Investigating the Importance of Electronic and Hydrophobic Effects for Ice Recrystallization Inhibition Using β-*O*-Aryl Glycosides

Matthew Alteen

Thesis submitted to the Faculty of Graduate and Postdoctoral Studies

University of Ottawa

in partial fulfillment of the requirements for the M.Sc. degree in the Ottawa-Carleton Chemistry Institute.

Candidate	Supervisor
_____	_____
Matt Alteen	Professor Robert N. Ben

Abstract

The cryopreservation of cells and tissues requires the addition of a cryoprotectant in order to prevent cellular damage caused by ice. Unfortunately, common cryoprotectants such as DMSO and glycerol exhibit significant toxicity which makes their use unfeasible for many clinical procedures. Our laboratory is interested in the development of alternative, non-toxic cryoprotectants which possess ice recrystallization inhibition (IRI) activity. Potent IRI activity has recently been discovered in certain small molecules, but the structural features required for this process are unclear. Herein we report the development of a library of *O*-aryl glycosides in order to probe the importance of electron density and hydrophobic moieties for IRI activity. It was found that the degree of electron density at the anomeric oxygen does not correlate with IRI ability in *para*-substituted aryl glycosides, nor does changing the position of the aryl substituent impart a predictable effect on activity. However, the addition of hydrophobic alkyl or acyl chains was beneficial for IRI activity; generally, increasing chain length was found to correlate with increasing activity. In some instances, an optimal alkyl chain length was identified, after which continued lengthening results in a loss of potency. We conclude from this study that a certain extent of hydrophobic character is beneficial for the IRI activity of aryl glycosides, and that a balance between hydrophobicity and hydrophilicity is required for optimum IRI ability. It is hoped that these findings will aid future efforts towards the rational design of novel cryoprotectants.

Acknowledgements

Many others besides myself have directly and indirectly contributed to the research presented in this document. I am deeply indebted to them, for without their support, my work would not have been possible.

Firstly, I would like to thank my supervisor, Dr. Robert Ben, for accepting me into his research group and for his constant direction, support and advice. I appreciate the faith he placed in me as a young, inexperienced graduate student two years ago, because without that leap of faith I would not have acquired the skills and knowledge I have today. Through lab meetings, courses, one-on-one discussions and once-terrifying problems at the blackboard, Rob has taught me to be a better chemist, teacher and critical thinker. I especially thank him for the constructive feedback he has provided me during the editing of this thesis. I am also grateful to the University of Ottawa for the funding I have received during my graduate studies.

I would also like to thank all the current and past members of the Ben Lab for their help with chemistry and for creating an enjoyable work environment. I owe a great deal of thanks to Dr. Mathieu Leclère, who provided invaluable training and advice during my first year. Thanks to Malay, for his help with chemistry and his endless insight into the world of mobile technology. Thanks to Anna, for our lively political debates and good times shared during the slow days. Thanks also to Chantelle, for her helpful advice with my own reactions and chemistry in general. To Jennie, Kyle, Ibrahim, Thomas, Devin, Stephanie, and all the other members of the lab: Thanks for the fond memories of our road trips to Montreal and Quebec, problems at the board, and Friday Beers. Thanks as well to Samantha Sherman for serving as a tireless and dedicated honours student.

I am very grateful for the help and support I have received from the Department of Chemistry during my time here. Thank you to Drs. Glenn Facey and Erik Ye for their help whenever I pushed the wrong button on the NMR. To Dr. Sharon Curtis and everyone at the uOttawa mass spectrometry facility, thank you for helping to verify my samples and for identifying the occasional "mystery" peak. Thanks to Drs. Chris Boddy, Jeff Keillor, Bill Ogilvie, Tony Durst, André Beauchemin, Louis Barriault, and all other members of the department for passing on their knowledge of chemistry to me in one form or another. Thank you to Dr. Alain St-Amant, for keeping in touch and always being available whenever I needed help, and to Louise Hotte, for letting me borrow the photocopier/scanner in the Dean's office numerous times and for always keeping the bowl of candy well-stocked.

To my parents, friends and family: Thank you for shaping who I am and for keeping me company on this multi-year journey. From family dinners to late nights at La Maison, these experiences have helped shape who I am. Finally, to my loving partner Jayme, for her constant motivation, support and the joy she brings to every aspect of my life: I couldn't do it without you at my side.

"Equipped with his five senses, man explores the universe around him and calls the adventure Science."
– Edwin Powell Hubble

Table of Contents

List of Figures

List of Tables

List of Graphs

List of Schemes

List of Abbreviations

α	alpha
β	beta
^{1}H	proton
^{13}C	carbon
3D	three-dimensional
Ac_2O	acetic anhydride
AFGP(s)	antifreeze glycoprotein(s)
AFP	antifreeze protein
Ala	alanine
Atm	atmosphere
$BF_3{\cdot}OEt_2$	boron trifluoride diethyletherate
br	broad
Cat.	catalytic
Cbz	carboxybenzyl
$CDCl_3$	deuterated chloroform
CD_3OD	deuterated methanol
CMC	critical micelle concentration
CPA	cryoprotective agent
d	doublet
D_2O	deuterium oxide
dd	doublet of doublets
DCM	dichloromethane
DIS	dynamic ice shaping
DMF	dimethylformamide
DMSO	dimethyl sulfoxide
dt	doublet of triplets
EDG	electron-donating group
ESI	electrospray ionization
Et	ethyl
Et_2O	diethyl ether
EtOAc	ethyl acetate
EWG	electron-withdrawing group
FBS	fetal bovine serum
Gal	galactose
Glc	glucose
Gly	glycine
HepG2	human hepatocellular carcinoma cell line
HES	hydroxyethyl starch
HTK	histidine-tryptophan-ketoglutarate
IIF	intracellular ice formation
INA	ice nucleating agent
IR resin	Amberlite ion exchange resin
IRI	ice recrystallization inhibition
kDa	kilodaltons

KGG	lysine-glycine-glycine
LiOH	lithium hydroxide
LRMS	low-resolution mass spectrometry
m	multiplet
M	molar
M^+	parent molecular ion
Man	mannose
Me	methyl
MEM	minimum essential medium
MeOH	methanol
MGS	mean grain size
$MgSO_4$	magnesium sulfate
MHz	mega Hertz
mM	millimolar
MS	molecular sieves
MTT	3-(4,5-dimethylthiazol-2-yl)-2,5-diphenyltetrazolium bromide
NaCl	sodium chloride
NADH	nicotine adenine dinucleotide
NADPH	nicotine adenine dinucleotide phosphate
NHAc	*N*-acetyl
NMR	nuclear magnetic resonance
OGG	ornithine-glycine-glycine
OBu	butoxy
OEt	ethoxy
OMe	methoxy
OPr	propoxy
PBS	phosphate buffered saline
$Pd(OH)_2$	palladium (II) hydroxide
PEG	polyethylene glycol
ppm	parts per million
Pr	propyl
PVP	polyvinylpyrollidone
q	quartet
QLL	quasi-liquid layer
s	singlet
SAR	structure-activity relationship
Ser	serine
SGG	serine-glycine-glycine
$SOCl_2$	thionyl chloride
t	triplet
TAA	threonine-alanine-alanine
Tal	talose
TFA	trifluoroacetic acid
TH	thermal hysteresis
THF	tetrahydrofuran
Thr	threonine
WRL-68	human embryonic liver cell line

Chapter 1: Introduction to Cryopreservation, the Mechanisms of Cryo-Injury and the Potential of Carbohydrate-Based Small Molecules as Cryoprotectants

1.1 Introduction

Cryopreservation is a technique which allows for the long-term storage of cells and tissues at very low temperatures (typically -78°C to -196°C).[1] At these temperatures, all biochemical processes are essentially halted and the degradation of cells over time is slowed significantly.[1] Since its first reported use in 1949,[2] the process of cryopreservation is now a procedure in clinical and research environments.[3-5] It also has applications in agriculture and the food industry.[6,7]

Despite the success of this technology over the past 60 years, numerous drawbacks still remain that limit the applicability of certain cryopreservation procedures. One of the most significant challenges is the prevention of ice formation which can impair cellular function in recovered samples post-thaw.[8-10] Therefore, the addition of a cryoprotectant to preserved samples is necessary in order to mitigate the damage associated with this process by limiting ice formation.[1,11] The most commonly-used cryoprotectants include cell-penetrating agents such as dimethyl sulfoxide (DMSO) and glycerol,[12-14] as well as non-penetrating agents such as salts, sugars and polymers.[15,16] Unfortunately, many of these cryoprotectants exhibit significant toxicity that negatively impacts cell viability and functionality and is harmful to patients receiving cryopreserved tissues. For example, cell lines used in certain regenerative medicine therapies require high post-thaw viability and functionality which is not yet attainable using currently-available cryopreservation techniques.[17-19] This severely curtails the feasibility of cryopreservation in medical settings.

One approach towards a solution to this pressing issue is the development of alternative cryoprotectants which are non-toxic to cells but are still capable of preventing damage from ice. The rational design of new cryoprotectants is challenging since the mechanisms by which they function are

complicated and not fully understood.[20-23] However, insight can be drawn from naturally-occurring biological antifreezes which protect organisms that live in sub-zero environments.[24] Using these compounds as a model, progress has been made towards understanding and reproducing the molecular processes by which these natural cryoprotectants function.[25] It is hoped that information obtained from these studies may someday lead to the rational design of effective, non-toxic cryoprotective agents. This following sections will summarize current knowledge relating to cryo-injury, the mechanisms through which cellular damage can be mitigated, and recent progress in the development of novel cryoprotectants.

1.2 Cryopreservation of cells, tissues and organs

1.2.1 Mechanisms of cellular damage during freezing

Freezing is a lethal process to almost all organisms. The cellular damage that occurs to biological samples during the freezing and thawing process is the greatest impediment utilizing cryopreservation techniques for novel biological samples.[26] Currently, no cryopreservation protocol ensures 100% cell viability post-thaw,[1] which is problematic for certain applications.[17-19] As such, there has been considerable research into the mechanism(s) by which this cellular damage occurs so that better ways of supressing the damage can be developed. While the exact causes remain unclear, a number of hypotheses surrounding eukaryotic cell damage have emerged.

Damage of the external cell membrane as a direct result of both extracellular and intracellular ice formation is one of the main proposed causes of cellular injury during cryopreservation.[27] Extracellular ice can damage membranes through three different processes: by increasing intracellular solute concentrations,[9-11] by influencing osmotic pressure across cell membranes,[28] and by mechanically stressing or shearing membranes with increasing crystal size.[8,29] The combined results of these

processes include osmotic shrinkage and distorted/deformed cell membranes. Intracellular ice formation (IIF) has also been identified as a possible source of cryo-injury. The freezing of the intracellular environment causes solutes present in the cytoplasm to precipitate out of solution. This alters the pH of the environment and, in turn, disrupts cellular metabolism.[1,9,11]

There has been some debate as to the importance of IIF for post-cryopreservation cell viability.[30,31] Toner and Mazur have argued that IIF is the major cause of cryopreservation damage since cellular functions are inhibited by freezing of the cytoplasm.[30,32] However, work by Salt and coworkers has indicated otherwise. They found that fat cells obtained from freeze-tolerant goldenrod gall fly larvae (*Eurosta solidaginis*) remain viable despite the presence of IIF. It was also noted that the ice crystals observed in the cells were relatively small.[33] This result questioned whether IIF alone is the most significant factor in cell damage and suggested intracellular and extracellular ice recrystallization may also be contributing.[33] Ice recrystallization is a thermodynamically favoured process involving the growth of larger ice crystals at the expense of smaller ones.[34] The large ice crystals that form create internal mechanical stress on the cell membrane and eventually lead to cell death.[1,34] Recrystallization takes place at higher temperatures and in the presence of smaller ice crystals and is therefore most damaging during the thawing stage of preservation.[35] In addition, Chaytor and colleagues have demonstrated that there is a positive correlation between ice recrystallization inhibition and the post-thaw cell viabilities in a variety of human cell lines.[36] Thus, while there are many processes which cause cellular injury during cryopreservation, inhibiting ice recrystallization appears to be a logical approach towards improving current protocols.

1.2.2 Cryoprotective agents and their toxicities

The addition of at least one cryoprotective agent (CPA) is necessary when cryopreserving cells in order to prevent cell death due to ice formation.[37] CPAs can be generally classified as belonging to one of two broad classes: cell penetrating CPAs and non-penetrating CPAs. The earliest cryoprotectants – glycerol and dimethyl sulfoxide (DMSO) – are both examples of penetrating CPAs.[2,38] Their effectiveness as cryoprotectants was discovered by accident in 1949, when Polge serendipitously found that glycerol improved the viability of frozen spermatocytes.[2] At the time, it was hypothesized that the penetrating ability of these compounds allowed them to solvate residual solutes on either side of the cell membrane, thus preventing osmotic efflux which leads to cell dehydration.[1,38,39] However, it has since been shown that non-penetrating CPAs are also capable of protecting against damage in certain applications, suggesting that the two types of cryoprotectants have distinct mechanisms of action. [16,37]

The most common cryoprotectant, DMSO, is proposed to operate in several different ways. Because it is capable of penetrating cells, it is thought to replace water inside the cell and dilute ionic solutes on the external surface of the cell.[38-41] This helps maintain the osmotic equilibrium inside and outside the cell, slowing the rate of cell dehydration and osmotic flux which leads to rupture of the cell membrane.[38-41] It is also surmised that the amphiphilic nature of DMSO allows it to insert itself within the lipid bilayer, which spaces out the fatty acid chains of the membrane and give it more flexibility to accommodate changes to cell volume.[40,41] Additionally, it has been shown that DMSO is capable of forming transient pores within the cell membrane, which increases cell permeability and allows further compensation against osmotic stress.[40-41]

The use of high-molecular weight polymers such as polyvinylpyrrolidone (PVP), polyethylene glycol (PEG) and hydroxyethyl starch (HES) as non-penetrating CPAs has also been documented.[14,21,42] However, the mechanism by which these macromolecules function is less clear.[43] It has been proposed

that the colligative properties of the polymers at high concentrations increase the viscosity of the aqueous solution outside of the cell, which restricts the rate at which water can be drawn across the cell membrane and reduces osmotic stress.[44] Another hypothesis is that the hydrogen bonding ability of these polymers to water depresses the freezing point of the solution and that the ability of the polymers to absorb high amounts of water reduces the availability of free water molecules to form ice crystals.[45] The use of such polymers as CPAs has been most successful in the preservation of red blood cells; on their own, they are not as effective at preserving nucleated cells as penetrating CPAs.[37] However, when used in combination with a penetrating CPA, they can improve post-thaw cell viabilities by reducing the amount of penetrating agent required, helping to avoid cytotoxicity.[37] To date, it is not known if PVP, PEG and HES inhibit ice recrystallization as studies have not been carried out to this effect.

Low-molecular weight carbohydrates such as D-sucrose and D-trehalose, which are non-penetrating, can also be used as cryoprotectants.[46] Sucrose has been shown to protect red blood cells, chloroplasts and bone marrow stem cells from cryo-injury at high concentrations (up to 0.350 M).[27] Carbohydrates such as these have been found to possess unique hydration properties which allow them to interact strongly with surrounding water molecules.[47,48] This strong interaction with bulk water may serve to restrict osmotic efflux and prevent ice crystal formation similar to the action of polymers described above. In addition, a wide range of monosaccharides and disaccharides display modest ice recrystallization inhibition (IRI) activity which has been shown to correlate with increased cell viability.[48]

1.2.3 Limitations of current cryopreservation technologies

After more than 60 years of development, cryopreservation has evolved to the point that it is now a routine procedure for the storage of various mammalian cell lines.[49] Indeed, it is difficult to imagine how biomedical research using cell cultures could be carried out without the ability to store

these cells before use. In addition to being used for research purposes, it is now possible to cryopreserve human sperm cells and oocytes for *in vitro* fertilization procedures as well as fertilized embryos.[50-52] Some success has also been documented in the cryostorage of ovarian tissues samples.[53]

However, despite these recent advances, the significant toxicity of commonly-used cryoprotectants such as DMSO is a serious limitation which prevents the use of cryopreserved cells for certain clinical procedures. While there is a net benefit to the use of DMSO when storing cells, not all cells remain viable after thawing due to the cytotoxic nature of this cryoprotectant.[54] For research purposes, reduced post-thaw cell viabilities are tolerable for starting most mammalian cell cultures. However, for some medical applications, high cell viabilities are required. Recent studies on the use of mesenchymal stem cells for regenerative medicine therapies are one example of this; a study by Quevedo *et al.* found that low cell survival rates after cryopreservation correlate with poor *in vivo* cell differentiation, questioning the feasibility of related procedures when DMSO is used.[55]

There are also drawbacks to the use of DMSO as a cryoprotectant in clinical settings.[17] Debilitating side effects have been reported in patients who have received cryopreserved cell transplants and bone marrow grafts which have been stored in DMSO.[56] While in most cases the observed side effects are mild to moderate (nausea, vomiting, shortness of breath, and changes in blood pressure) serious cardiac-related side effects can sometimes occur.[57] Even if these side effects prove to be non-lethal, they contribute to increased morbidity, prolonged hospitalization times and increased treatment-related costs.[58]

The above examples demonstrate the need for improved cryoprotective agents. Currently, a trade-off exists between the prevention of damaging ice formation and the toxic effects of DMSO. In order to expand the scope of biological specimens which can be cryopreserved, it is necessary to

develop alternative cryoprotectants which protect cells from freezing damage yet do not exhibit the potent cytotoxicity of DMSO. This has been an ongoing area of research by our laboratory.

1.3 Antifreeze Glycoproteins (AFGPs) and their properties

1.3.1 Origin, structure and function of biological antifreezes

Biological Antifreezes are a unique class of biomacromolecules which are capable of protecting organisms which inhabit sub-zero environments from the growth of ice.[59] First isolated from Arctic and Antarctic Teleost fish in the late 1960's, variants were later identified from amphibians, insects and plants.[60] These compounds allow fish such as Atlantic Cod (*Gadus morhua)* and Antarctic Notothenioid (*Pagothenia borchgrevinki)* to survive in water which can reach temperatures of -1.9°C due to high concentrations of sea salt.[61,62] The plasma of these fish contain only about one-third the concentration of solutes as the surrounding water, meaning that their isolated blood serum should freeze at -0.7°C.[63,64] This 1.2°C difference in freezing points led researchers to hypothesize that some other component was present in the plasma of the fish which allowed them to survive.

Figure 1.1: Atlantic Cod (*Gadus morhua*) (**A**) and Antarctic Notothenioid (*Pagothenia borchgrevinki*) (**B**).[59,60]

Five classes of biological antifreezes found in fish have been identified thus far, including four types of antifreeze proteins (AFPs) designated type I, II, III and IV, and a fifth class of antifreeze glycoprotein (AFGP).[65,66] While the four types of AFPs all share similar function, their structures are

quite varied (Table 1.1). Type I and type IV AFPs consist of a single α-helix or an α-helix bundle, respectively. Type II and type III AFPs contain more irregular secondary and tertiary structure; type II exists as a disulfide-rich mixed coil while type III forms a globular β-sandwich.[65]

Table 1.1: Comparison of the origins, sizes and representative structural features of antifreeze protein (AFP) types I-IV and antifreeze glycoproteins (AFGP).[65,66]

Characteristic	Type I AFP	Type II AFP	Type III AFP	Type IV AFP	AFGP
Mass (kDa)	3.3 – 4.5	11 – 24	6.5	12	2.6-33
Representative Structure					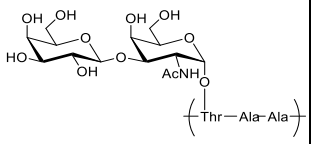
Key Structural Properties	Alanine-rich α-helix	Disulfide-rich mixed coil	Globular β-sandwich	Alanine-rich helical bundle	Disaccharide + (TAA)-repeat
Natural Source	Right-eyed flounders; sculpins	Sea raven; smelt; herring	Ocean pout wolfish; eel pout	Longhorn sculpin	Antarctic notothenioids; northern cods

In contrast, AFGPs share similar structural features across different species and are capable of being synthesized *in vitro* using solid phase peptide synthesis.[61,62,67] This has made structure-function studies of AFGPs more attractive than AFPs. AFGPs consist of a repeating threonyl-alanyl-alanyl peptide sequence and a β-D-galactosyl-(1,3)-α-D-*N*-acetylgalactosamine disaccharide.[68] The peptide is glycosylated at the secondary hydroxyl group of each threonine residue.[68] This structural sequence is highly conserved with only minor amino acid variation observed between AFGPs of different species. [62] Some glycoproteins have been identified in which the second alanine reside of the Thr-Ala-Ala repeat has been replaced with proline, and in some species of cod the glycosylated threonine reside is occasionally replaced with an arginine.[69,70] In contrast to their high sequence homology, AFGPs vary substantially in molecular weight based on the number of repeating glycopeptide units and have thus

been classified into eight subtypes according to their weight.[71] AFGPs 1-5 are the largest, containing up to 50 units with molecular weights of 20-30 kDA. AFGPs 6-8 are smaller, containing as little as four repeating units in the case of AFGP 8. While they are believed to function through similar mechanisms, the larger AFGPs display more potent antifreeze activity than the smaller ones.[71]

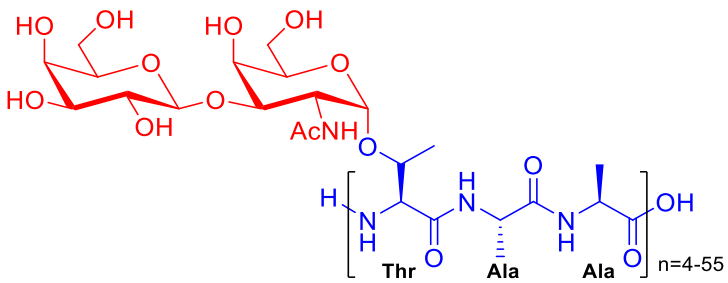

Figure 1.2: Native structure of antifreeze glycoproteins.[68]

AFPs and AFGPs have evolved as natural cryoprotectants and are essential to the species which produce them. Because of their unique properties, they have garnered great interest as a source of inspiration for alternative CPAs to be used for the cryopreservation of cells and tissues.[72] They are also of interest for their potential applications in cryosurgery, food preservation and agriculture.[73-75] As such, extensive studies have been carried out on these compounds in order to elucidate their mechanism of action in preventing ice formation.[76-78] It is now generally accepted that AFPs and AFGPs depress the freezing point of water by binding to specific faces of a growing ice lattice in order to prevent further growth.[79,80] However, certain aspects of their mode of action remain unclear. The following section will summarize the properties of ice formation and the two proposed processes by which AF(G)Ps inhibit ice crystal growth: thermal hysteresis (TH) and ice recrystallization inhibition (IRI).

1.3.2 Thermal Hysteresis

One main feature of biological antifreezes is their ability to depress the freezing point of a solution relative to its melting point, a process defined as thermal hysteresis (TH).[64] This results in a gap between the melting and freezing points of the solution (known as a thermal hysteretic gap) and within this gap the solution does not freeze (Figure 1.3). The localized depression of the freezing point caused by these proteins is a non-colligative phenomenon (i.e. depression of the freezing point does not occur proportionally to the concentration of active compound, Figure 1.4).[63,81] This is in contrast to other antifreeze solutes such as NaCl or galactose that display a linear correlation indicative of colligative freezing point depression.[63,81] Interestingly, the combination of AFGP with NaCl results in a synergistic improvement in freezing point depression which retains a non-colligative profile, indicating that the freezing point depression of AFGP is a result of its specific structural nature.[63,81]

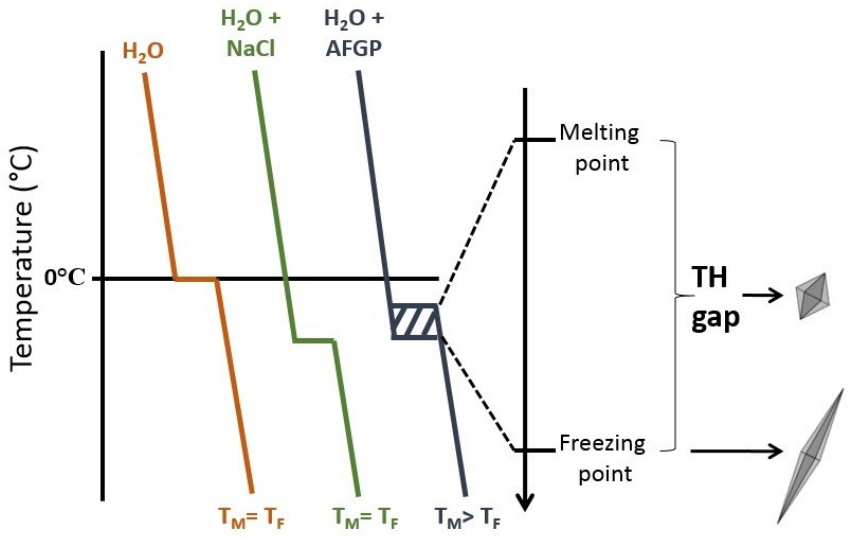

Figure 1.3: Schematic representation of thermal hysteresis: freezing curves for pure water (orange), NaCl solution (green) and AFGP 8 (**1**) solution (blue). A thermal hysteretic gap exists for the AFGP 8 solution.[82-85]

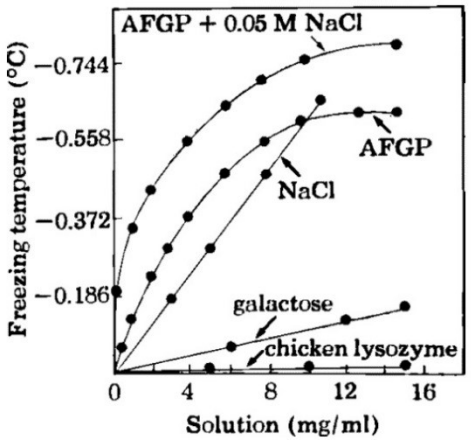

Figure 1.4: Change in freezing temperature (°C) of various aqueous solutions as a function of solute concentration. Linear correlations indicate colligative freezing point depression; non-linear correlations indicate non-colligative freezing point depression.[60,63]

As a result of their non-colligative properties, biological antifreezes are capable of lowering the freezing point of solutions at much lower concentrations; it is believed their antifreeze activity is 200-500 times greater than NaCl and related colligative solutes.[60, 81] This proves beneficial for the organisms in question since the low concentrations of antifreeze compound required cause less osmotic stress to the cells. The maximum TH activity of fish AF(G)Ps is approximately 1.5°C.[24] However, certain insect AFPs have been discovered which possess hyperactive TH activity of greater than 6.0°C (Table 1.2).[86]

Table 1.2: Maximum Thermal Hysteresis (TH) activity of antifreeze proteins and glycoproteins from various sources.[87]

Source of Biological Antifreeze	Maximum TH Activity
Bacterial/fungal AFPs	Negligible (IRI activity only)
Plant AFPs	0.2 – 0.4 °C
Fish AFPs	0.6 – 1.5 °C
Fish AFGPs	0.6 – 1.2 °C
Insect AFPs	> 6.0 °C

The observed TH activity of AFPs and AFGPs has been attributed to their ability to bind to ice.[85,86] In doing so, the antifreezes induce a phenomenon known as dynamic ice shaping (DIS) which alters the growth rate and morphology of the ice crystals that form.[88] In pure water, ice crystals are disk-like in shape and will grow by the addition of water molecules to the prism faces (a-axes) of the ice crystal (Figure 1.5).[88,89] This outward growth along the prismatic face of the crystal will form sheets of ice.[88] However, when AF(G)Ps are present, they too will preferentially bind to the prism faces of the ice crystal and prevent typical prismatic face growth observed in pure water.[90] With this face blocked by the antifreeze compounds, the water molecules will instead add to the basal face (c-axis) of the crystal.[89,90] This results in the formation of hexagonal bipyramidal ice crystals that ultimately form long, needle-like structures once the temperature drops below the lower limit of the TH gap.[90,65]

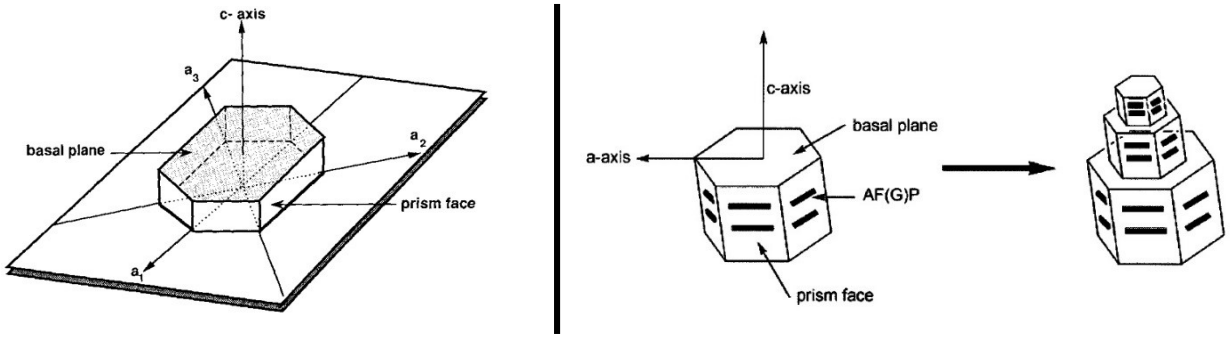

Figure 1.5: Schematic representation of the ice crystals which form in pure water (**A**) and in a solution containing a biological antifreeze (**B**). In pure water, additional water molecules bind to the prism face of the ice crystal, causing the crystal to expand outwards along the a-axes. In the presence of antifreeze compounds, the water molecules are restricted to adding along the basal plane, forming hexagonal bipyramidal crystals which grow lengthwise along the c-axis.[24,89]

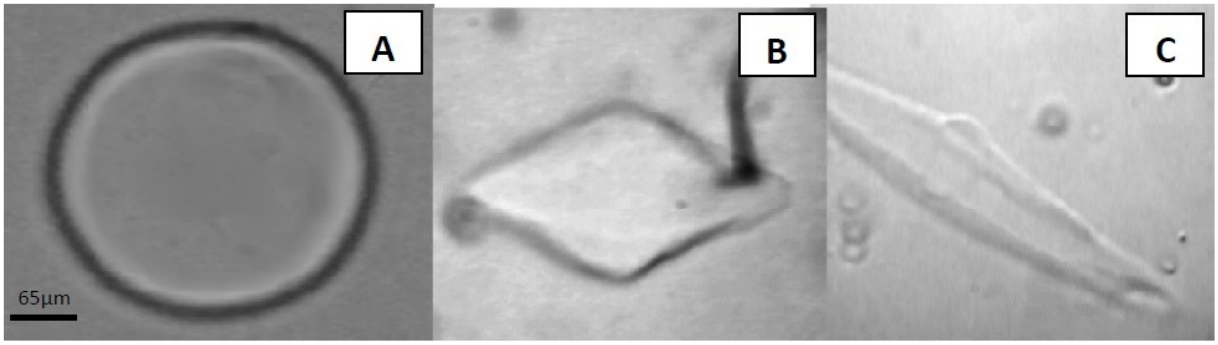

Figure 1.6: Magnified view of ice crystal morphology when grown in (**A**) distilled water, (**B**) an AFGP solution at temperatures within the thermal hysteretic (TH) gap, and (**C**) an AFGP solution at temperatures below the TH gap. The morphology of the crystals in (**B**) and (**C**) are altered due to dynamic ice shaping.[65]

1.3.3 Ice Recrystallization Inhibition

The second process by which biological antifreezes act as cryoprotectants is their ability to inhibit ice recrystallization. Ice recrystallization is defined as the growth of large ice crystals at the expense of smaller ones.[91,92] This thermodynamically favoured process takes place at temperatures below 0°C and is driven by a reduction in grain boundary energy, since the grain boundary of two smaller ice crystals will be reduced if the crystals merge into one larger crystal.[91,92] This effect is detrimental in living systems because the resulting large ice crystals cause mechanical stress to plasma membranes and damage the cells. AFPs and AFGPs are capable of inhibiting the recrystallization process, limiting the size of ice crystals and, in turn, reducing cellular damage.[91,92,93] Figure 1.7 depicts the extremely small ice crystals which form in a 10 mg/mL AFGP 8 solution, which is a potent inhibitor of ice recrystallization (**A**). This is in stark contrast to the large ice crystals which form in an untreated phosphate-buffered saline solution (**B**).[94]

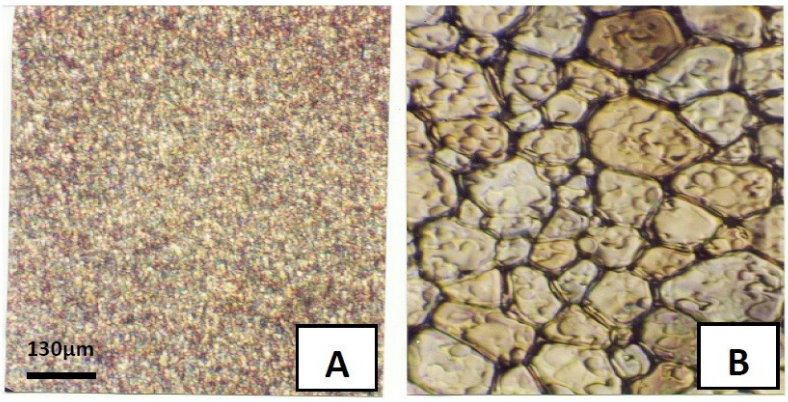

Figure 1.7: Magnified view of (**A**) the ice crystals formed in a 5.5 x 10^{-6} M solution of IRI-active AFGP 8 and (**B**) the ice crystals formed in a phosphate buffered saline solution (Ben Lab, unpublished results). Magnification factors used in each photo are identical.

Ice Recrystallization Inhibition (IRI) is believed to be a desirable property for the cryopreservation of biological samples. As such, several studies have explored this property for the development of alternative cryoprotectants.[36,95,96] A recent report by Chaytor and coworkers on the cryopreservation of human HepG2 and WRL-68 cell lines using IRI-active carbohydrates has found that increased IRI ability correlates with improved cell viabilities post-thaw.[36] Similar results were obtained by Wu *et al.* in the carbohydrate-mediated preservation of human umbilical cord blood.[95] However, the mechanism of ice recrystallization inhibition is poorly understood, as are the important structural features possessed by compounds which are capable of inhibiting ice recrystallization. This makes the rational design of ice recrystallization inhibitors challenging. Over the past decade, numerous structure-activity relationship studies have been carried out on AFGPs to gain insight into this phenomenon.[97-100] While it was initially believed that IRI and TH activities were inextricably linked, this has since been disproven; ice recrystallization inhibition has been observed in the absence of thermal hysteresis in both natural and synthetically-derived AFGP analogues.[99,101] This makes it possible to explore the structural features responsible for both processes separately in greater detail.

1.3.4 AFGPs as Cryoprotectants

Given the exceptional protection which biological antifreezes provide to their host organisms in sub-zero environments, it was originally envisioned that AFPs and AFGPs could be used as cryoprotectants. However, while attractive in principle, AFGPs generally make poor cryoprotectants for a number of reasons. The thermal hysteretic activity of AFGP, though beneficial for species living within the temperature range of the TH gap, proves detrimental to cells once the temperature falls below the lower limit of the gap.[60,102,103] This is because AFGPs bind specifically to the prismatic face of growing ice crystals, which alters the morphology of the ice lattice.[65,90] Although ice growth is controlled within the TH gap, once the solution temperature falls below the freezing point, rapid growth of long spicule-shaped ice crystals occurs (Figure 1.6).[65,90] These spicules cause significant damage to the plasma membranes of cells and reduce the cell viability of the sample.[102,103,105] Limited success has been obtained using AFGPs to preserve pig oocytes, mouse embryos, carp spermatozoa and human platelet cells, but in the majority of cases AFGPs cannot effectively preserve cell viabilities after cryostorage.[85,104-106]

Even if the problems associated with dynamic ice shaping caused by AFGPs could be overcome, it would be difficult to obtain large enough quantities to use it as a cryoprotectant on a commercial scale. The isolation of AFGPs from natural sources is difficult and expensive, making such approaches unfeasible.[97] A total synthesis of AFGP 8 has been reported, but the synthesis of such glycoconjugates results in low overall yields and is also costly.[97,107] Another unexpected drawback of AFGPs is cytotoxicity. AFGPs were once thought to be a non-toxic alternative to DMSO, but it has since been discovered that AFGP 8 is itself cytotoxic to human liver and kidney cell lines.[108] This effectively eliminates the main advantage of any alternative cryoprotectant over DMSO. As a result of these limitations, biological antifreezes themselves are not currently used in any regular cryopreservation

protocol. However, a great deal of information can be obtained from the structure and activity of AFGPs which would assist in the development of novel cryoprotectants. The following section will summarize these efforts and the subsequent development of synthetic AFGP analogues.

1.4 AFGP Analogues and Carbohydrates as Ice Recrystallization Inhibitors

1.4.1 1st and 2nd Generation C-linked AFGP Analogues

The discovery of the cryoprotectant properties which AFGPs possess (namely, thermal hysteresis and ice recrystallization inhibition) led researchers to investigate the structural features of the glycoproteins which confer these abilities. Various structure-activity relationship (SAR) studies have been performed to identify the components of the AFGP which are necessary for TH activity. It was discovered that increasing molecular weight of the AFGPs is correlated with increased TH activity.[109] AFGP 8, which contains four repeating glycopeptide units, displays 70% less TH activity than AFGP 1, which contains 55 repeating units.[109] Modifications to the carbohydrate portion of the AFGP, including oxidation and acetylation of the pyranose hydroxyl groups, all result in decreases in activity.[76,110] Complexation of the carbohydrate to borate was also found to inactivate the compound, suggesting that the presence of free hydroxyl groups is important for antifreeze activity.[111]

Extensive SAR studies on the TH activity of AFGP 8 (1) were performed by Nishimura.[78] Substitution of a monosaccharide for the disaccharide or removal of the C2-*N*-acetyl group on the first pyranose ring was not tolerated, nor was modifying the glycosidic bond of the disaccharide to the peptide backbone from an α to a β linkage.[78] Investigation of the peptide units found that the hydrophobic methyl groups on the alanine and threonine residues were also important for activity. These conclusions are summarized in Figure 1.8.[78] Unfortunately, this study and all others relating to the antifreeze activity of AFGPs focused exclusively on TH activity, with no assessment of IRI activity.

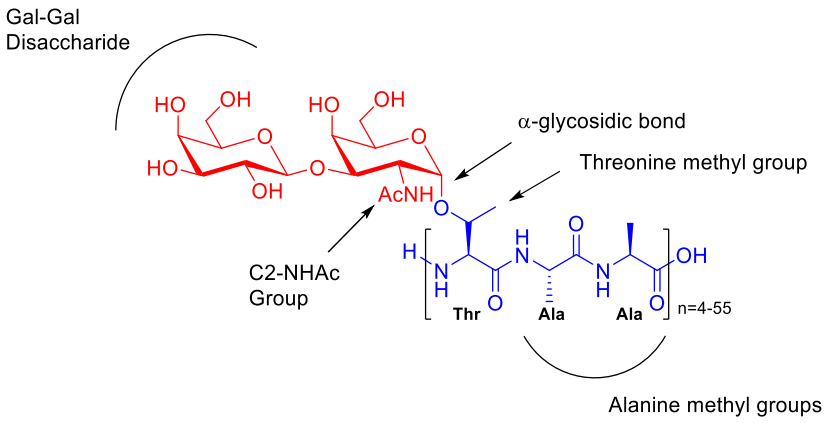

Figure 1.8: Important structural features required for thermal hysteresis (TH) activity in AFGP 8.[78]

In light of this, Ben *et al.* sought to develop synthetic analogues of AFGPs in order to better understand their molecular mechanism(s) of action. This was, and remains today, a difficult undertaking due to the structural complexity of glycopeptides, the need for orthogonal carbohydrate and peptide protecting groups, and the instability of the glycosidic bond between the anomeric carbon and oxygen in acidic or basic conditions.[112,113] Few total syntheses of AFGP 8 has so far been reported due to these challenges. Instead, Ben *et al.* chose to synthesize *C*-linked AFGP analogues.[23] *C*-linked glycosidic bonds have been shown to possess increased stability to acid, base or glycosidase hydrolysis relative to typical *O*-linked glycosides, making them a judicious choice in the development of structurally-diverse glycoprotein analogues.[114] The first reported AFGP analogue, [*C*-(KGG)-gal]$_4$ (**2**) possessed a number of strategic structural modifications in order to simplify its synthesis (Figure 1.9).[23] First, The β-D-galactosyl-(1,3)-α-D-*N*-acetylgalactosamine disaccharide was replaced with one molecule of commercially-available D-galactose. Secondly, the Thr-Ala-Ala peptide unit found in native AFGP 8 was replaced with a Lys-Gly-Gly sequence. Lysine was chosen since it is similar in length to arginine, which sometimes replaces threonine in smaller native AFGPs, and the alanines were replaced with glycine to eliminate the possible formation of stereoisomers during the synthesis of the peptide.

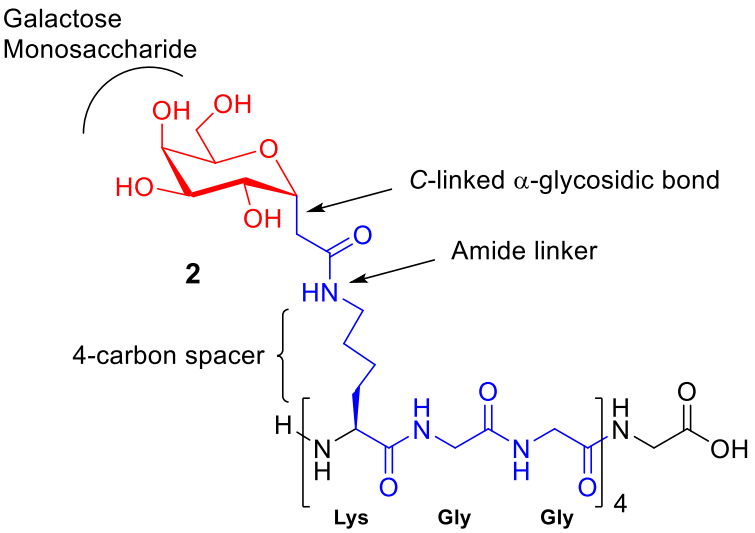

Figure 1.9: First-generation *C*-linked AFGP analogue [*C*-(KGG)-Gal]$_4$ (**2**) indicating key structural features.[23]

The synthesis of (**2**) demonstrated the effectiveness of *C*-glycosides as an approach towards rationally-designed AFGP analogues.[23,99] However, the IRI activity of (**2**) was found to be substantially lower than native AFGP 8 (Graph 1.1).[100] As such, additional *C*-linked AFGP analogues were produced (Figure 1.10).[99,100] Second-generation analogues (**3**) and (**4**) displayed surprising antifreeze activity in that they both possessed potent IRI ability comparable to that of AFGP 8 (Graph 1.1) but did not show TH activity.[99,100] This provided conclusive evidence that IRI and TH activity are not directly linked, making it possible to synthesize targets which possess only one type of antifreeze activity.[99] Both compounds also showed very little DIS activity, which is a desirable property for cryopreservation.[99,100] Cytotoxicity of the second-generation analogues towards human liver and kidney cell lines was also assessed.[99,108] It was found that [*C*-(OGG)-Gal]$_4$ (**3**) did not confer toxicity towards the examined cell lines at concentrations from 0.63 mg/mL to 2.0 mg/mL, indicating that the toxicity of AFGP 8 can also be modulated through structural variation.[99,108] The increased IRI activity of the *C*-serine analogue (**4**) over the ornithine analogue (**3**) prompted studies investigating whether the decreased length of the aliphatic linker was responsible. After synthesis and assessment of various derivatives with longer alkyl chain

lengths, [*C*-(SGG)-Gal]$_4$ (**4**) remained the most potent inhibitor.[115] Subsequent studies on the solution conformation of AFGP analogues have revealed that the length of the linker affects the orientation of the carbohydrate unit relative to the peptide backbone, which may in turn influence IRI activity by altering the hydration of the glycopeptide.[115]

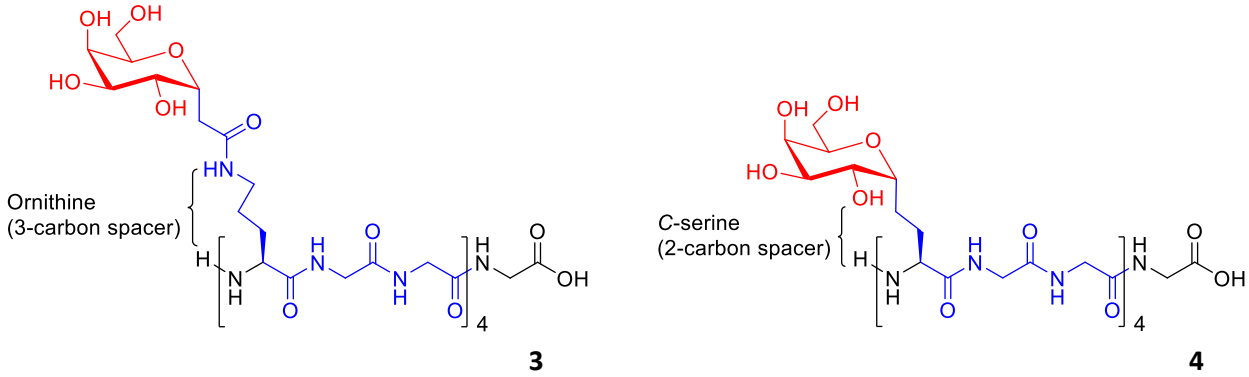

3 **4**

Figure 1.10: Second-generation *C*-AFGP analogues [*C*-(OGG)-Gal]$_4$ (**3**) and [*C*-(SGG)-Gal]$_4$ (**4**).[99,100]

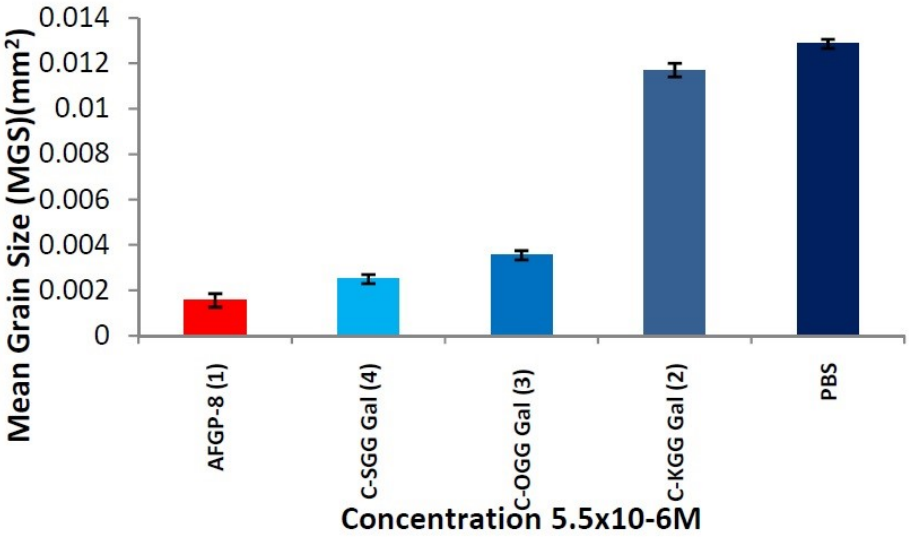

Graph 1.1: Ice Recrystallization Inhibition (IRI) activity of AFGP 8 (**1**), *C*-linked AFGP analogues (**2**, **3**, **4**), and phosphate buffered saline (PBS) as a negative control. Error bars represent standard error of the mean (SEM).[23,99,100]

In response to the promising IRI activities shown by *C*-AFGP analogues (**3**) and (**4**), Leclère and colleagues assessed the performance of these compounds as cryoprotectants in comparison to DMSO (Graph 1.2).[96] WRL-68 human embryonic liver cells were intentionally chosen for this study as they represent a possible source of stem cells for regenerative medicine therapies.[116] Cells were slow-frozen in the presence of *C*-AFGP or DMSO, stored for 6 days at -196°C, thawed quickly, and then assessed for cell viability after 2 hours. At 1.5 mg/mL concentration, [*C*-(OGG)-Gal]$_4$ (**3**) resulted in total cell viability which was statically identical to a 2.5 % solution of DMSO. [*C*-(SGG)-Gal]$_4$ (**4**) displayed slightly lower cell viability, possibly due to increased cytotoxicity relative to (**3**). This was the first reported use of IRI-active and TH-inactive AFGP analogues as effective cryoprotectants, demonstrating their potential as an alternative to DMSO. Additional cryopreservation experiments were carried out including one hour of pre-incubation with analogue (**3**) since previous studies with these analogues indicated they are quickly internalized by human liver cells. However, there was no discernable improvement in cell viability observed, suggesting that penetration of the cell membrane by AFGP analogues is not necessary for successful cryopreservation.[96]

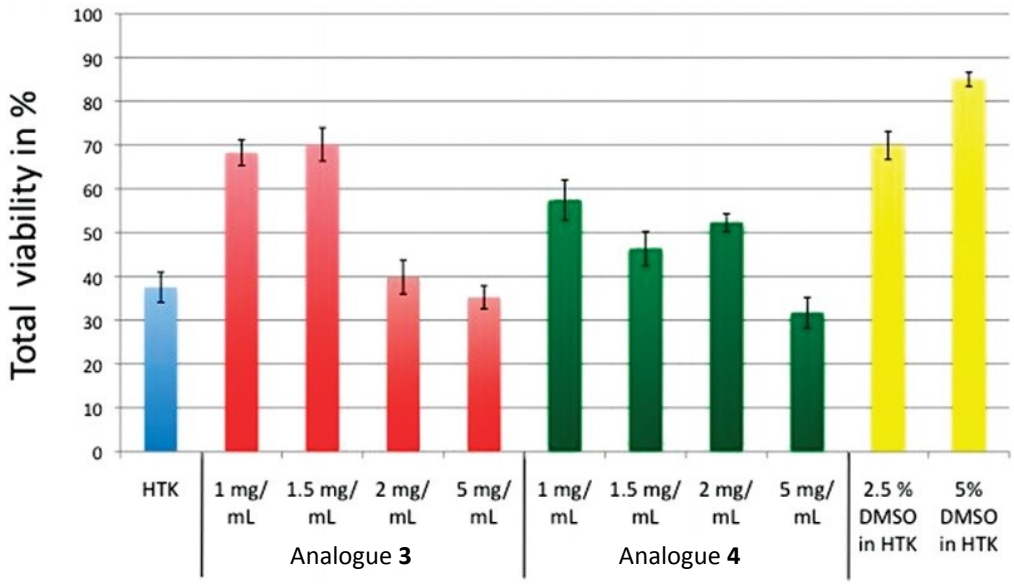

Graph 1.2: WRL-68 cell viability 2 hours post-thaw after cryostorage with C-AFGP analogues (**3**) or (**4**) compared to 2.5% or 5% DMSO. Cells were preserved in histidine-tryptophan-ketoglutarate (HTK) custodiol solution. Error bars represent standard error of the mean (SEM).[96]

1.4.2 Carbohydrate Hydration and its Effect on IRI Activity

The encouraging IRI activities observed in *C*-linked AFGP analogues (**3**) and (**4**) prompted a series of structure-activity relationship studies by Czechura and colleagues to identify structural features important for IRI.[117] One such study involved the modification of the carbohydrate unit to determine the effect of hydroxyl group stereochemistry, since it was been hypothesized that these groups play an important role in the activity of biological antifreezes. Three derivatives of [*C*-(OGG)-Gal]$_4$ (**3**) were produced in which the pyranose ring was substituted with glucose (**5**), mannose (**6**) and talose (**7**) (Figure 1.11) and these analogues were then assessed for their corresponding IRI activity (Graph 1.3).[117]

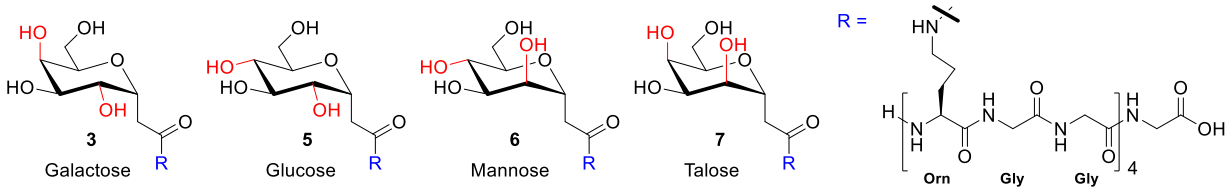

Figure 1.11: *C*-AFGP analogues [*C*-(OGG)-Gal]$_4$ (**3**), [*C*-(OGG)-Glc]$_4$ (**5**), [*C*-(OGG)-Man]$_4$ (**6**) and [*C*-(OGG)-Tal]$_4$ (**7**) produced by Czechura *et al.*[117]

An interesting trend emerged from this analysis. Among the AFGP analogues tested, increased IRI activity was correlated with decreased partial molar compressibility values for the free pyranose rings as calculated by Galema and Høiland (Figure 1.12).[118,119] These values represent the degree of fit of the hydrated sugar within the three-dimensional network of surrounding bulk water and were obtained using molecular dynamic simulations, kinetic experiments and ultrasound measurements. A high molar compressibility value indicates a good hydrogen-bonding "fit" of the molecule in the surrounding aqueous solvent.[118,119] Thus, it appeared from the data that disrupting the compatibility of the glycoconjugates in the 3D hydrogen-bonding network leads to an increase in IRI activity.[117] The IRI activities of the individual monosaccharides followed the same trend; galactose (**8**), with the lowest molar compressibility value and poorest "fit", was the most active carbohydrate, while talose (**11**), with the highest molar compressibility, was the least active.[117]

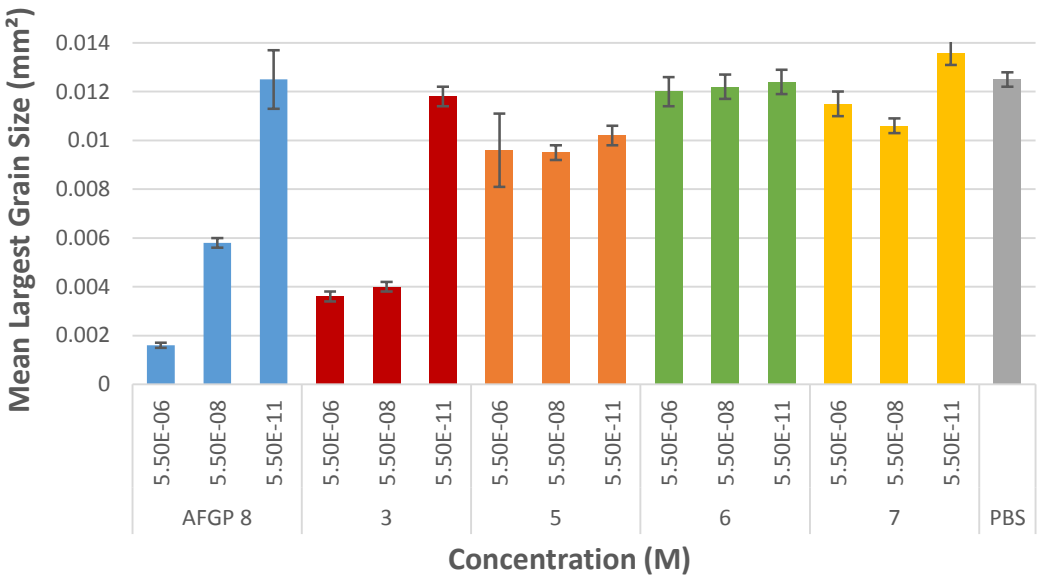

Graph 1.3: IRI Activities of *C*-AFGP analogues (**3**, **5-7**) in comparison with AFGP-8 (positive control) and phosphate-buffered saline (negative control). Errors bars indicate standard error of the mean (SEM).[117]

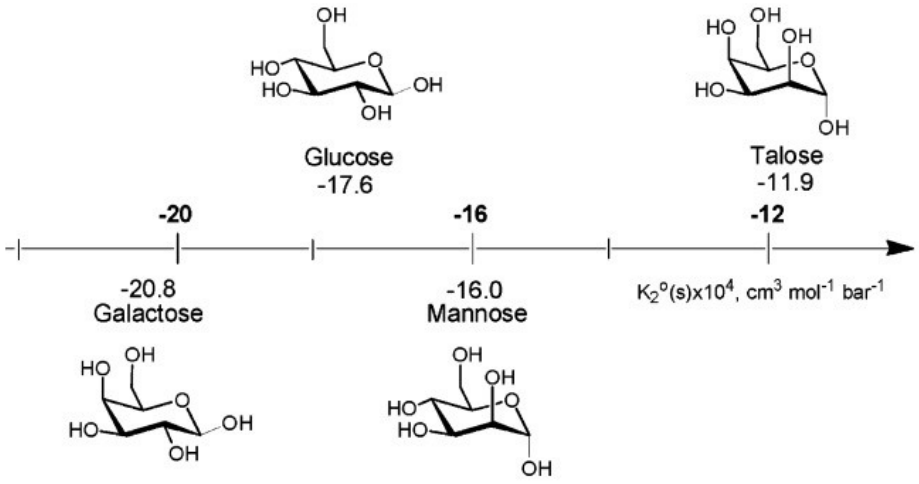

Figure 1.12: Calculated partial molar compressibility values for galactose (**8**), glucose (**9**), mannose (**10**), and talose (**11**) in aqueous solution at 298°C. Values are representative of the dominant conformer of each monosaccharide.[117]

The intriguing relationship between the hydration of monosaccharides and their IRI ability led Tam *et al.* to examine whether this correlation extended to disaccharides.[48] Five disaccharides with previously-reported hydration values were therefore assessed for IRI ability: D-melibiose (**12**), D-Lactose

(**13**), D-trehalose (**14**), D-maltose (**15**), and D-sucrose (**16**). Table 1.3 depicts the molar compressibility, hydration number and partial molar volume of monosaccharides (**8-11**) and disaccharides (**12-16**).[48,117-119]

Table 1.3: Calculated molar compressibility ($10^4K_2°(s)$, $cm^3\ mol^{-1}\ bar^{-1}$), hydration number and partial molar volume (cm^3) of selected monosaccharides and disaccharides. [117-119]

Carbohydrate	Molar Compressibility ($K_2^O(s)$ x $10^4cm^3mol^{-1}bar^{-1}$)	Hydration Number (0.1)	Partial Molar Volume (cm^3)	Carbohydrate	Molar Compressibility ($K_2^O(s)$ x $10^4cm^3mol^{-1}bar^{-1}$)	Hydration Number (0.1)	Partial Molar Volume (cm^3)
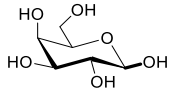 D-Galactose (**8**)	-20.8 ± 0.5 -20.4 ± 0.4	8.7	110.2 ± 0.3	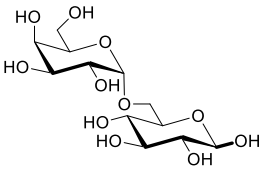 D-Melibiose (**12**)	-30.2 ± 0.3	15.5	204.0 ± 0.2
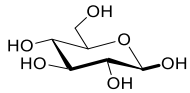 D-Glucose (**9**)	-17.6 ± 0.3	8.4	111.7 ± 0.3	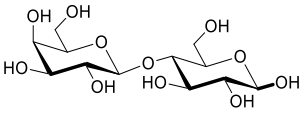 D-Lactose (**13**)	-31.1 ± 0.2 -30.4 ± 1.0	15.3	207.6 ± 0.2
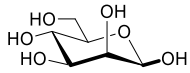 D-Mannose (**10**)	-16.0 ± 0.5	8.1	111.3 ± 0.2	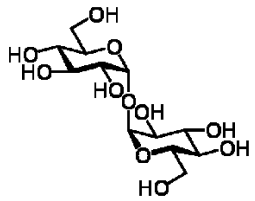 D-Trehalose (**14**)	-30.2 ± 0.3	15.3	206.9 ± 0.5
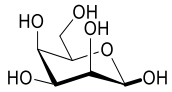 D-Talose (**11**)	-11.9 ± 0.3	7.7	112.5 ± 0.1	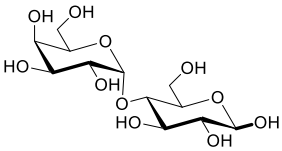 D-Maltose (**15**)	-23.7 ± 1.0	14.5	208.8 ± 0.3
				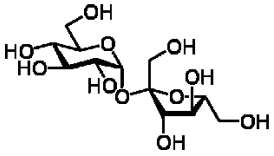 D-Sucrose (**16**)	-17.8 ± 0.5	13.9	210.2 ± 0.3

The hydration number of a compound represents the number of water molecules which are tightly bound to it in the first hydration shell.[118] This differs from the partial molar compressibility values, which take into account the first two hydration shells surrounding the molecule of interest.[118] Thus, hydration numbers are viewed as a somewhat more precise representation of the number of water molecules interacting with the solute in its immediate vicinity.[118,119] Partial molar volumes are also shown in Table 1.3, which describe the volume of the carbohydrate and its first hydration shell.[118,119] Graph 1.4 depicts the IRI activity at 22 mM concentration of the monosaccharides (**8-11**) and disaccharides (**12-16**) as a function of their calculated hydration numbers.[48]

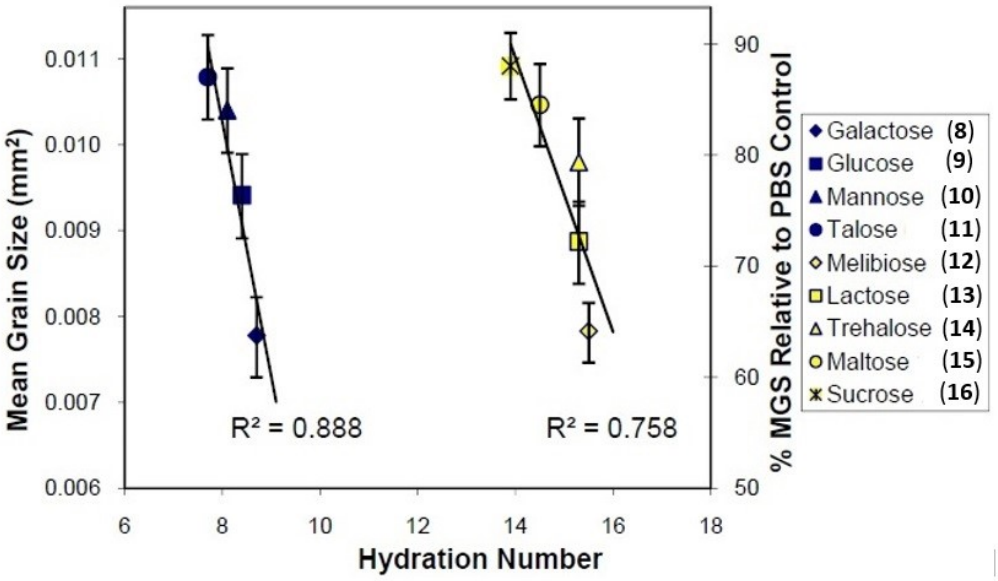

Graph 1.4: IRI activity of monosaccharides (**8-11**) and disaccharides (**12-16**) at 22 mM concentration plotted against their calculated hydration numbers.[48,118,119]

From the graph, it is evident that the disaccharides evaluated possess a similar correlation between degree of recrystallization inhibition and hydration number; as the hydration of the carbohydrates increase, so too does their IRI activity.[48] However, instead of one continuous trend, there are two distinct linear correlations for the monosaccharides and disaccharides which do not match with each other. The IRI of galactose and melibiose were found to be statistically identical despite a

substantial difference in hydration number (8.7 *vs*. 15.5, respectively). Additionally, the IRI activity of sucrose was substantially less than that of galactose even though it has a higher hydration number (13.9 *vs*. 8.7). This experiment suggested that the IRI activities of monosaccharides cannot be compared with disaccharides using hydration number alone.[48]

Tam *et al.* hypothesized that the difference in molecular weight between monosaccharides and disaccharides may also play a role in governing their net IRI activities.[48] To overcome this, the authors divided the hydration numbers of the carbohydrates by their partial molar volume. This provided hydration values which accounted for the difference in steric volumes between the monosaccharides and disaccharides, similar to the approach used in an unrelated experiment by Parke *et al.* comparing the taste properties of carbohydrates per unit volume of solute.[120] Tam and co-workers described these values as the *hydration index*.[48] By plotting the IRI activities of the nine carbohydrates vs their hydration index, a single linear correlation emerges (Graph 1.5). This demonstrates the usefulness of the hydration index method in explaining the IRI activity of carbohydrates by taking into consideration the difference in their molar volumes. While this method has yet to be applied to other substituted and non-substituted carbohydrates, it offers useful insight into the properties which govern the IRI activities of these compounds.

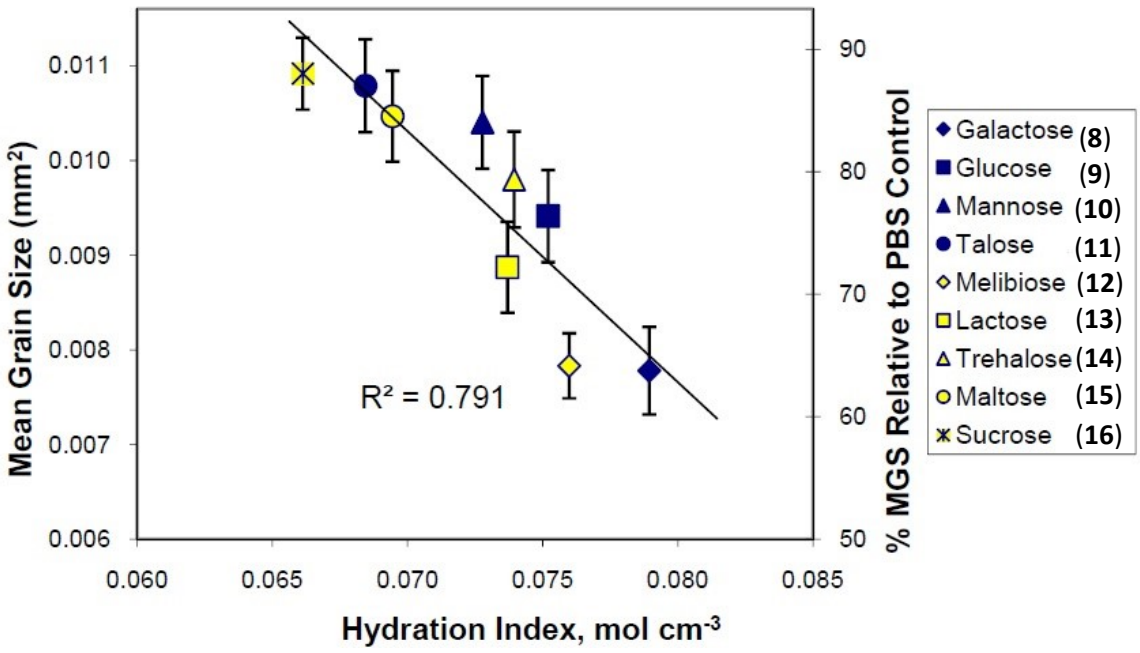

Graph 1.5: IRI activities of carbohydrates (**8-16**) at 22 mM concentration as a function of hydration index (hydration number divided by partial molar volume, $mol^{-1}\,cm^{-3}$).[48]

The discovery of the link between hydration and IRI activity in carbohydrates offers clues into the mechanism by which these compounds inhibit ice recrystallization.[48] As aqueous solutions are cooled below their freezing point, the formation of hydrogen bonds between water molecules becomes less reversible.[121] Eventually the water molecules begin to arrange themselves into an ordered ice lattice. Between the liquid water molecules and the newly-formed ice crystals there is believed to exist a nanometer-thick layer of water in a semi-ordered state.[122,123] This interface between the solid and liquid states is referred to as the quasi-liquid layer (QLL), through which a molecule of water must first pass before being added to a growing ice crystal.[122,123] Since small-molecule inhibitors of ice recrystallization generally do not possess TH activity, it is believed that they do not bind to ice in order to operate as compounds possessing TH activity do. Instead, it is more logical that these compounds are interacting with water molecules in the QLL.[117]

It has been hypothesized by the Ben Lab that the hydration of carbohydrates is important for ice recrystallization inhibition activity because of their tendency to disrupt the ordering of surrounding bulk water in solution (Figure 1.13).[48,117] Since carbohydrates are capable of tightly binding with water molecules around them, the three dimensional network of remaining water molecules in the first hydration shell is altered from its native form. By extension, this will disrupt the bulk water layer from forming the semi-ordered arrangement required to enter the QLL before they join with the ice lattice.[48,117] As a result, more energy is required for the water molecules to organize themselves into the proper structure, slowing the process of ice recrystallization. This hypothesis would explain why the poor "fit" of galactose-based compounds in solution results in higher IRI values.

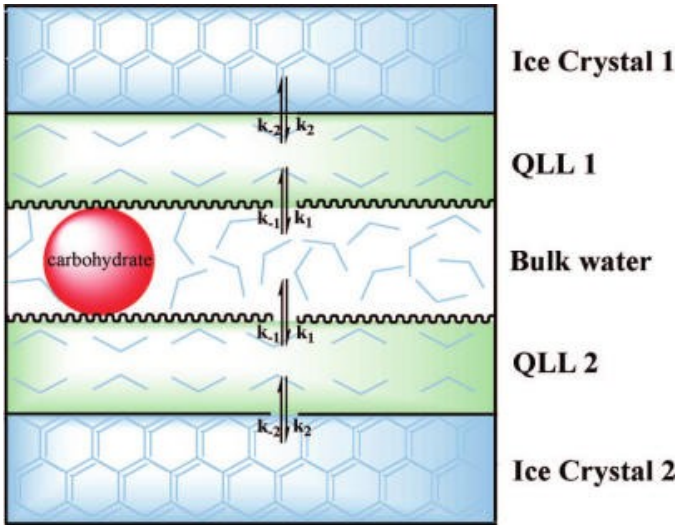

Figure 1.13: Schematic representation of the ice-water interface and the possible effect of carbohydrates on ice recrystallization. Bulk water interacting with the carbohydrate is unable to order itself into a quasi-liquid layer (QLL) before adding to the growing ice lattice.[48,117]

1.4.3 Potent Small-Molecule Inhibitors of Ice Recrystallization

The discovery that simple carbohydrates possess moderate ice recrystallization inhibition activity was significant because it was the first time that an antifreeze property had been demonstrated in small molecules. Although the IRI activity of these compounds was much lower than that of AFGP 8 and *C*-AFGP analogues (**3**,**4**), further research demonstrated that potent IRI activity can be obtained from small-molecule carbohydrate derivatives. Capicciotti *et al.* have assessed the IRI ability of carbohydrate-based non-ionic surfactants (**17**, **18**), alditols (**19, 20**) and hydrogelators (**21**, **22**) at low-milimolar concentrations (Figure 1.14).[124] It was found that *n*-octyl-β-D-galactopyranoside (**18**) displayed potent IRI activity in a concentration-dependent manner, while *n*-octyl-β-D-glucopyranoside (**17**) showed very little IRI activity (Graph 1.6).[124] This result was in agreement with previous studies in which galactose-based carbohydrate derivatives had been shown to possess higher IRI activity than glucose-based derivatives, possibly due to the overall hydration of the molecule.[48,117] It was noted that IRI activity was present in (**18**) at concentrations below the critical micelle concentration (CMC) of the surfactant, which indicates that micelle formation is not a requirement for IRI activity.[124]

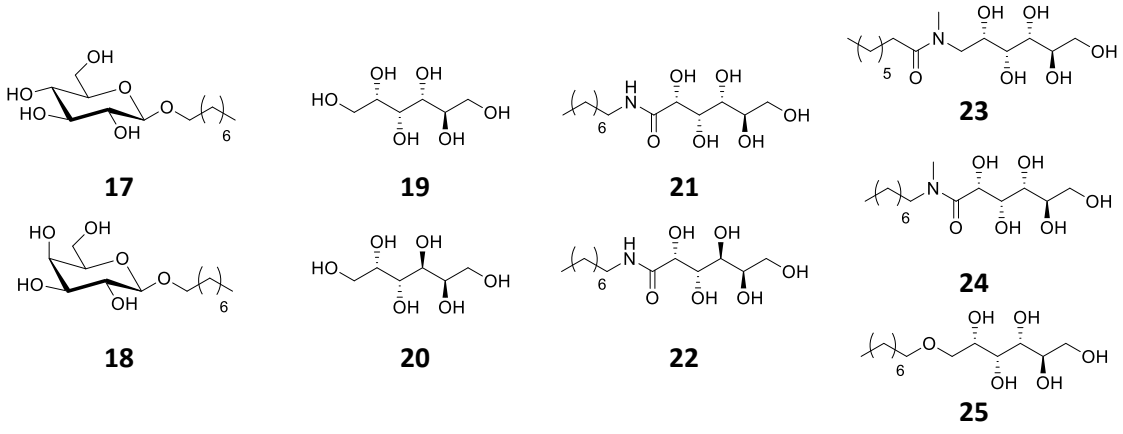

Figure 1.14: Carbohydrate-based surfactants, hydrogelators and related derivatives synthesized and assessed for IRI activity by Capicciotti *et al.*[124]

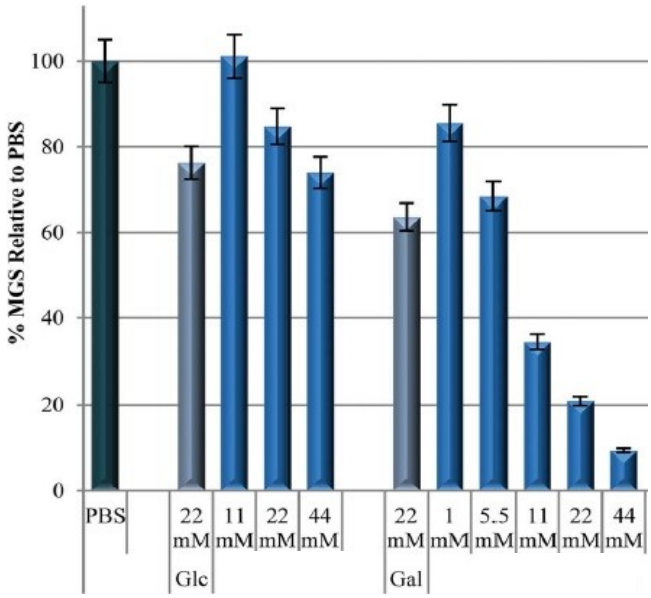

Graph 1.6: IRI Activities of *n*-octyl-β-D-glucopyranoside (**17**) and *n*-octyl-β-D-galactopyranoside (**18**) compared with their corresponding free reducing sugars.[124]

Open-chain sugars sorbitol (**19**) and dulcitol (**20**) had only weak IRI abilities. However, surprising results were obtained with their *N*-octylaldonamide derivatives. Very potent IRI activity was observed in *N*-octyl-D-gluconamide (**21**) even at concentrations as low as 0.5 mM, while *N*-octyl-D-galactonamide (**22**) showed poor activity at the same concentration. This was the first time a glucose-based compound was shown to possess higher IRI activity than the corresponding galactose epimer. To examine the importance of hydrogen bond donation in the amide linkage of (**21**), *N*-methylated derivatives (**23**) and (**24**) were synthesized and tested. In both cases a significant loss of IRI activity resulted, suggesting that the amide N-H bond is important for the potent IRI activity of (**21**), possibly due to hydrogen bonding interactions. An ether-linked analogue of *N*-octyl-D-gluconamide (**25**) was also found to have reduced IRI activity, further supporting the importance of the amide group. Based on the results from this series, it was concluded that hydrogelation ability is not tied to IRI activity since both (**21**) and (**22**) are hydrogelators but displayed substantially different IRI activities.[124]

Recent investigations of other classes of small molecules suggests that IRI activity is not limited to carbohydrate derivatives. Balcerzak and colleagues synthesized a variety of lysine-based surfactants, hydrogelators and anti-ice nucleating agents (INAs) to assess their effectiveness as ice recrystallization inhibitors.[125] The anti-INA activity of quaternary ammonium surfactants (Figure 1.15A) were found to be independent of their IRI activity; despite the fact that all compounds in the series were known anti-INA agents, the observed IRI activities of the compounds was highly variable.[125] Interestingly, very potent IRI activity was obtained from lysine-based surfactants (Figure 1.15B) with long alkyl chains at the *C*-terminus. A similar effect was seen with lysine-based hydrogellators (Figure 1.15C) whereby increasing hydrophobic character resulted in increasing IRI activity, although this trend was dependent on the site of alkylation and there was a limit to the length of hydrocarbon chain tolerated. It was also noted that hydrogellation ability of these was not connected with their IRI activities, consistent with the observations of Capicciotti *et al.* in *N*-octyl-aldonamide hydrogelators.[124,125]

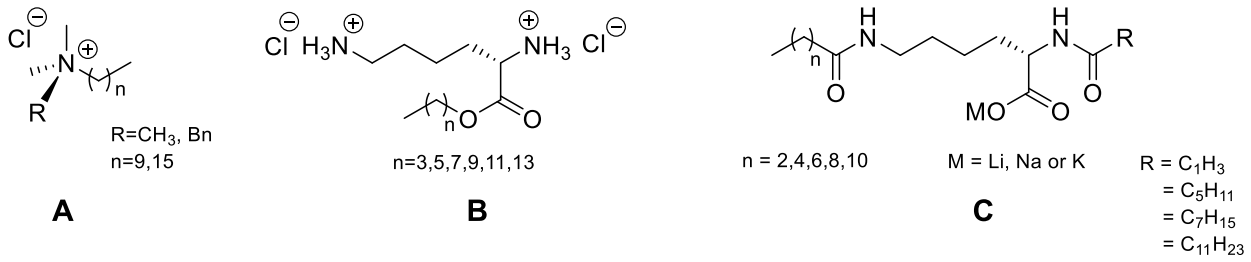

Figure 1.15: General structures of cationic anti-INAs (**A**), lysine surfactants (**B**), and lysine-based hydrogelators (**C**) assessed for IRI activity by Balcerzak *et al.*[125]

1.5 Towards the Rational Design of Small-Molecule Cryoprotectants

While *C*-linked AFGP analogues such as (**3**) have been shown to possess promising cryoprotective abilities, there a numerous drawbacks associated with the development of these compounds as cryoprotectants.[112,126] One major barrier to their use is the difficulty associated with

accessing large quantities of glycoproteins. Automated methods for the synthesis of glycoproteins have not yet been developed to the same extent as those used to produce nucleic acids or proteins, meaning that custom-designed synthetic routes using traditional approaches are instead required.[112] Although some progress has been made in this area in the past several decades, the synthesis of glycoconjugates remains a formidable challenge due the large size and structural complexity of glycoconjugates, combined with the need for selective protection of carbohydrate hydroxyl groups possessing similar reactivity.[112,126] This makes for a laborious and expensive process with generally poor overall yields which is likely not feasible for production on an industrial scale.

In contrast, small-molecule ice recrystallization inhibitors represent a more viable alternative to large glycoconjugates as cryoprotectants for a number of reasons. From a synthetic standpoint, they can generally be produced in a more efficient manner since they possess simpler structures and fewer steps are required to make them. Secondly, small molecules tend to possess more "drug-like" properties in terms of cell permeability and are more capable of crossing plasma membranes than macromolecules. Another advantage of small molecules is that less amount of compound is required on a per-mass basis than a glycoprotein at the same molar concentration, which results in further cost-effectiveness. The combination of these factors makes low-molecular weight cryoprotectants much more attractive from a commercial and economic standpoint than large glycoconjugates.

The discovery that ice recrystallization inhibition activity can be conferred by various classes of small-molecules opens the door to many new possibilites of in the search for alternative CPAs.[124,125] However, without adequate knowledge of the mechanism or structural features required for IRI activity, this search remains a daunting task. Unlike in medicinal chemistry, there are no facilities which are equipped for high-throughput screening of IRI activity. As such, a random approach towards identifying lead compounds would be enormously time-consuming and inefficient. However, with a better understanding of the processes which prevent ice recrystallization, the rational design of specific CPA

candidates becomes a possibility. Such information would streamline efforts towards an effective and non-toxic replacement for DMSO.

In native AFGPs, both hydrogen bond donation from the carbohydrate unit as well as hydrophobic components of the peptide backbone are believed to contribute to their antifreeze activity. Whether one or both of these properties is responsible for ice recrystallization inhibition in small molecules remains to be conclusively established. Hence, a systematic evaluation of each of these phenomena in small molecules is warranted in order to obtain a better understanding of their mode of action at the ice-water interface. With this information in hand, the development of novel cryoprotectants can proceed in a rational and more efficient manner. These goals form the basis of the present study and are described in greater detail in the following chapter.

References

1. Mazur, P., Cryobiology: The Freezing of Biological Systems. *Science **1970**, 168, 939-949.*

2. Polge, C.; Smith, A.V.; Parkes, A.S., Revival of spermatozoa after vitrification and dehydration at low temperatures. Nature **1949**, 164, 666.

3. Gosden, R. G.; Picton, H. M.; Nugent, D.; Rutherford, A. J., Gonadal tissue cryopreservation: clinical objectives and practical prospects. *Human Fertility* **1992**, 2, 107-114.

4. Loken, S. D.; Demetrick, D. J., A novel method for freezing and storing research tissue bank specimens. *Human Pathology* **2005**, 36, 977-980.

5. Can, A.; Karahuseyinoglu, S., Concise Review: Human umbilical cord stroma with regard to the source of fetus-derived stem cells. *Stem Cells* **2007**, 25, 2886-2895.

6. Wallis, J. G.; Wang, H.; Guerra, D. J., Expression of a synthetic antifreeze protein in potato reduces electrolyte release at freezing temperatures. *Plant Mol. Biol.* **1997**, 35, 323-354.

7. Griffith, M.; Ewart, K. V., Antifreeze proteins and their potential use in frozen foods. *Biotech. Adv.* **1995**, 13, 375-403.

8. Mazur, P., The role of cell membranes in the freezing of yeast and other single cells. *Ann. N. Y. Acad. Sci.* **1965**, 125, 658-676.

9. Lovelock, J. E., The haemolysis of human red blood-cells by freezing and thawing. *Biochim. Biophys. Acta.* **1953**, 10, 414.

10. Meryman, H. T.; Williams, R. J.; Douglas, M. S., Freezing injury from "solution effects" and its prevention by natural or artificial cryoprotection. *Cryobiology* **1977**, 14, 287-302.

11. Lovelock, J. E., The mechanism of the protective action of glycerol against haemolysis by freezing and thawing. *Biochim. Biophys. Acta.* **1953**, 11, 28.

12. McNiven, M. A.; Gallant, R. K.; Richardson, G. F., Dimethyl-Acetamide as a Cryoprotectant for Rainbow Trout Spermatozoa. *Theriogenology* **1993**, 40, 943-948.

13. Chen, F. *et al.,* Cryopreservation of tissue-engineered epithelial sheets in trehalose. *Biomaterials* **2011**, 32, 8426-8435.

14. Stolzing, A.; Naaldiijk, Y.; Fedorova, V.; Sethe, S., Hydroxyethylstarch in cryopreservation – Mechanisms, benefits and problems. *Transfus. Apher. Sci.* **2012**, 46, 137-147.

15. McGann, L. E., Differing Actions of Penetrating and Nonpenetrating Cryoprotective Agents. *Cryobiology* **1978**, 15, 382-390.

16. Doebbler, G. F.; Rinfret, A. P., The influence of protective compounds and cooling and warming conditions on hemolysis of erythrocytes by freezing and thawing. *Biochim. Biophys. Acta* **1962**, 58, 449-458.

17. Davis, J. M.; Rowley, S. D.; Braine, H. G.; Piantadosi, S.; Santos, G. W., Clinical toxicity of cryopreserved bone marrow graft infusion. *Blood* **1990**, 75, 781-786.

18. Elmoazzen, H. Y.; Poovadan, A.; Law, G. K.; Elliott, J. A. W.; McGann, L. E.; Jomha, N. M., Dimethyl sulfoxide toxicity kinetics in intact articular cartilage. *Cell Tissue Bank* **2007**, 8, 125-133.

19. Liseth, K.; Abrahamsen, J. F.; Bjorsvik, S.; Grottebo, K.; Bruserud, O., The viability of cryopreserved PBPC depends on the DMSO concentration and the concentration of nucleated cells in the graft. *Cytotherapy* **2005**, 7, 328-333.

20. Anchordoguy, T. J.; Cecchini, C. A.; Crowe, J. H.; Crowe, L. M., Insights into the cryoprotective mechanism of dimethyl sulfoxide for phospholipid bilayers. *Cryobiology* **1991**, 28, 467-473.

21. Kuleshova, L. L.; Shaw, J. M.; Trounson, A. O., Studies on Replacing Most of the Penetrating Cryoprotectant by Polymers for Embryo Cryopreservation. *Cryobiology* **2001**, 43, 21-31.

22. Wang, J.-H., A Comprehensive Evaluation of the Effects and Mechanisms of Antifreeze Proteins during Low-Temperature Preservation. *Cryobiology* **2000**, 41, 1-9.

23. Eniade A.; Hauer, L.; Ben, R.N., Synthesis of a C-linked antifreeze glycoprotein (AFGP) mimic: Probes for investigating the mechanism of action. *Org. Lett.* **1999**, 1, 1759-1762.

24. Davies, P. L.; Hew, C. L., Biochemistry of fish antifreeze proteins. *FASEB J.* **1990**, 4, 2460-2468.

25. Capicciotti, C. J.; Doshi, M.; Ben, R. N., Ice Recrystallization Inhibitors: From Biological Antifreezes to Small Molecules. *Recent Developments in the Study of Recrystallization*, Peter Wilson (Ed.), Intech **2013**, 177-224.

26. Gao, D.; Critser, J. K., Mechanisms of Cryoinjury in Living Cells. *ILAR J.* **2000**, 41, 187-196.

27. Mazur, P.; Farrant, J.; Leibo, S. P.; Chu, E. H. Y., Survival of hamster tissue culture cells after freezing and thawing: Interactions between protective solutes and cooling and warming rates. *Cryobiology* **1969**, 6, 1-9.

28. Merryman, H. T., Osmotic stress as a mechanism of freezing injury. *Cryobiology* **1971**, 8, 489-500.

29. Tonino, G. J. M.; Steyn-Parve, E. P., Localization of some phosphatases in yeast. *Biochim. Biophys. Acta* **1963**, 67, 453.

30. Toner, M.; Karel, M.; Cravalho, E., Thermodynamics and kinetics of intracellular ice formation during freezing of biological cells. *J. Appl.Phys*. **1990**, 67, 1582-1593.

31. Muldrew, K.; McGann, L. E., Mechanisms of intracellular ice formation. *Biophys. J.* **1990**, 57, 525-532.

32. Mazur, P., The role of intracellular freezing in the death of cells cooled at supraoptimal rates. *Cryobiology* **1977**, 14, 251-272.

33. Salt, R. W., Survival of Frozen Fat Body Cells in an Insect. *Nature* **1959**, 184, 1426-1427.

34. Tomczak, M. M.; Marshall, C. B.; Gilbert, J. A.; Davies, P. L., A facile method for determining ice recrystallization inhibition by antifreeze proteins. *Biochem. Biophys. Res. Commun.* **2003**, 311, 1041-1046.

35. Kingery, W. D., Regelation, surface diffusion, and ice sintering. *J. Appl. Phys.* **1960**, 31, 833-838.

36. Chaytor, J. L. *et al.*, Inhibiting ice recrystallization and optimization of cell viability after cryopreservation. *Glycobiology* **2012**, 22, 123-133.

37. Fuller, B. J., Cryoprotectants: The essential antifreezes to protect life in the frozen state. *CryoLetters* **2004**, 25, 375-388.

38. Lovelock, J. E.; Bishop, M. W. H., Prevention of Freezing Damage to Living Cells by Dimethyl Sulphoxide. *Nature* **1959**, 4672, 1394-1395.

39. Lovelock, J. E., The Protective Action of Neutral Solutes against Haemolysis by Freezing and Thawing. *Biochem. J*. **1954**, 56, 265-270.

40. Notman, R.; Noro, M.; O'Malley, B.; Anwar, J., Molecular Basis for Dimethylsulfoxide (DMSO) Action on Lipid Membranes. *J. Am. Chem. Soc.* **2006**, 128, 13982-13983.

41. Gurtovenko, A. A.; Anwar, J., Modulating the Structure and Properties of Cell Membranes: The Molecular Mechanism of Action of Dimethyl Sulfoxide. *J. Phys. Chem. B*, **2007**, 111, 10453-10460.

42. O'Neil, L.; Paynter, S. J.; Fuller, B. J.; Shaw, R. W., Vitrification of Mature Mouse Oocytes: Improved Results Following Addition of Polyethylene Glycol to a Dimethyl Sulfoxide Solution. *Cryobiology* **1997**, 34, 295-301.

43. Thirumala, S.; Wu, X.; Gimble, J. M.; Devireddy, R. V., Evaluation of Polyvinylpyrrolidone as a Cryoprotectant for Adipose Tissue-Derived Adult Stem Cells. *Tissue Eng. Part C*, **2010**, 16, 783-792.

44. Takahashi, T.; Hirsh, A.; Erbe, E.; Williams, R. J., Mechanism of Cryoprotection by Extracellular Polymeric Solutes. *Biophys J.* **1988**, 54, 509-518.

45. Farrant, J., Is there a common mechanism of protection of living cells by polyvinylpyrrolidone and glycerol during freezing? *Nature* **1969**, 222, 1175-1176.

46. Smorag, Z.; Heyman, Y.; Garnier, V.; Gajda, B., The effect of sucrose and trehalose on viability of one- and two-cell rabbit embryos. *Theriogenology* **1990**, 33, 741-747.

47. Sei, T.; Gonda, T.; Arima, Y., Growth rate and morphology of ice crystals growing in a solution of trehalose and water. *J.Cryst. Growth* **2002**,240, 218-229.

48. Tam R.Y.; Ferreira, S. S.; Czechura, P.; Chaytor, J. L.; Ben, R. N., Hydration Index – A Better Parameter for Explaining Small Molecule Hydration in Inhibition of Ice Recrystallization. *J. Am. Chem. Soc.* **2008**, 130, 17494–17501.

49. Kawamoto, J. C.; Barrett, J. N., Cryopreservation of Primary Neurons for Tissue Culture. *Brain Res.* **1986**, 384, 84-93.

50. Calamera, J. C. *et al.*, Effect of thawing temperature on the motility recovery of cryopreserved human spermatozoa. *Fertility and Sterility* **2010**, 93, 789-794.

51. Gearhart, J.; Coutifaris, C., *In Vitro* Fertilization, the Nobel Prize, and Human Embryonic Stem Cells. *Cell Stem Cell* **2011**, 8, 12-15.

52. Ginsburg, E. S.; Yanushpolsky, E. H.; Jackson, K. V., *In vitro* fertilization for cancer patients and survivors. *Fertility and Sterility* **2001**, 75, 705-710.

53. Donnez, J.; *et al.*, Livebirth after orthotopic transplantation of cryopreserved ovarian tissue. *The Lancet* **2004**, 364, 1405-1410.

54. Pal, R.; Mamidi, M. K.; Das, A. K.; Bhonde, R., Diverse effects of dimethyl sulfoxide (DMSO) on the differentiation potential of human embryonic stem cells.

55. Quevedo, H. C. *et al.*, Allogeneic mesenchymal stem cells restore cardiac function in chronic ischemic cardiomyopathy via trilineage differentiating capacity. *Proc. Natl. Acad. Sci. USA* **2009**, 106, 14022-14027.

56. Berz, D.; McCormack, E. M.; Winer, E. S. Colvin, G. A.; Quesenberry, P. J., Cryopreservation of Hematopoietic Stem Cells. *Am. J. Hematol.* **2007**, 82, 463-472.

57. Martino, M.; Morabito, F.; Messina, G.; Irrera, G.; Pucci, G.; Iacopino, P., Fractionated infusions of cryopreserved stem cells may prevent DMSO-induced major cardiac complications in graft recipients. *Haematologica* **1996**, 81, 59-61.

58. Syme, R.; Bewick, M.; Stewart, D.; Porter, K.; Chadderton, T.; Glück, S., The Role of Depletion of Dimethyl Sulfoxide before Autografting: On Hematologic Recovery, Side Effects, and Toxicity. *Biol. Blood Marrow Transplant.* **2004**, 10, 135-141.

59. Duman, J. G.; DeVries, A. L., The Role of Macromolecular Antifreezes in Cold Water Fishes. *Comparative Biochemistry and Physiology Part A: Physiology* **1975**, 52, 193-199.

60. Yeh, Y.; Feeney, R.E., Antifreeze proteins: structures and mechanism of action. *Chem. Rev.* **1996**, 96, 601-617.

61. Scholander, P. F.; Van Dam, L.; Kanwisher, J. W.; Hammel, H. T.; Gordon, M. S., Supercooling and osmoregulation in Arctic fish. *J. Cell Com. Physiol.* **1957**, 49, 5-24.

62. Chen, L. B.; DeVries, A. L.; Cheng, C. H. C., Convergent Evolution of antifreeze glycoproteins in Antartic notothenoid fish and Arctic cod. *Proc. Natl. Acad. Sci. USA*. **1997**, 94, 3811-3816.

63. Feeney, R. E.; Hofmann, R., Depression of freezing point by glycoproteins from an Antarctic fish. *Nature (London)* **1973**, 243, 237-238.

64. Scholander, P.F.; Maggert, J. E., Supercooling and ice propagation in blood from Arctic fishes. *Cryobiology* **1971**, 8, 371-374.

65. Davies, P. L.; Sykes, B. D., Antifreeze Proteins. *Curr. Opin. Struct. Biol.* **1997**, 7, 828-834.

66. Harding, M. M.; Anderberg, P. I.; Haymet, A. D. J., 'Antifreeze' glycoproteins from polar fish. *Eur. J. Biochem.* **2003**, 270, 1381–1392.

67. Tseng, P.-H.; Jiaang, W.-T.; Chang, M.-Y.; Chen, S.-T., Facile Solid-Phase Synthesis of an Antifreeze Glycoprotein. *Chem. Eur. J.* **2001**, 7, 585-590.

68. Komatsu, S. K.; DeVries, A. L.; Feeney, R. E., Studies of the structure of freezing point-depressing glycoproteins from an Antarctic fish. *J. Biol. Chem.* **1970**, 245, 2909-2913.

69. Morris, H. R.; Thompson, M. R.; Osuga, D. T.; Ahmed, A. I.; Chan, S. M.; Vandenheede, J. R.; Feeney, R. E., Antifreeze Glycoproteins from the Blood of an Antarctic Fish: The Structure of the Proline-Containing Glycopeptides. *J. Biol. Chem.* **1978**, 253, 5155-5162.

70. Burcham, T. S.; Osuga, D. T.; Rao, B. N. N.; Bush, C. A.; Feeney, R. E., Purification and Primary Sequences of the Major Arginine-containing Antifreeze Glycopeptides from the Fish *Eleginus gracilis. J. Biol. Chem.* **1986**, 261, 6384-6389.

71. Hew, C. L.; Slaughter, D.; Fletcher, G. L.; Joshi, S., Antifreeze glycoproteins in the plasma of Newfoundland Atlantic cod (*Gadus morhua*). *Can. J. Zool*. **1981**, 60, 348-355.

72. Rubinsky, B.; Arav, A.; DeVries, A. L., The cryoprotective effect of antifreeze glycopeptides from Antarctic fishes. *Cryobiology* **1992**, 29, 69-79.

73. Pham, L.; Dahiya, R.; Rubinsky, B., An *in vivo* study of antifreeze protein adjuvant cryosurgery. *Cryosurgery* **1999**, 38, 169-175.

74. Griffith, M.; Ewart, K. V., Antifreeze proteins and their potential use in frozen foods. *Biotech. Adv*. **1995**, 13, 375-403.

75. Wallis, J. G.; Wang, H.; Guerra, D. J., Expression of a synthetic antifreeze protein in potato reduces electrolyte release at freezing temperatures. *Plant Mol. Biol*. **1997**, 35, 323-354.

76. Vandenheede, J. R.; Ahmed, A.I.; Feeney, R. E., Structure and role of carbohydrate in freezing point-depressing glycoproteins from an Antarctic fish. *J. Biol. Chem.* **1972**, 247, 7885–7889.

77. Burcham, T. S.; Knauf, M. J.; Osuga, D.T.; Feeney, R.E.; Yeh, Y., Antifreeze glycoproteins: Influence of polymer length and ice crystal habit on activity. *Biopolymers* **1984**, 23, 1379–1395.

78. Tachibana, Y.; Fletcher, G. L.; Fujitani, N.; Tsuda, S.; Monde, K.; Nishimura, S., Antifreeze glycoproteins: Elucidation of the structural motifs that are essential for antifreeze activity. *Angew. Chem. Int. Ed.* **2004**, 43, 856-862.

79. Brown, R. A.; Yeh, Y.; Burcham, T. S.; Feeney, R. E., Direct Evidence for Antifreeze Glycoprotein Adsorption onto an Ice Surface. *Biopolymers* **1985**, 24, 1265-1270.

80. Kuiper, M. J.; Lankin, C.; Gauthier, S. Y.; Walker, V. K.; Davies, P. L., Purification of antifreeze proteins by absorption to ice. *Biochem. Biophys. Res. Comm.* **2003**, 300, 645-648.

81. DeVries, A. L.; Komatsu, S. K.; Feeney, R. E., Chemical and Physical Properties of Freezing Point-Depressing Glycoproteins from Antarctic fish. *J. Biol. Chem*. **1970**, 245, 2901-2908.

82. Gibson, M.I., Slowing the Growth of Ice with Synthetic Macromolecules: Beyond Antifreeze(glyco) Proteins. *Polymer Chemistry* **2010**, 1141-1152.

83. Wilson, P. W.; Leader, J. P., Stabilization of supercooled fluids by thermal hysteresis proteins. *Biophys. J*. **1995**, 68, 2098-2107.

84. Hall, D. G.; Lips, A., Phenomenology and Mechanism of Antifreeze Peptide Activity. *Langmuir* **1999**, 15, 1905.

85. Knight, C. A.; Cheng, C. C.; DeVries, A. L., Adsorption of a-helical antifreeze peptides on specific ice crystal surface planes. *Biophys. J.* **1991**, 59, 409-418.

86. Graham, L. A.; Yin-Cheung, L.; Walker, V. K.; Davies, P. L., Hyperactive antifreeze protein from beetles. *Nature* **1997**, 388, 727-728.

87. Venketesh, S.; Dayananda, C., Properties, Potentials and Prospects of Antifreeze Proteins. *Crit. Rev. Biotechnol.* **2008**, 19, 57-82.

88. Raymond, J.A.; Wilson, P. W.; DeVries, A.L., Inhibition of growth of non-basal planes in ice by fish antifreezes. *Proc. Natl Acad. Sci. USA* **1989**, 86, 881–885.

89. Hew, C. L.; Yang, D. C., Protein Interaction with ice. *Eur. J. Biochem*. **1992**, 203, 33-42.

90. Wilson, P. W.; Beaglehole, D.; DeVries, A. L., Antifreeze glycopeptides adsorption on single crystal ice surfaces using ellipsometry. *Biophys. J*. **1993**, 64, 1878-1884.

91. Knight, C. A.; Wen, D.; Laursen, R. A., Nonequilibrium antifreeze peptides and the recrystallization of ice. *Cryobiology* **1995**, 32, 23-34.

92. Knight, C. A.; Hallet, J.; DeVries, A. L., Solute effects on ice recrystallization: An assessment technique. *Cryobiology* **1988**, 25, 55-60.

93. Larese, A.; Acker, J.; Muldrew, K.; Yang, H. Y.; McGann, L., Antifreeze protein induce intracellular nucleation. *Cryo Letters* **1996**, 17, 175-182.

94. Tokarew, J., Ph.D. Dissertation, University of Ottawa, **2011**.

95. Wu, L. K.; Tokarew, J. M.; Chaytor, J. L.; von Moos, E.; Li, Y. Palii, C.; Ben, R. N.; Allan, D. S., Carbohydrate-mediated inhibition of ice recrystallization in cryopreserved human umbilical cord blood. *Carb. Res.* **2011**, 346, 86-93.

96. Leclère, M.; Kwok, B. K.; Wu, L. K.; Allan, D. S.; Ben, R. N., *C*-Linked Antifreeze Glycoprotein (*C*-AFGP) Analogues as Novel Cryoprotectants. *Bioconjugate Chem.* **2011**, 22, 1804-1810.

97. Ben, R. N., Antifreeze glycoproteins – preventing the growth of ice. *Chem. Bio. Chem.* **2001**, 2, 161-166.

98. Eniade A.; Hauer, L.; Ben, R.N., Synthesis of a C-linked antifreeze glycoprotein (AFGP) mimic: Probes for investigating the mechanism of action. *Org. Lett.* **1999**, 1, 1759-1762.

99. Eniade, A.; Purushotham. M.; Ben, R. N.; Wang, W.; Horwarth, K., A serendipitous discovery of antifreeze protein-specific activity in C-linked antifreeze glycoprotein analogs. *Cell Biochem. Biophys.* **2003**, 38, 115-124.

100. Liu, S.; Ben, R. C-Linked Galactosyl Serine AFGP Analogues as Potent Recrystallization Inhibitors. *Org. Lett.* **2005**, 7, 2385-2388.

101. Sidebottom, C.; Buckley, S.; Pudney, P.; Twigg, S.; Jarmann, C.; Holt, C.; Telford, J.; McArthur, A.; Worrall, D.; Hubbard, R.; Lillford, P., Phytochemistry: Heat-stable antifreeze protein from grass. *Nature* **2000**, 406, 256-257.

102. Koushafar, H.; Pham, L.; Lee, C.; Rubinsky, B., Chemical adjuvant cryosurgery with antifreeze proteins. *J. Surg. Oncol.* **1997**, 66, 114-121.

103. Rubinsky, B.; DeVries, A. L., Effect of ice crystal habit on the viability of glycerol-protected red blood cells. *Cryobiology* **1989**, 26, 580.

104. Rubinsky,B.; Arav, A.; Mattiolo, M.; DeVries, A.L., The effect of antifreeze glycopeptides on membrane potential changes at hypothermic temperatures. *Biochem. Biophys. Res. Commun.* **1990**, 173, 1369-1374.

105. Rubinsky, B.; Arav, A.; DeVries, A.L., The cryoprotective effect of antifreeze glycopeptides from Antarctic fishes. *Cryobiology* **1992**, 29, 69-79.

106. Tablin, F.; Oliver, A. E.; Walker, N. J.; Crowe, L. M.; Crowe, J. H., Membrane phase transition of intact human platelets: Correlation with cold-induced activation. *J. Cell. Physiol.* **1996**, 168, 305-313.

107. Filira, F.; Biondi, L.; Scolaro, B.; Foffani, M.T.; Mammi, S.; Peggion, E.; Rocchi, R., Solid phase synthesis and conformation of sequential glycosylated polytripeptide sequences related to antifreeze glycoproteins. *Int. J. Biol. Macromol*. **1990**, 12, 41–49.

108. Liu, S.; Wang, W.; von Moos, E.; Jackman, J.; Mealing, G.; Monette, R.; Ben, R. N., *In Vitro* Studies of Antifreeze Glycoprotein (AFGP) and a C-Linked AFGP Analogue. *Biomacromolecules* **2007**, 8, 1456-1462.

109. Burcham, T.S.; Knauf, M.J.; Osuga, D.T.; Feeney, R.E.; Yeh, Y., Antifreeze glycoproteins: Influence of polymer length and ice crystal habit on activity. *Biopolymers* **1984**, 23, 1379–1395.

110. Osuga, D.T.; Feather, M.S.; Shah, M.J.; Feeney, R.E., Modification of galactose and *N*-galactoseamine residues by oxidation of *C*-6 hydroxyls to the aldehydes followed by reductive amination: Model systems and antifreeze glycoproteins. *J. Prot. Chem*. **1989**, 8, 519–528.

111. Ahmed, A.I.; Yeh, Y.; Osuga, D.T.; Feeney, R.E., Antifreeze glycoproteins from Antarctic fish: inactivation by borate. *J. Biol. Chem.* **1976**, 251, 3033–3036.

112. Boltje, T. J.; Buskas, T.; Boons, G.-J., Opportunities and challenges in synthetic oligosaccharide and glycoconjugate research. *Nature chemistry* **2009**, 1, 611-622.

113. Sjölin, P.; Kihlberg, J., Use of Fluorobenzoyl Protective Groups in Synthesis of Glycopeptides: β-Elimination of O-Linked Carbohydrates Is Suppressed. *J.Org. Chem*. **2001**, 66, 2957-2965.

114. Marcaurelle, L. A.; Bertozzi, C. R., New Directions in the Synthesis of Glycopeptide Mimetics. *Chem. Eur. J.* **1999**, 5, 1384-1390.

115. Tam, R.Y.; Rowley, C. N.; Petrov, I.; Zhang,T.; Afagh, N. A.; Woo T. K.; Ben, R. N., Solution Conformation of C-Linked Antifreeze Glycoprotein Analogues and Modulation of Ice Recrystallization, *J. Am. Chem. Soc*. **2009**, 131, 15745-15753.

116. Petrenko, Y. A.; Jones, D. R. E.; Petrenko, A. Y., Cryopreservation of human fetal liver hematopoietic stem/progenitor cells using sucrose as an additive to the cryoprotective

medium. *Cryobiology* **2008**, 57, 195– 200.

117. Czechura, P.; Tam, R.Y.; Dimitrijevic, E; Murphy, A.V; Ben, R. N., The Importance of Hydration for Inhibiting Ice Recrystallization with C-Linked Antifreeze Glycoproteins, *J. Am. Chem. Soc.,* **2008**, 130 (10) 2928-2929.

118. Galema, S. A.; Høiland, H., Stereochemical Aspects of Hydration of Carbohydrates in Aqueous Solutions. 3. 1Density and Ultrasound Measurements*. J. Phys. Chem*. **1991**, 95, 5321.

119. Høiland, H.; Hølvik, H., Partial Molar Volumes and Compressibilities of Carbohydrates in Water. *J. Solution Chem*. **1978**, 7, 587-596.

120. Parke, S.A.; Birch, G. G,; Dijk, R., Some Taste Molecules and their Solution Properties. *Chem. Senses* **1999**, 24, 271- 279.

121. Malenkov, G., Liquid water and ices: understanding the structure and physical properties. J. *Phys.: Condens. Matter* **2009**, 21, 283101-283136.

122. Karim, O. A.; Haymet, A. D., The ice/water interface: A molecular dynamics simulation study. *J. Chem. Phys*. **1988**, 89, 6889.

123. Sadtchenko, V.; Ewing, G. E., Interfacial melting of thin ice films: An infrared study. *J. Chem. Phys.* **2002**, 116, 4686.

124. Capicciotti, C. J. *et al.*, Potent inhibition of ice recrystallization by low molecular weight carbohydrate-based surfactants and hydrogelators. *Chem. Sci.* **2012**, 3, 1408-1416.

125. Balcerzak, A. K.; Febbraro, M.; Ben, R. N., The importance of hydrophobic moieties in ice recrystallization inhibitors. *RSC Adv.* **2013**, 3, 3232-3236.

126. Davis, B. G., Synthesis of Glycoproteins. *Chem. Rev.* **2002**, 102, 579-601.

Chapter 2: Goals and Objectives

2.1 Introduction

The inherent toxicity of currently-available cryoprotectants severely limits their applications in clinical and medical settings[1-4]. Thus, there is an urgent need to develop and commercialize alternative cryoprotectants which prevent damage to biological samples due to ice formation while remaining non-toxic to cells and human patients. Identifying and optimizing candidate compounds for this purpose has been a major focus of the Ben research group over the past decade. Extensive structure-function studies of antifreeze glycoproteins and related analogues led to the discovery of IRI-active *C*-linked AFGP analogues (**3**) and (**4**), demonstrating that it is possible to develop synthetic, "custom-tailored" derivatives that possess cryoprotectant abilities without the undesirable property of thermal hysteresis (TH) found in natural AFGPs[5,6,7]. It has also been shown by our laboratory that ice recrystallization inhibition (IRI) activity correlates with improved cell viabilities after cryopreservation, a property which can be measured with relative ease to assist in the screening of compounds.[8,9]

Despite progress in this area of research, the mechanism by which certain molecules are capable of inhibiting ice recrystallization remains unclear. This makes the rational design of IRI-active compounds extremely difficult and requires time-consuming structure activity relationship studies to be carried out on compounds which are already known to inhibit recrystallization. A better understanding of this process would allow a more systematic approach to the development of novel cryoprotectants and would expedite the discovery of non-toxic alternatives to DMSO and glycerol. As previously mentioned, the IRI activity of certain carbohydrates is believed to be linked with their ability to interact strongly with the layer of bulk water which solvates the molecule in aqueous solution.[10,11] If so, disrupting or improving these interactions should produce a consistent effect on IRI activity. It was therefore decided that a study be carried out on the effects of varying non-covalent interactions, such as

hydrogen bonding and hydrophobic interactions, in carbohydrates derivatives. This will provide insight into the molecular properties which are beneficial for IRI activity and perhaps lead to a rational approach towards better cryoprotectants.

2.2 Objective 1: Examining the effect of anomeric electron density and C4 stereochemistry on the IRI activity of aryl glycosides

It has been documented that the hydration of carbohydrates in aqueous solution is influenced by the stereochemistry of the hydroxyl groups at the C2 and C4 positions.[12-14] These effects have been attributed to differences in the hydrogen-bonding abilities of the OH groups to surrounding water molecules due to steric crowding or competition from intramolecular hydrogen bonds.[12-14] Less is known about the importance of the anomeric oxygen on the hydration abilities of carbohydrates. However, Aicart *et al.* have calculated the hydration values of α and β anomers of *p*-nitrophenyl glucosides, galactosides and mannosides.[15] Their results showed that the hydration numbers depend not only on the stereochemistry at C2 and C4, but also vary significantly between the α and β anomers of each glycoside.[15] This suggests that the hydrogen-bonding abilities of the C1 oxygen may be important for hydration. Additionally, the presence of the *p*-nitrophenyl group was found to impart an increase of approximately 4 water molecules in the first hydration shell of the carbohydrates compared to previously-computed hydration values for *O*-methylglycosides.[15] In a separate study, Simons and colleagues have researched the solution conformations of singly-hydrated *O*-phenyl glycosides.[16] They report that the presence of the phenyl ring at the anomeric position allows for the insertion of a water molecule into the pyranose ring. This insertion replaces one weak intramolecular hydrogen bond with two stronger intermolecular interactions between the carbohydrate and the water molecule, producing a significant conformational change.[16]

The studies by Aicart and Simons indicate that *O*-aryl glycosides are capable of significantly influencing the interactions between a carbohydrate and its surrounding hydration shell. Since Tam and coworkers have reported that greater hydration correlates with greater IRI activity in simple carbohydrates,[10] the increased hydration numbers of the *p*-nitrophenyl glycosides studied by Aicart generates interest in these compounds as potential inhibitors of ice recrystallization. In addition, since the hydrogen-bonding properties of the anomeric oxygen may be important for IRI, the use of aryl glycosides provides a means of probing this effect. The electronic properties of a *para*-substituted aryl ring is expected to influence the electron density of the anomeric oxygen through resonance contributions. Thus, the strength of the oxygen atom as a hydrogen bond acceptor can be modulated by increasing or decreasing its basicity.

To the best of our knowledge, there have been no published reports of the effect of electron density at the anomeric centre on the hydration behaviour of carbohydrates or the impact of electron density on IRI ability. It is conceivable that increased electron density would result in stronger hydrogen bonding interactions between the anomeric oxygen and the surrounding water molecules, disrupting the ordering of bulk water and thereby slowing the incorporation of water molecules into the ice lattice (Figure 2.1A). The opposite effect could be envisioned when decreasing the electron density of the anomeric oxygen; a less basic oxygen would hypothetically form weaker hydrogen bonds, resulting in a more ordered hydration shell and a reduced capacity to inhibit ice recrystallization (Figure 2.1B). Deliberately varying the electronic properties of the carbohydrate in this fashion may provide insight into the importance of hydrogen bonding at this position and could potentially translate into an observable effect on the IRI activities of small molecule carbohydrates.

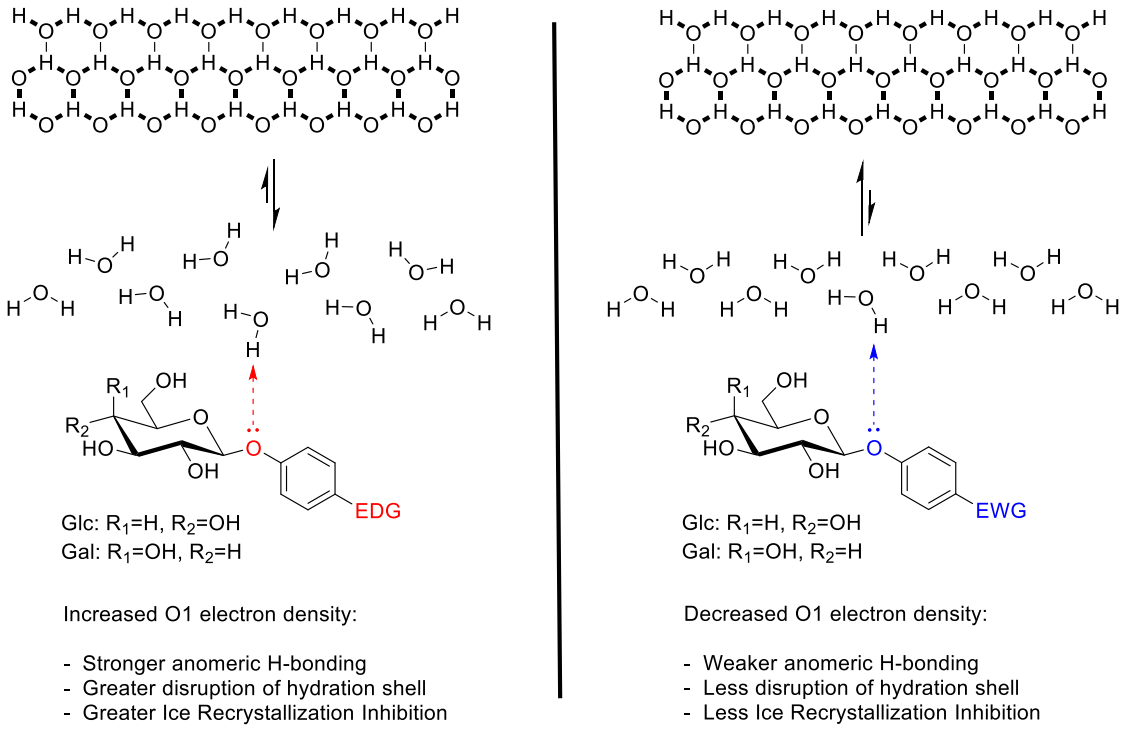

Figure 2.1: The potential hydrogen-bonding interactions of the anomeric oxygen during ice formation as influenced by electron-donating groups (**A**) and electron-withdrawing groups (**B**) on the aryl ring.

Recent work by Trant and colleagues sought to address this question by synthesizing and assessing the IRI activity of various *O*-aryl galactosides (**26-31**) outlined in Figure 2.2.[17] This class of compound is ideal for evaluating the importance of anomeric hydrogen bonding ability since the electron density of the phenolic substituent can easily be manipulated based on the presence of electron-withdrawing or electron-donating groups on the aryl ring. The IRI activities of the six mono-substituted aryl galactosides tested are summarized in Figure 2.2.

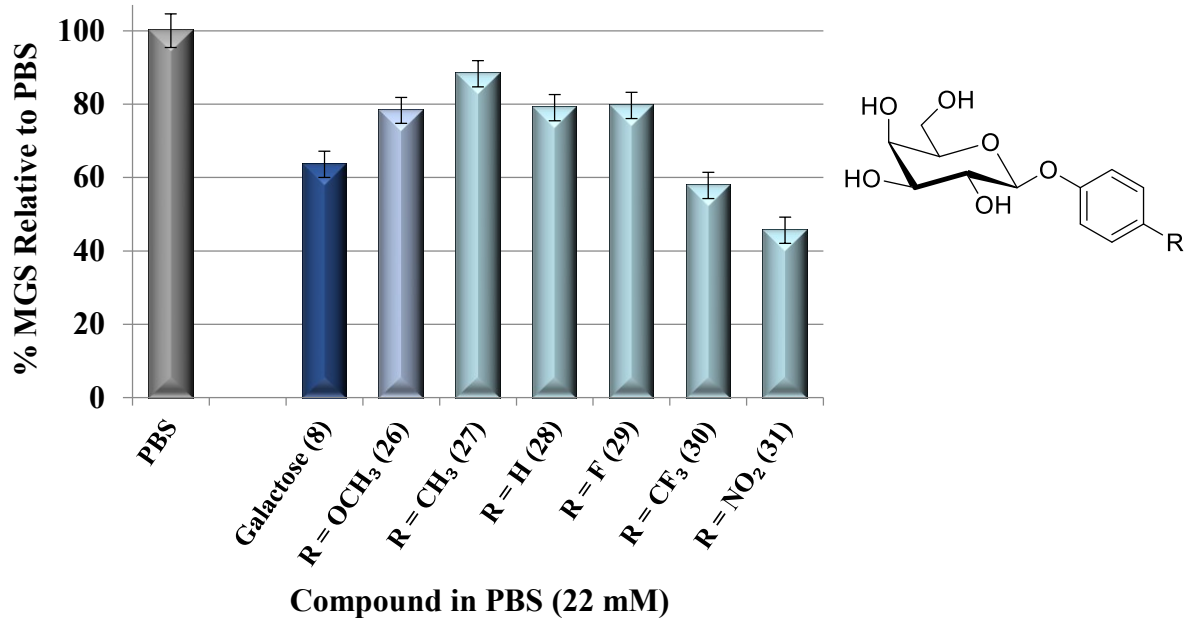

Figure 2.2: IRI activities of substituted β-*O*-aryl galactosides produced by Trant *et al.*[17]

The results obtained by Trant did not support the initial hypothesis. In fact, the opposite effect was observed: The most strongly electron-donating substituent, *p*-methoxyphenyl-β-D-galactopyranoside (**26**) displayed poorer IRI activity than galactose (**8**), suggesting the donating effect of the OCH_3 group was not beneficial for IRI ability.[17] In contrast, *p*-nitrophenyl-β-D-galactopyranoside (**31**), with strong electron-withdrawing properties, had the best IRI activity of the compounds tested.[17] A similar improvement was seen with *p*-trifluoromethylphenyl-β-D-galactopyranoside (**30**), although to a lesser extent.[17] These results questioned whether hydrogen bonding ability at the anomeric oxygen is truly important for ice recrystallization inhibition, although it was acknowledged that further studies were required in order to verify this conclusively.

Previous studies by Czechura *et al.* have linked the IRI activity of simple carbohydrates and *C*-linked AFGP derivatives to the overall hydration of the monosaccharide unit.[18] It is hypothesized that a more hydrated sugar is more capable of disrupting the 3-dimensional network of surrounding bulk

water through strong hydrogen bonding interactions, which prevents the water from organizing itself into the arrangement necessary to enter the ice lattice.[18] Thus, the initial study of aryl glycosides focused only on galactopyranose derivatives since galactose has a higher hydration number compared to glucose, mannose or talose. However, subsequent work in this area revealed that the IRI activity of *p*-methoxyphenyl-β-D-glucopyranoside (**32**) was substantially greater than its corresponding galactopyranoside (**26**).[17,19] This result was unexpected based on the hydration hypothesis and was the first example of a glucose derivative which proved more active than its galactose epimer.

In light of this discovery, Capicciotti and coworkers produced a series of analogues of **32** to determine if other aryl glucosides can display potent IRI ability (**33**-**42**) (Figure 2.3).[19] Again, there was no apparent trend based solely on the electronics of the aryl ring, as both an electron-donating methoxy group and an electron-withdrawing fluorine resulted in comparable IRI activity. The series of compounds investigated was expanded to include hydroxyl and methyl ester groups (**34**, **37**), both of which showed only moderate activity.[19] However, the halogenated derivatives *p*-chloro- and *p*-bromo-β-D-glucopyranoside (**41**, **42**) displayed very potent activity beyond that of the *p*-fluoro glycoside (**40**), demonstrating that glucose-based compounds have potential as ice recrystallization inhibitors.[19] Galactose analogues of the *p*-hydroxyl, *p*-chloro and *p*-bromo compounds were subsequently synthesized for comparison (Figure 2.4). Interestingly, the *p*-hydroxyphenyl galactose (**43**) and *p*-chlorophenyl galactose (**44**) were less active than their glucose counterparts, but *p*-bromophenyl galactose (**45**) proved more active.[19]

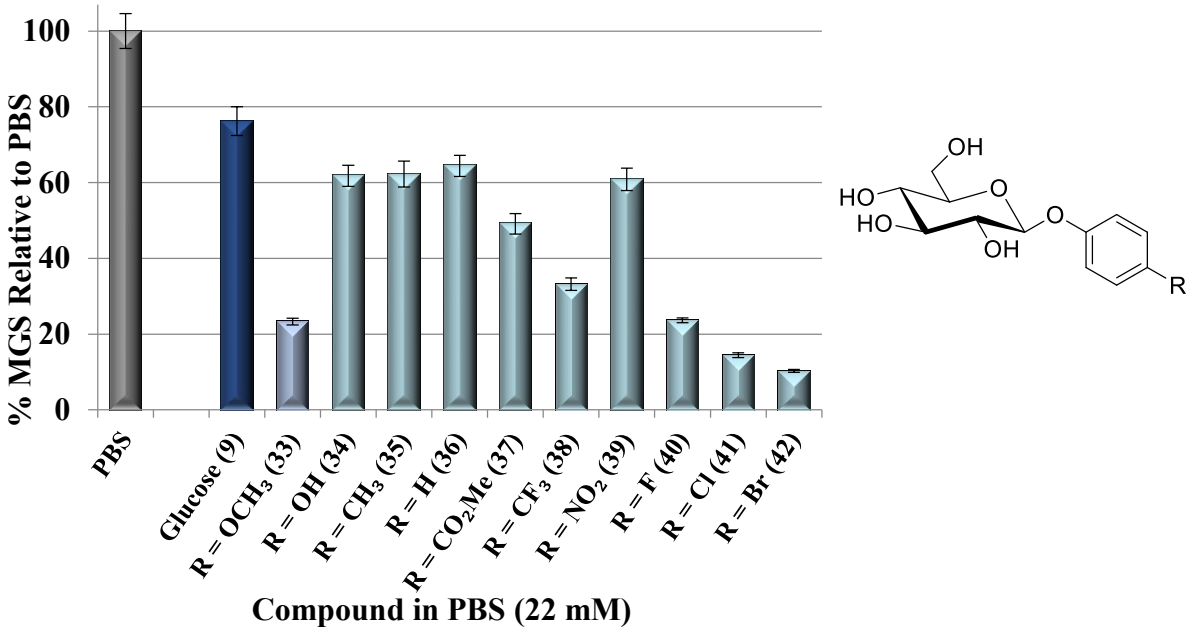

Figure 2.3: IRI activities of aryl glucosides (**33**-**42**) synthesized by Capicciotti.[19]

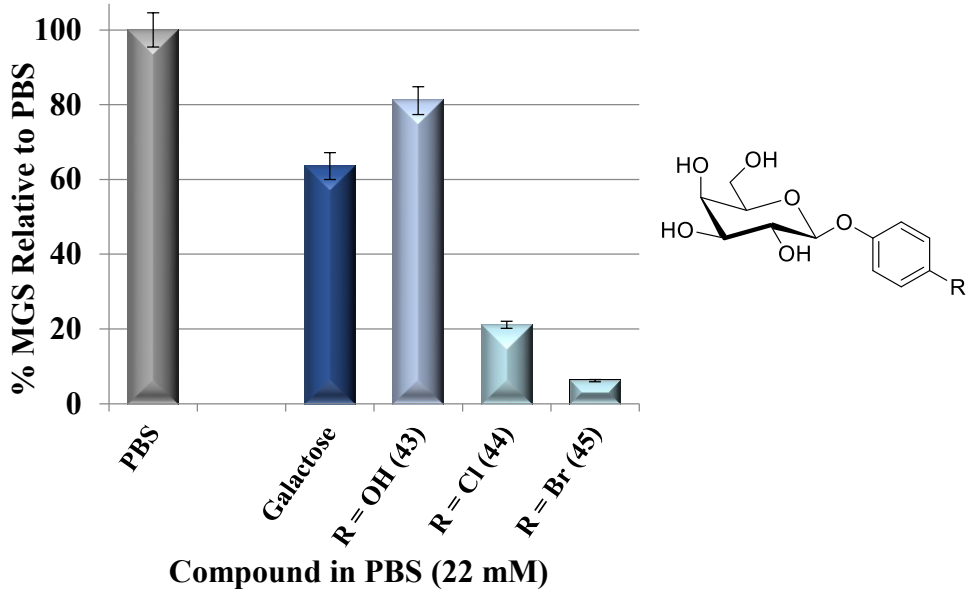

Figure 2.4: IRI activities of aryl galactosides (**43**-**45**) synthesized by Capicciotti.[19]

Based on these results, it appears that there are a combination of factors at play in determining the IRI activity of aryl glycosides, including the stereochemistry at C4 as well as the choice of substituent on the aryl ring. To obtain a more complete picture of the IRI activities of these compounds, seven additional aryl glycosides (**46**-**52**) will be synthesized (Figure 2.5) and then tested for IRI activity. This will expand the scope of the two series to include an additional strongly electron-donating *p*-amino group, a weak electron-donating *N*-acetyl group and one additional electron-withdrawing substituent in the form of a para-carboxylic acid group. In addition, a galactose analogue of methyl ester derivative (**37**) will be completed. This will allow for a systematic evaluation of the ability to inhibit ice recrystallization in relation to the electronic properties of thirteen different aryl substituents.

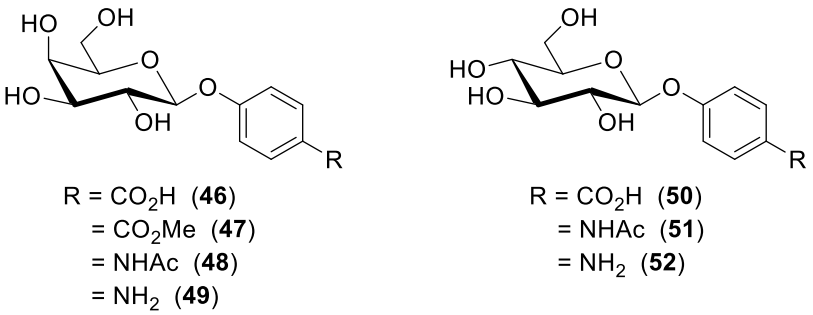

Figure 2.5: Structures of target *para*-substituted aryl galactosides (**46-49**) and aryl glucosides (**50-52**).

If a trend emerges from the data, it would provide support for the hypothesis that hydrogen bonding interactions at the anomeric oxygen play a role in mediating the IRI activity of these compounds. In addition to electronic factors, the examination of both glucose and galactose-based compounds containing identical aryl functionalities will allow for a global comparison amongst these two epimers. Although previous studies have shown that the choice of pyranose ring governs IRI activity in similar compounds, it is unclear whether the trends observed between different carbohydrates are consistent when broadly applied to an entire class of compound such as the aryl glycosides. As such, this study will aid in determining whether there is a consistent trend amongst IRI activities when

modifying only the stereochemistry of the C4 hydroxyl group. If a trend is identified, it may provide insight into the most logical choice of monosaccharide when designing and optimizing future cryoprotectants.

The following goals provide a brief summary of this research objective:

1. Synthesize aryl glycosides (**46-52**) and assess each for IRI activity at 22 mM concentration.
2. Assess whether a correlation exists between the electron densities of the aryl substituents tested and the IRI activities of the corresponding aryl glycosides.
3. Compare the IRI activities of glucose- and galactose-based aryl glycosides and determine whether a significant difference in IRI ability is present between the two epimers.

2.3 Objective 2: Assessing the influence of substituent position on the ice recrystallization inhibition activity of aryl glycosides

The degree of electron density on the anomeric oxygen of aryl glycosides is presumed to be governed principally by the resonance contributions of the substituent at the para position. For example, the presence of a *para*-substituted electron-withdrawing group would be expected to reduce the electron density and hydrogen bonding ability of the anomeric oxygen due to the major resonance forms which result. Because the lone pairs of the oxygen are involved in resonance with the aryl group, they are less available to accept a hydrogen bond from nearby water molecules (Figure 2.6A). If the EWG is relocated to the *meta* position, this effect is not as pronounced due to the fact that the electrons cannot be dispersed among the atoms of the withdrawing group. As a result, the overall electron density of the C1 oxygen would now theoretically be greater since donation of the oxygen's lone pairs into the aryl ring will be less predominant (Figure 2.6B). If the hydrogen bonding ability of the anomeric

oxygen plays a large role in the IRI activity of the compound, the effect of moving the substituent from the *para* to the *meta* position should produce a consistent result in IRI activity.

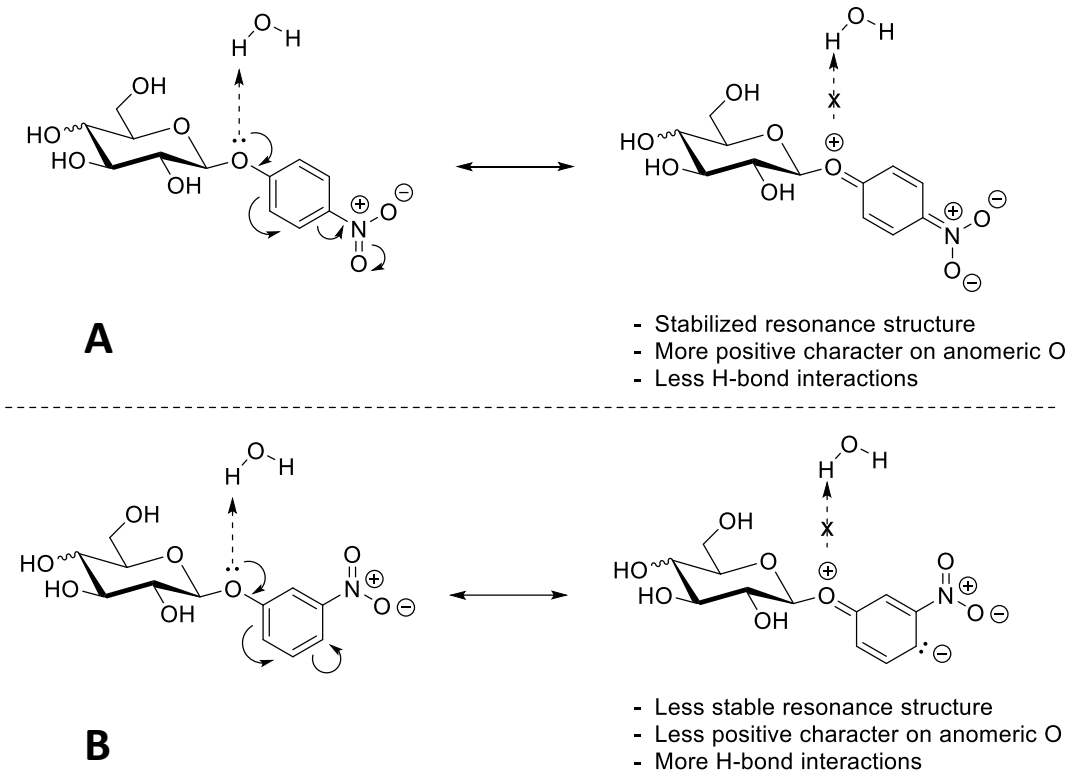

Figure 2.6: The effect of substituent position on the electron density of the anomeric oxygen in *para*-substituted (**A**) and *meta*-substituted (**B**) aryl glycosides based on resonance contributions.

In order to verify this hypothesis, a series of *meta*-substituted aryl glycosides (**53**-**56**) will be synthesized and assessed for IRI activity relative to the *para*-substituted isomers (Figure 2.7). A combination of electron-donating and electron-withdrawing substituents will be sampled to determine whether an inverse effect in IRI activity is observed between each type. Additionally, a brominated species will be examined due to the very potent IRI activity observed in *para*-bromo aryl glycosides. The electronic effects of halogens are more complex since they possess both electron-donating and

electron-withdrawing properties, but it is of interest to determine whether the potent activity of this functional group extends to other regioisomers.

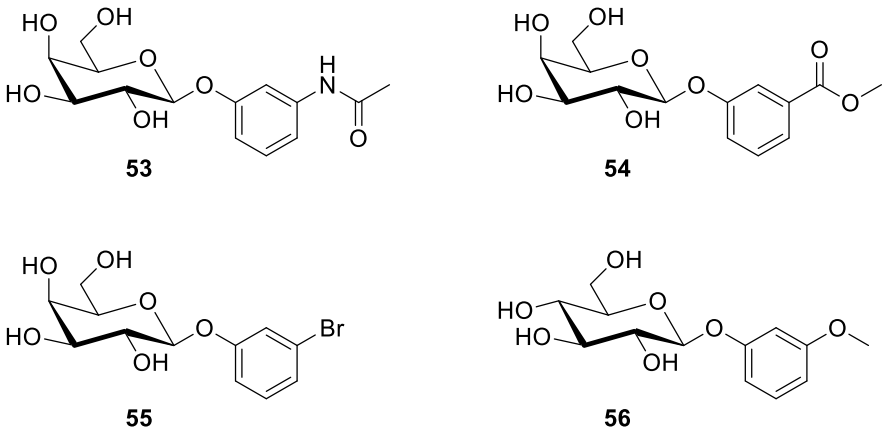

Figure 2.7: Structures of target *meta*-substituted aryl glycosides (**53-56**) to be assessed for IRI activity.

The effect of *ortho*-substitution on the IRI activity of aryl glycosides is more difficult to predict. If resonance-based electronic effects do influence IRI activity, it is plausible that *ortho*-substituted compounds should possess similar potency to their *para*-substituted analogues. However, it is also conceivable that the presence of a functional group at the *ortho* position may influence IRI activity due to its proximity to the anomeric oxygen as well as the other hydroxyl groups of the carbohydrate. This may disrupt the hydrogen-bonding abilities of the carbohydrate due to steric constraints, which could also affect the activity of the compound. Nonetheless, it remains worthwhile to investigate these compounds as they have not yet been assessed for IRI activity. Hence, *ortho*-substituted aryl glycosides (**57**-**60**) shown in Figure 2.8 will be similarly synthesised and tested to compare their activities to the *ortho*- and *meta*- compounds in the series.

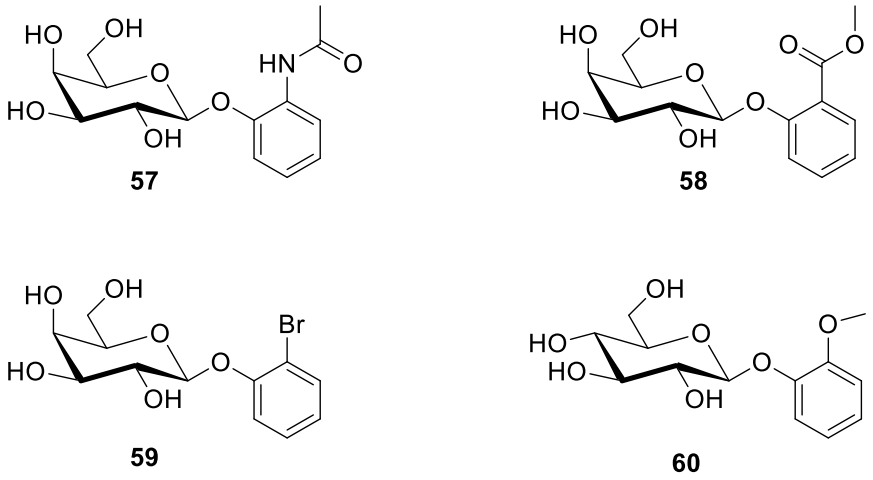

Figure 2.8: Structures of target *ortho*-substituted aryl glycosides to be assessed for IRI.

The research objectives of this section can be summarized as follows:

1. Synthesize target *meta*-substituted aryl glycosides (**53**-**56**) and *ortho*-substituted aryl glycosides (**57**-**60**).
2. Assess the IRI activity of these compounds at 22 mM concentration.
3. Determine if modifying substituent position on the aryl ring affects IRI activity in a predictable manner based on the corresponding electron density of the anomeric oxygen.

2.4 Objective 3: Investigating the effect of increasing hydrophobic character on the aromatic ring of aryl glycosides

Over the past several decades, a number of studies have investigated the importance of hydrophilic and hydrophobic regions on the cryoprotectant abilities of AFPs and AFGPs. Much of this work has centered around the importance of hydrophobicity for TH activity. For example, work by Haymet and colleagues on mutant type I winter flounder AFPs found a significant contribution to antifreeze activity from the hydrophobic methyl groups of alanine and valine mutants, contradicting previous hypothesis which advocated the importance of hydrogen bonding interactions from threonine

OH groups.[20,21] Similarly, studies of the solution structure of type III AFP by Sönnichsen *et al.* found that the OH groups of the relevant peptide residues were too sterically encumbered to be accessible for binding of the peptide to water through hydrogen bonding.[22] They also suggest hydrophobic interactions are responsible for ice binding in the case of type III AFP.[22]

Unfortunately, far fewer studies have been published on the link between hydrophobicity and ice recrystallization inhibition. Since TH and IRI are purported to operate via separate mechanisms,[10,11] hydrophobic interactions may not necessarily be a governing factor for IRI. As such, separate studies have been performed by our laboratory to specifically address the influence of hydrophobic moieties on IRI activity. To this end, Chaytor and Ben have synthesized and tested a fluorinated AFGP analogue (**61**) and compared its IRI activity to that of [*C*-(OGG)-Gal]$_4$ (**3**) and AFGP 8 (**1**).[23,24] Additionally, a fluorinated galactose derivative (**62**) was produced in order to examine the effect of a pseudo-hydrophobic moiety on IRI ability relative to galactose (**8**) (Figure 2.9).[23,24] It was found that the incorporation of fluorine groups resulted in a decrease in IRI activity of the compounds tested, an outcome which was rationalized by the hydrophobic character of the fluorinated moieties.[23,24] Based on the hydration hypothesis of carbohydrate-mediated recrystallization inhibition, a more potent inhibitor of ice recrystallization is one which better disrupts the layer of bulk water surrounding the inhibitor.[10] Fluorine atoms have been shown to facilitate the ordering of water molecules in a manner similar to hydrocarbons. Therefore, based on the hydration hypothesis, this ordering would facilitate ice recrystallization by more easily allowing the transfer of water molecules into the ice lattice.[10,25] From this study, it appears that hydrophobic interactions are detrimental for ice recrystallization inhibitors.

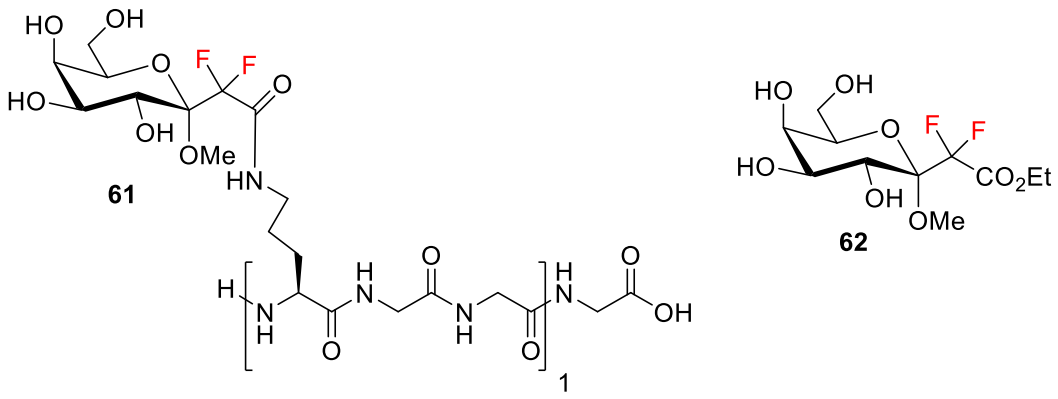

Figure 2.9: Fluorinated *C*-AFGP analogue (**61**) and galactose analogue (**62**) synthesized by Chaytor and colleagues.[23,24]

However, subsequent experiments on the effects of hydrophobic moieties have provided contradictory results. In a recent paper by Capicciotti and co-workers, a variety of non-ionic surfactants and hydrogelators were screened for IRI activity (Figure 1.14, page 29).[26] Interesting results were obtained from carbohydrate-based surfactants *n*-octyl-β-D-glucopyranoside (**17**) and *n*-octyl-β-D-galactopyranoside (**18**). It was found that (**17**) had IRI activity comparable to that of the parent glucose at several different concentrations.[26] However, the IRI activity of (**18**) was greatly enhanced at 22 mM concentration compared to galactose, and its activity varied in a concentration-dependent fashion.[26] In this situation, it does not appear as though the hydrophobic *n*-octyl chain on (**18**) is detrimental to IRI activity, since the only difference between (**17**) and (**18**) is the stereochemistry at C4.[26] In a similar vein, Balcerzak *et al.* examined the IRI abilities of lysine-based surfactants and gelators and discovered that long hydrophobic chains, upwards of 12 carbons in length, were very beneficial for IRI activity (Figure 1.15, page 31).[27] In both these studies, it is noted that the activity of potent ice recrystallization inhibitors is independent of the critical micelle concentration (CMC) of the surfactants tested.[26,27] As well, the ability of some IRI-active compounds to form hydrogels is not correlated with recrystallization inhibition activity.[27] This suggests that neither of these two processes (micelle formation or gelation) is

involved in the mechanism of IRI. It is clear from these studies, however, that hydrophobic effects are not always an impediment to potent IRI activity. In contrast, it appears they may actually be beneficial in some cases.

The unexpected effects of hydrophobic moieties on the IRI activity of these small molecules warrants further study. Of particular importance is whether this phenomenon is specific to surfactants and gelators. If the addition of hydrophobic character has a beneficial effect on the IRI activities of other classes of compounds, it would represent a new avenue towards novel, rationally-designed cryoprotectants. Therefore, two series of aryl glycosides shown in Figure 2.10 will be synthesized and assessed for IRI activity in order to gauge the effect of increasing hydrophobicity in an incremental fashion. The use of *p*-alkamidophenyl (Figure 2.10A) and *p*-alkoxyphenyl (Figure 2.10B) substituents is deliberate in that it will allow a comparison of the IRI activity of longer alkyl chain derivatives with the less-hydrophobic parent compounds, for which IRI activity has already been measured. The targets in both these series can be easily synthesized with commercially available starting materials using established literature conditions.

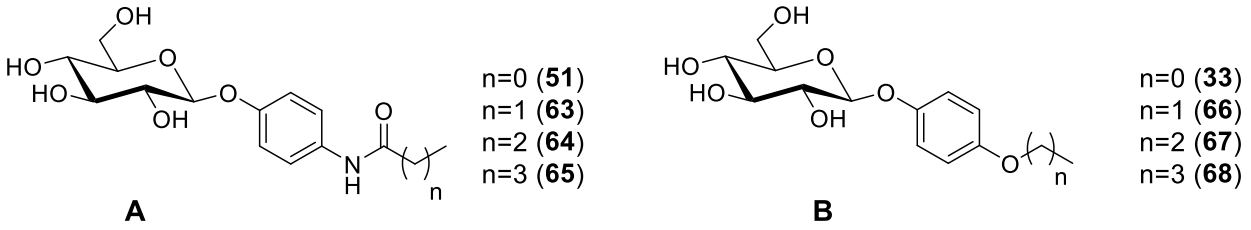

Figure 2.10: Structures of target *p*-alkamidophenyl glucosides (**A**) and *p*-alkoxyphenyl glucosides (**B**) to be assessed for IRI activity.

It is hypothesized that a trend in IRI activity (either increasing or decreasing) will emerge with the addition of each carbon unit to the hydrophobic tail of the compounds. This will provide insight into the effect and magnitude of small changes in hydrophobicity to the observed IRI activities. Studies will

be limited to *para*-substituted compounds to minimize potential interference of the aryl substituents with the carbohydrate unit of the compounds.

The following goals provide a brief summary of this research objective:

1. Synthesize *p*-alkamidophenyl glucosides (**63**-**65**) and *p*-alkoxyphenyl glucosides (**66-68**) and assess these compounds for ice recrystallization inhibition activity at 22 mM concentration
2. Determine whether a correlation exists between increasing alkyl chain length (hydrophobic character) and IRI activity for each aryl glycoside series.

References

1. Davis, J.M.; Rowley, S.D.; Braine, H. G.; Piantadosi, S.; Santos, G.W., Clinical toxicity of crypreserved bone marrow graft infusion. *Blood* **1990**, 75, 781-786.

2. Liseth, K.; Abrahamsen, J.F.; Bjorsvik, S.; Grottebo, K.; Bruserud, O., The viability of cryopreserved PBPC depends on the DMSO concentration and the concentration of nucleated cells in the graft. *Cytotherapy* **2005**, 7, 328-333.

3. Mazur, P.; Farrant, J.; Leibo, S.P.; Chu, E.H.Y., Survival of hamster tissue culture cells after freezing and thawing: Interactions between protective solutes and cooling and warming rates. *Cryobiology* **1969**, 6, 1-9.

4. Meryman, H.T., Osmotic stress as a mechanism of freezing injury. *Cryobiology* **1971**, 8, 489-500.

5. Eniade, A.; Hauer, L; Ben, R.N. Synthesis of a *C*-linked antifreeze glycoprotein (AFGP) mimic; Probes for investigating the mechanism of action. *Org. Lett.* **1999**, 1, 1759-1762.

6. Eniade, A.; Purushotham, M.; Ben, R.N.; Wang, W.; Horwarth, K.A. Serendipitous discovery of antifreeze protein-specific activity in *C*-linked antifreeze glycoprotein analogs. *Cell Biochem. Biophys.* **2003**, 38, 115-124.

7. Liu, S.; Ben, R.N. *C*-linked galactosyl serine AFGP analogues as potent recrystallization inhibitors. *Org. Lett.* **2005**, 7, 2385-2388.

8. Wu, L. K.; Tokarew, J. M.; Chaytor, J. L.; von Moos, E.; Li, Y. Palii, C.; Ben, R. N.; Allan, D. S., Carbohydrate-mediated inhibition of ice recrystallization in cryopreserved human umbilical cord blood. *Carb. Res.* **2011**, 346, 86-93.

9. Tokarew, J., Ph.D. Dissertation, University of Ottawa, **2011**.

10. Tam R.Y.; Ferreira, S. S.; Czechura, P.; Chaytor, J. L.; Ben, R. N., Hydration Index – A Better Parameter for Explaining Small Molecule Hydration in Inhibition of Ice Recrystallization. *J. Am. Chem. Soc.* **2008**, 130, 17494–17501.

11. Czechura, P.; Tam, R.Y.; Dimitrijevic, E; Murphy, A.V; Ben, R. N., The Importance of Hydration for Inhibiting Ice Recrystallization with C-Linked Antifreeze Glycoproteins, *J. Am. Chem. Soc.,* **2008**, 130 (10) 2928-2929.

12. Galema, S. A.; Høiland, H., Stereochemical Aspects of Hydration of Carbohydrates in Aqueous Solutions. 3. ^{1}Density and Ultrasound Measurements, *J. Phys. Chem.* **1991**, 95, 5321-5326.

13. Høiland, H.; Hølvik, H., Partial Molar Volumes and Compressibilities of Carbohydrates in Water. *J. Solution Chem.* **1978**, 7, 587-596.

14. Dashnau, J.; Sharp, K. A.; Vanderkooi, J. M., Carbohydrate Intramolecular Hydrogen Bonding Cooperativity and its Effect on Water Structure. *J. Phys. Chem. B* **2005**, 109, 24152-24159.

15. Junquera, E.; Olmos, D.; Aicart, E., Carbohydrate-water interactions of *p*-nitrophenylglycosides in aqueous solution. Ulstrasonic and densitometric studies. *Phys. Chem. Chem. Phys.* **2002**, 4, 352-357.

16. Simons, J. P. *et al.*, Hydrogen Bonding and Cooperativity in Isolated and Hydrated Sugars: Mannose, Galactose, Glucose and Lactose. *J. Am. Chem. Soc.* **2005**, 127, 11414-11425.

17. Trant, J. T.; Doshi, M.; Ben, R. N., unpublished results, **2010**.

18. Czechura, P.; Tam, R. Y.; Dimitrijevic, E.; Murphy, A. V.; Ben, R. N., The Importance of Hydration for Inhibiting Ice Recrystallization with *C*-Linked Antifreeze Glycoproteins. *J. Am. Chem. Soc.* **2008**, 130, 2928-2929.

19. Capicciotti, C. J.; Mancini, R.; Ben, R. N., unpublished results, **2011**.

20. Haymet, A. D. J.; Ward, L. Gl; Harding, M. M., Winter Flounder "Antifreeze" Proteins: Synthesis and Ice Growth Inhibition of Analogues that Probe the Relative Importance of Hydrophobic and Hydrogen-Bonding Interactions. *J. Am. Chem. Soc.* **1999**, 121, 941-948.

21. Sicheri, F.; Yang, D. S. C., Ice-binding structure and mechanism of an antifreeze protein from winter flounder. *Nature* **1995**, 375, 427-31.

22. Sönnichsen, F. D.; DeLuca, C. I.; Davies, P. L.; Sykes, B. D., Refined solution structure of type III antifreeze protein: hydrophobic groups may be involved in the energetics of the protein-ice interactions. *Structure* **1996**, 4, 1325-1337.

23. Chaytor, J. L.; Ben, R. N., Assessing the ability of a short fluorinated antifreeze glycopeptide and a fluorinated carbohydrate derivative to inhibit ice recrystallization. *Bioorg. Med. Chem. Lett.* **2010,** 20, 5251-5254.

24. Chaytor, J. L., Ph.D. Dissertation, University of Ottawa, **2010**.

25. Biffinger, J. C.; Kim, H. W.; DiMagno, S. G., The Polar Hydrophobicity of Fluorinated Compounds. *ChemBioChem* **2004**, 5, 622-627.

26. Capicciotti, C. J. *et al.*, Potent inhibition of ice recrystallization by low molecular weight carbohydrate-based surfactants and hydrogelators. *Chem. Sci.* **2012**, 3, 1408-1416.

27. Balcerzak, A. K.; Febbraro, M.; Ben, R. N., The importance of hydrophobic moieties in ice recrystallization inhibitors. *RSC Adv.* **2013**, 3, 3232-3236.

Chapter 3: Synthesis of *O*-Aryl-β-D-glycosides and Assessment of the Role of Electronic Effects on Ice Recrystallization Inhibition

3.1 Introduction

Over the past decade, the Ben Laboratory has demonstrated that it is possible to design and synthesize analogues of native AFGPs that exhibit custom-tailored antifreeze activity. Specifically, these analogues display potent ice recrystallization inhibition (IRI) activity without thermal hysteresis (TH) activity.[1-3] Increased IRI activity has been found to correlate with improved post-thaw cell viabilities in cryopreserved human liver and kidney cell lines,[4] and consequently the *C*-linked AFGP analogue [*C*-(OGG)-Gal]$_4$ (**3**), which is a potent inhibitor of ice recrystallization, has been shown to be as effective as a 2.5% solution of DMSO, demonstrating the potential of this and other related compounds as novel cryoprotectants.[5]

Recently, our laboratory has reported that many different classes of small molecules can exhibit potent IRI activity.[6,7] This is an important breakthrough as it no longer limits the search for potential new cryoprotectants to large, complex glycoconjugates. Generally speaking, small molecules are more attractive as cryoprotectants due to their lower production cost and ease of synthesis (relative to the *C*-glycoconjugates). Hence, our laboratory has begun focusing on the development of these compounds for various medical and commercial applications.

While the IRI ability of simple carbohydrates has been linked to the degree of hydration,[8] the specific factors governing the hydration of a small molecule are not well understood. It has been suggested that the hydrogen bonding propensity of sugars is likely responsible for increased recrystallization inhibition and that this occurs by disrupting the three-dimensional network of surrounding bulk water.[9] Therefore, compounds with a greater degree of hydration would be expected to display more potent IRI activity. Ultrasonic and densitometric studies of *p*-nitrophenyl glycosides

have revealed that the hydration (quantified using a hydration number) of these compounds are greater than their corresponding reducing sugar.[17] Subsequent screening of *O*-aryl glycoside analogues by our laboratory identified *p*-methoxyphenyl-β-D-glucopyranoside as a potent inhibitor of ice recrystallization, generating further interest in this class of compound.[11]

It has been reported that the hydrogen-bonding abilities of the C2 and C4 hydroxyl groups of carbohydrates are important in governing the hydration of the molecules.[15] However, the importance of hydrogen bonding at C1 is less clear. *O*-Aryl glycosides provide a means of probing the importance of hydrogen bonding ability at the anomeric oxygen since the electron density of the oxygen atom can be modified based on the presence of electron-donating or electron-withdrawing substituents on the aryl ring. A systematic study of these electronic effects on the IRI activity of aryl glycosides will provide insight into the role of hydrogen bonding in this process. With this understanding, the rational design and optimization of novel cryoprotectants may become possible.

3.2 Synthesis and IRI Activity of Para-Substituted Aryl Galactosides and Aryl Glucosides

The initial study of aryl glycosides was carried out by Trant and Doshi to examine whether electron density of the anomeric oxygen correlates with IRI activity.[10] To this end, a series of six *para*-substituted aryl galactosides (**26**-**31**) were synthesized and assessed. Although no discernable trend was identified, it was observed that some molecules displayed activity greater than D-galactose. Capicciotti and Mancini compared the IRI activity of these compounds to the IRI activity of the corresponding aryl glucosides (**33**-**42**) and found that the glucose-based compounds were, in some cases, more active than their galactose-based counterparts.[11] Unfortunately, the relationship between the stereochemistry at C4 and its effect on IRI activity was not clear. In an attempt to better understand this observation, the synthesis of seven additional aryl galactosides (**46**-**49**) and aryl glucosides (**50**-**52**) were synthesized.

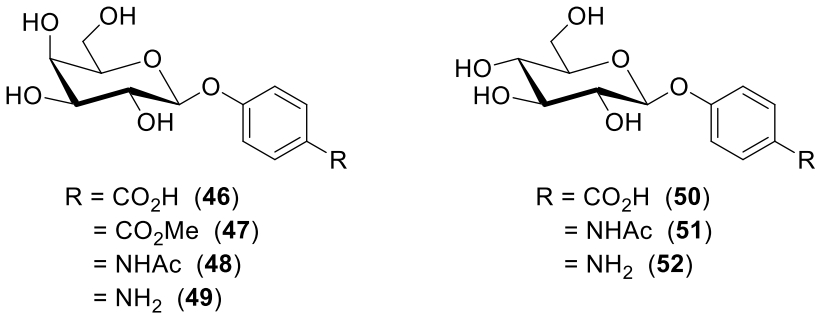

Figure 3.1: Structures of aryl glycoside targets (**46-52**) synthesized for assessment of IRI activity.

*3.2.1 Synthesis of methyl 4-(*β-D-*galactopyranosyloxy)benzoate (**47**), 4-(*β-D-*galactopyranosyloxy)benzoic acid (**46**), and 4-(*β-D-*glucopyranosyloxy)benzoic acid (**50**).*

As outlined in Scheme 3.1, methyl 4-hydroxybenzoate (**71**) was produced via esterification of 4-hydroxybenzoic acid (**70**) using thionyl chloride in methanol. **71** was then reacted with galactose pentaacetate (**69**) using boron trifluoride diethyletherate. This provided **72** in 55% yield, which was subsequently deprotected using a catalytic amount of potassium carbonate in methanol and purified by recrystallization to give methyl 4-(β-D-galactopyranosyloxy)benzoate (**47**) in 68% yield. Saponification of **47** using lithium hydroxide in 2:1 H_2O:THF provided 4-(β-D-galactopyranosyloxy)benzoic acid (**46**) in near-quantitative yield. An identical approach was used for the synthesis of 4-(β-D-glucopyranosyloxy)benzoic acid (**50**) by instead using glucose pentaacetate as the glycosyl donor (Scheme 3.2).

Scheme 3.1: Synthesis of methyl 4-(β-D-galactopyranosyloxy)benzoate (**47**) and 4-(β-D-galactopyranosyloxy)benzoic acid (**46**).

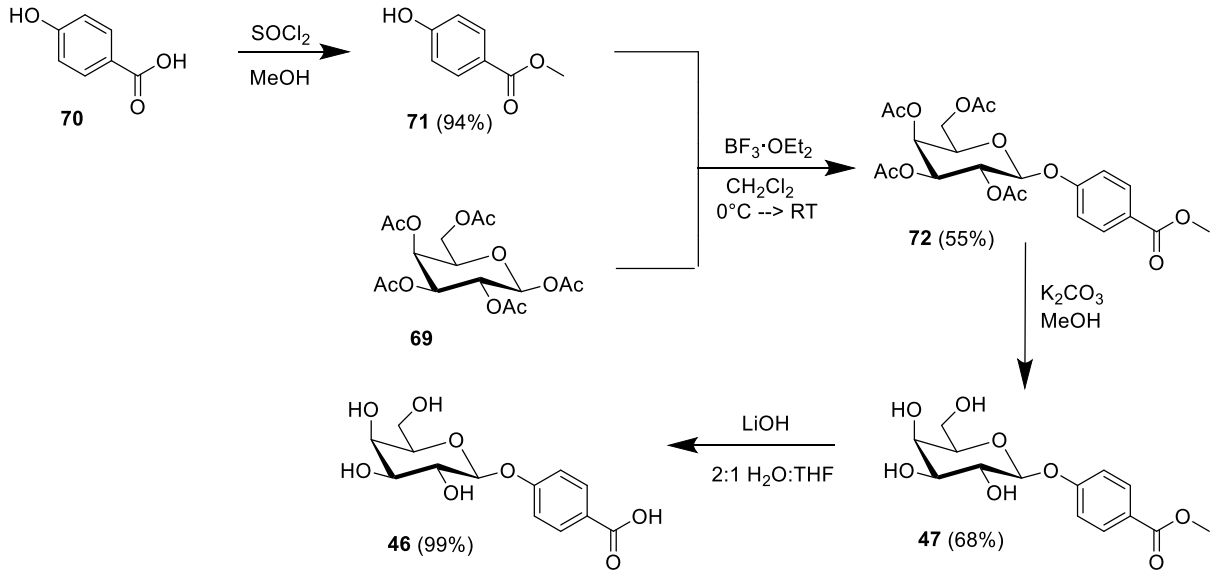

Scheme 3.2: Synthesis of 4-(β-D-glucopyranosyloxy)benzoic acid (**50**).

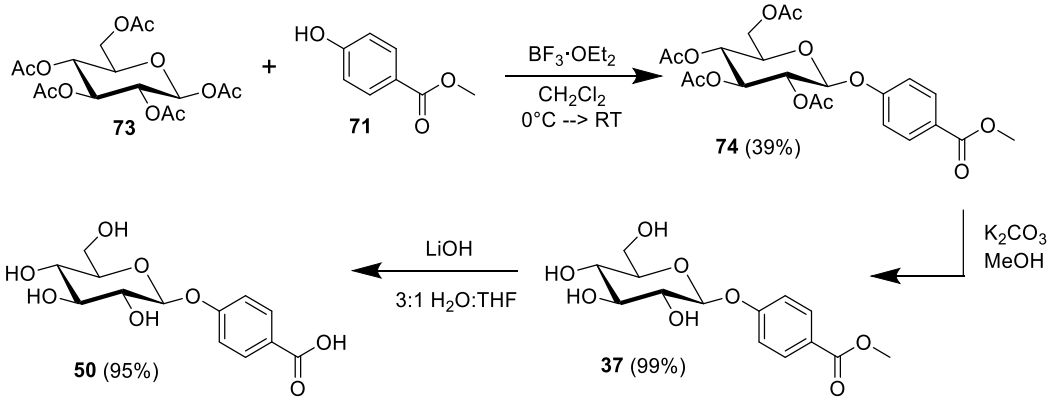

*3.2.2 Synthesis of 4-aminophenyl-*β-D-*galactopyranoside (**49**) and 4-aminophenyl-*β-D-*glucopyranoside (**52**).*

The synthesis of amino-substituted glycosides (**49**, **52**) was initially attempted by protecting the aniline unit of 4-aminophenol (**75**) with a *t*-Boc protecting group using di-*tert*-butyl dicarbonate in the presence of mild base. While the selective protection of the aniline was easily accomplished, attempts

to remove the *t*-Boc group after glycosidation were unsuccessful. Deprotection was attempted using a 1:1 mixture of trifuloroacetic acid in dichloromethane as well as anhydrous 4M HCl in dioxane. However, both reaction conditions resulted in cleavage of the glycosidic bond. In light of this, a new approach was attempted by instead protecting the aniline with a Cbz protecting group, which can be removed by hydrogenolysis. This strategy, which was adapted from a procedure by Perron and colleagues, [12] was successful in isolating the desired aryl glycosides (Scheme 3.3). 4-aminophenol (**75**) was first reacted with benzyl chloroformate under acidic conditions (10% aq. acetic acid/dioxane) to furnish the protected 4-(benzyloxycarbonyl)aminophenol (**76**) in 88% yield. This substrate was then reacted with either galactose pentaacetate (**69**) or glucose pentaacetate (**73**) in the presence of $BF_3{\cdot}OEt_2$ to yield the corresponding Cbz-protected aryl glycoside (**77** or **78**). Deprotection of the acetate groups with potassium carbonate in methanol furnished **79** (53%) or **80** (54%). This was followed by removal of the Cbz protecting group by hydrogenolysis with palladium hydroxide and one atmosphere of hydrogen gas to furnish 4-aminophenyl-β-D-galactopyranoside (**49**) or 4-aminophenyl-β-D-glucopyranoside (**52**) in quantitative yields.

Scheme 3.3: Synthesis of 4-aminophenyl-β-D-galactopyranoside (**49**) and 4-aminophenyl-β-D-glucopyranoside (**52**).

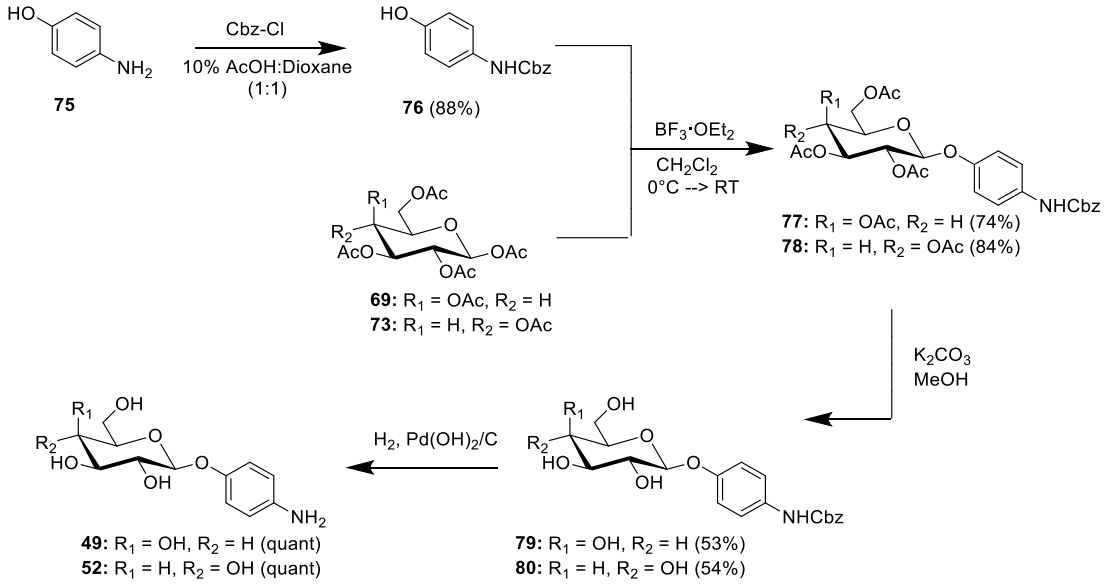

*3.2.3 Preparation of 4-acetamidophenyl-β-D-galactopyranoside (**48**), and 4-acetamidophenyl-β-D-glucopyranoside (**51**).*

The synthesis of 4-acetamidophenyl-β-D-galactopyranoside (**48**) was accomplished by first acetylating **75** with acetic anhydride in water to obtain 4-acetamidophenol (**81**) in 55% yield (Scheme 3.4). This compound was then reacted with peracetylated galactose or glucose using previously-mentioned conditions, providing the protected aryl glycoside **82.** Deprotection of the *O*-acetyl groups provided **48** in 49% yield. The epimer of **48**, 4-acetamidophenyl-β-D-glucopyranoside (**51**), was instead produced from the non-acetylated glycoside **52** since a large batch of this compound had already been prepared (Scheme 3.5). Selective acetylation of the unprotected glycoside was achieved using acetic anhydride in water followed by filtration to give pure **51** in 74% yield.

Scheme 3.4: Synthesis of 4-acetamidophenyl-β-D-galactopyranoside (**48**).

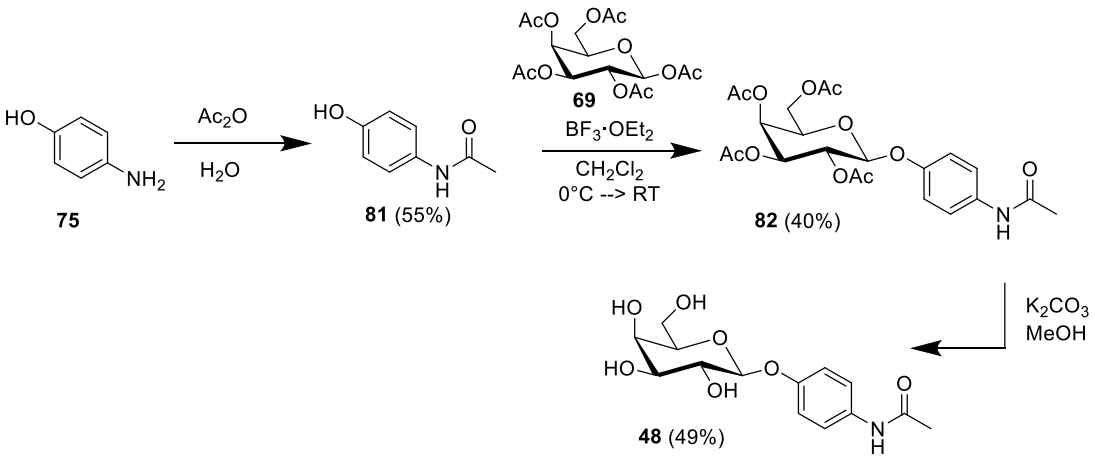

Scheme 3.5: Synthesis of 4-acetamidophenyl-β-D-glucopyranoside (**51**).

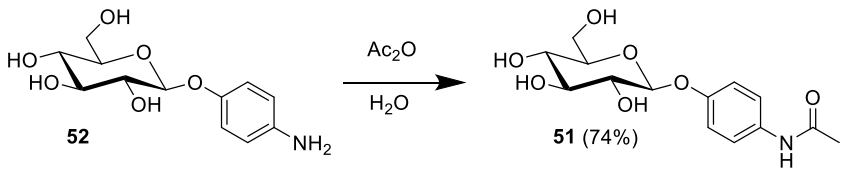

*3.2.4 Assessment of IRI activity of para-substituted O-aryl galactosides (**46**-**49**) and O-aryl glucosides (**50**-**52**).*

The IRI activity of aryl glycosides (**46**-**52**) was assessed using the previously-established "splat cooling" method.[13] In this assay, a 10 µL drop containing the compound dissolved in phosphate-buffered saline (PBS) is dropped from a height of 2 metres onto a pre-cooled aluminum block at -78°C. The flash-frozen ice wafer is then transferred to a cooling unit held at -6.4°C for 30 minutes, during which time recrystallization occurs. At the end of this annealing period, the resulting ice crystals formed are photographed and the average area of the ice crystals in the field of view are analyzed using a novel domain recognition software.[18] The mean grain (or ice crystal) size (MGS) of the sample is compared to the MGS of a control PBS solution from the same day of testing, and the IRI activity is reported as the percentage of the MGS relative to the control.

The IRI activity of the aryl galactosides (**46-50**) at 22 mM concentration are shown in Graph 3.1 in comparison to galactose (**8**) and the previously-assessed compounds produced by Trant and Capicciotti (**26**-**31**, **43**-**45**). Similarly, Graph 3.2 depicts the activity of newly synthesized aryl glucosides (**50-52**) alongside aryl glucosides (**33-42**) prepared by Capicciotti. It was hypothesized that the ability of the anomeric oxygen to hydrogen bond with surrounding bulk water may be one of the contributing factors of the IRI activity displayed by carbohydrates.[10,11] If so, it is expected that the presence of an electron-donating functional group on the aryl ring would increase the electron density of the anomeric oxygen, allowing it to form stronger hydrogen bonds. Similarly, the presence of an electron-withdrawing group should have the opposite effect, reducing the effectiveness of an aryl glycoside as an inhibitor of ice recrystallization.

Unfortunately, the IRI activities exhibited by compounds **46**-**52** do not support this hypothesis, nor do they help to establish a trend when viewed in conjunction with the first generation of aryl glycosides synthesized (Graphs 3.1 and 3.2). For example, it would be expected that the strongly-

donating amino group of **49** impart higher IRI activity than the unsubstituted phenyl ring on **28**. In fact, both compounds have very similar activities. Interestingly, the methyl ester on **47** appears to substantially increase its IRI activity, which is unexpected given the electron-withdrawing nature of this functional group. Additionally, although the carboxylic acid and ester groups of **46** and **47** have similar electron-withdrawing ability, they display very different IRI activities. The results of the aryl glucoside series are similarly difficult to rationalize. Of the three new aryl glucosides produced, the compound possessing an amino group (**52**) again displays the lowest IRI activity. Carboxylic acid and *N*-acetyl derivatives (**50**, **51**) both show activity comparable to that of glucose (**9**), despite their differing electronic properties.

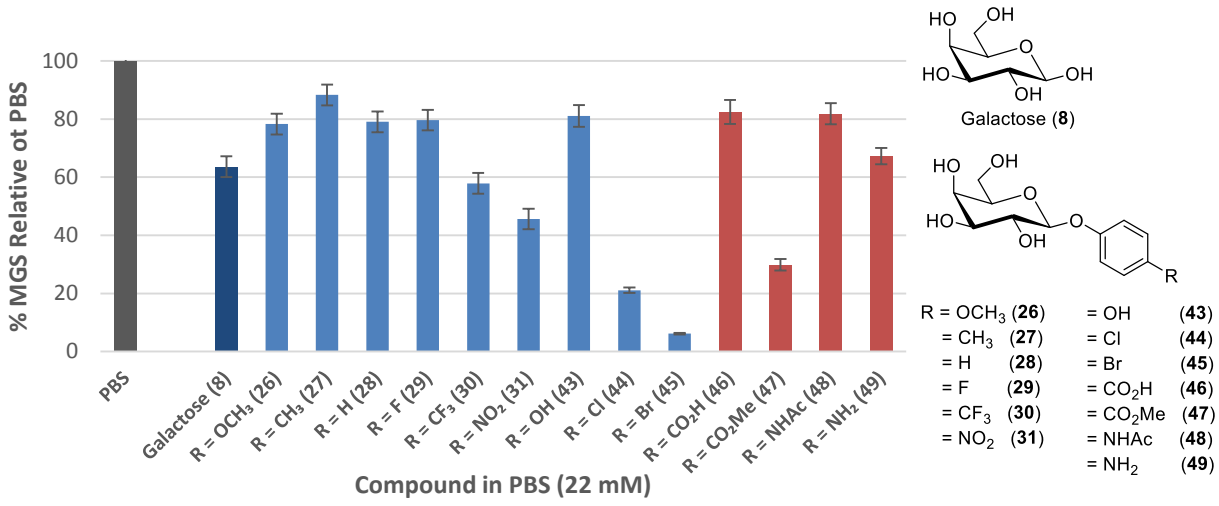

Graph 3.1: IRI Activities of aryl galactosides (**46-49**) (red bars) in comparison to previously-synthesized compounds in the series (blue bars).

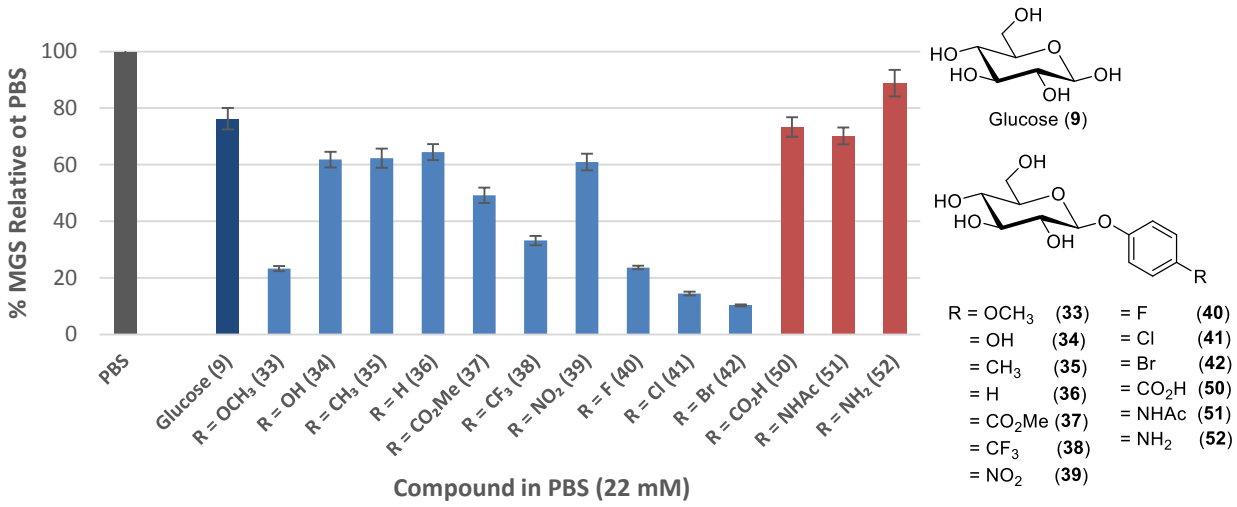

Graph 3.2: IRI Activities of aryl glucosides (**50-52**) (red bars) in comparison to previously-synthesized compounds in the series (blue bars).

Based on these results, it cannot be concluded that an increase in electronic density at the anomeric oxygen translates into an increase in IRI activity of an aryl glycoside. There is no apparent correlation in IRI activity based solely on the electronic properties of the aryl ring, since both electron-donating substituents (i.e R=OMe, **33**) and electron-withdrawing substituents (i.e. R=F, **40**) were capable of conferring potent IRI activity in certain compounds. This suggests that hydrogen bonding ability of the anomeric oxygen is not an important factor for IRI ability. We therefore conclude that other interactions are responsible for the variation in IRI activities observed in the series of aryl glycosides assessed. Further studies are underway to elucidate the specific factors involved in this phenomenon.

As shown in Graph 3.3, the combination of the aryl glucoside and aryl galactoside data allows for a comparison of IRI activity based on the stereochemistry at C4 of the pyranose ring. Significant variations in activity are observed between many of the epimers, suggesting that the arrangement of the hydroxyl group at this position plays an important role in the IRI ability of these compounds.

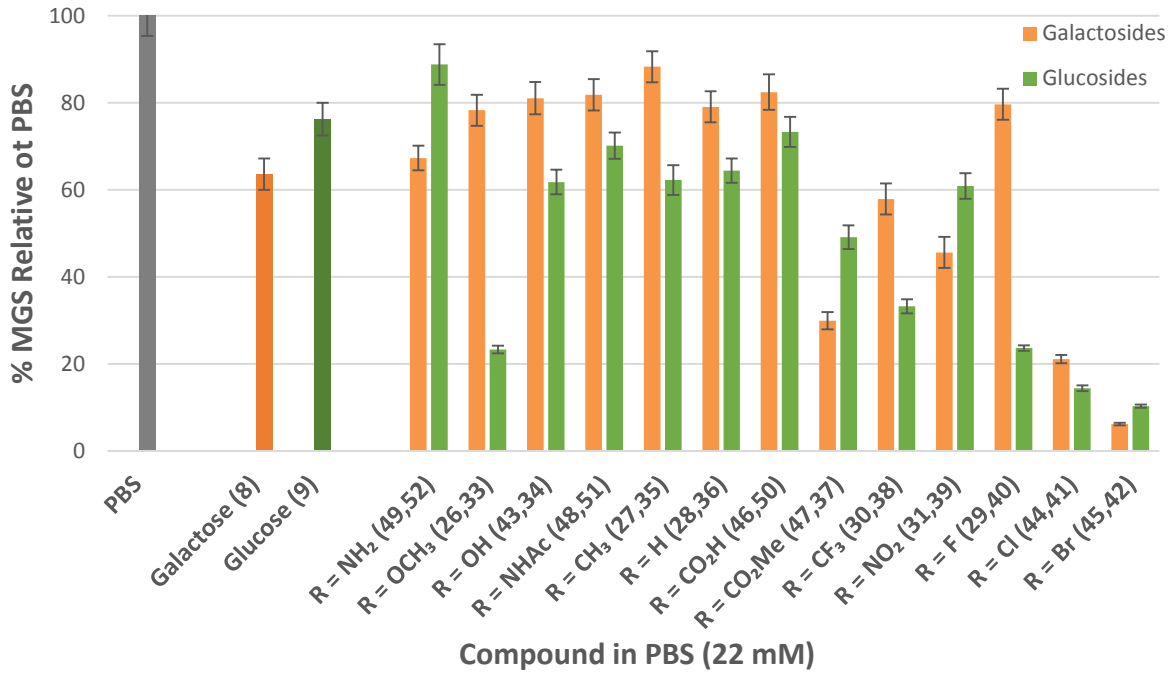

Graph 3.3: Comparison of IRI activities displayed by *para*-substituted aryl glycosides produced by Trant (**26-31**), Capicciotti (**33-45**) and those assessed during the present study (**46-52**) .[10,11]

Many of the compounds from the aryl glucoside series possess more potent IRI activity than the corresponding galactosides. Of the thirteen functional groups assessed, only four (R=NH_2, R=CO_2Me, R=NO_2, R=Br) resulted in significantly higher IRI activity in the presence of galactose *vs*. glucose. All others in the series were more active as glucosides rather than as galactosides. Additionally, the average mean grain size of the two series was calculated to be 51 ± 2.4 % for the aryl glucosides and 62 ± 3.0 % for the aryl galactosides. These results are contrary to what would be expected based on the observations by Tam and Czechura relating to hydration and IRI activity.[8,9] Since galactose is more hydrated and more IRI-active than glucose, it is surprising that the addition of an identically-substituted phenyl ring to both sugars can invert their activity profiles. It is possible that the presence of a β-substituted phenyl ring alters the hydration characteristics of the carbohydrates, which in turn has an effect on the corresponding IRI activities of the compounds. Unfortunately, because the hydration values of these aryl glycosides have not been reported, it is not possible verify whether the activities of

these compounds correlate with their hydration indices as is the case with the unsubsitituted sugars as well as *C*-linked glycopeptides (**3**, **5-7**). Calculation of these hydration values is therefore necessary for a more complete understanding of the results.

3.3 Investigating the effect of substituent position on the IRI activities of aryl glycosides.

As discussed in the previous section, the electron-donating or electron-withdrawing character of the *para*-substituent of an aryl glycoside does not appear to be linked with its IRI ability. This suggests that the basicity of the anomeric oxygen is not an important component for IRI. The initial study of anomeric electron density included only *para*-substituted glycosides, since these compounds are expected to have the greatest effect on electron density at C1 based on resonance contributions. Thus, another way of corroborating the above conclusions is through the generation of *ortho*- and *meta*-substituted regioisomers of the aryl glycoside series. Moving the substituent from the *para* to the *meta* position alters the electron density experienced by the anomeric oxygen through resonance. If electron density of the anomeric oxygen is important, the IRI activity of the compound would be expected to change between regioisomers in a predictable fashion. The placement of a substituent at the *para*-position also minimizes possible steric interactions between the substituent and the hydroxyl groups of the carbohydrate ring. The generation of *meta*- and *ortho*-substituted regioisomers may interfere with the ability of the pyranose ring to interact with the surrounding hydration shell through hydrogen bonding, a process which is believed to be important for IRI activity. Hence, these isomers may provide insight into the role of steric effects if IRI activity is subsequently lost. To determine the effect of substituent position on IRI activity, the synthesis of *meta*-substituted aryl glycosides (**53**-**55**) and *ortho*-substituted aryl glycosides (**57**-**60**) was undertaken.

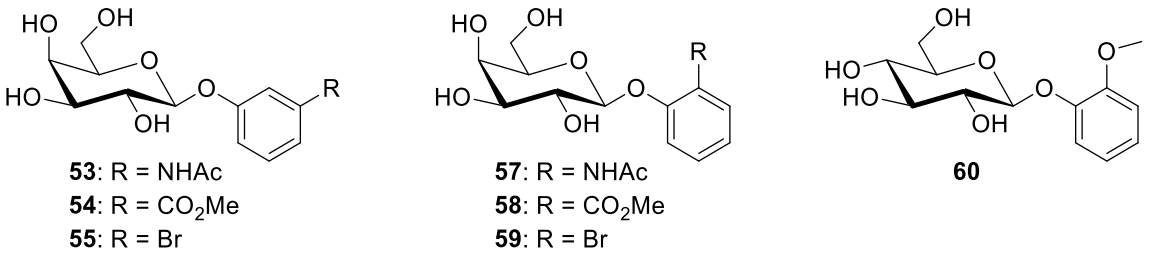

Figure 3.2: Structures of target *ortho*- and *meta*-substituted aryl glycosides (**53**-**60**).

3.3.1 Preparation of 3-acetamidophenyl-β-D-*galactopyranoside (**53**) and 2-acetamidophenyl*-β-D-*galactopyranoside (**57**).*

The synthesis of **53** was achieved by first acetylating 3-aminophenol using one equivalent of acetic anhydride in water to provide 3-acetamidophenol (**84**) in 52% yield (Scheme 3.6). Glycosidation was achieved through reaction of **84** with galactose pentaacetate to give the protected glycoside **85**, which was then deacetylated with potassium carbonate in methanol to afford 3-acetamidophenyl-β-D-galactopyranoside (**53**) in 79% yield. Preparation of the ortho-substituted isomer 2-acetamidophenyl-β-D-galactopyranoside (**57**) was accomplished through the same approach starting from 2-aminophenol. (Scheme 3.6).

Scheme 3.6: Synthesis of 3-acetamidophenyl-β-D-galactopyranoside (**53**) and 2-acetamidophenyl-β-D-galactopyranoside (**57**).

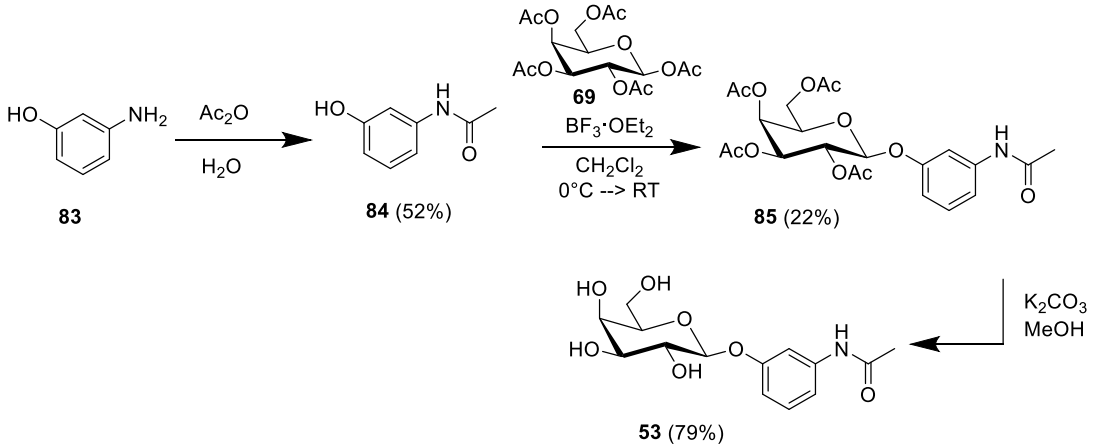

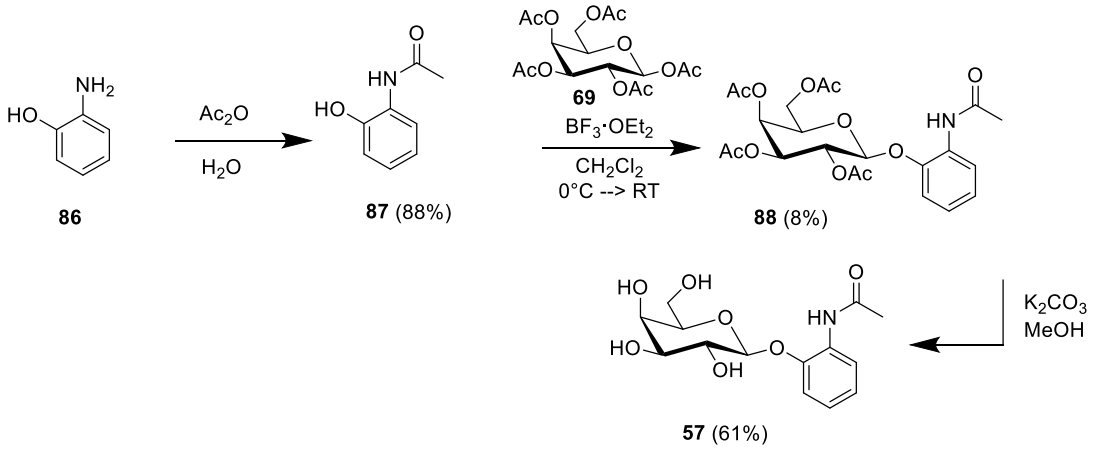

*3.3.2 Preparation of methyl 3-(*β-D-*galactopyranosyloxy)benzoate (**54**) and methyl 2-(*β-D-*galactopyranosyloxy)benzoate (**58**).*

As outlined in Scheme 3.7, the synthesis of methyl ester derivative **54** began with the commercially-available phenol **89** which was then reacted with galactose pentaacetate using previously-described conditions. The protected glycoside **90** was then deprotected to yield methyl 3-(β-D-galactopyranosyloxy)benzoate (**54**) in 50% overall yield. Due to time constraints, the methyl 2-(β-D-galactopyranosyloxy)benzoate (**58**) isomer could not be completed. Production of this compound should be possible using the same strategy as was used for **54** by instead starting from the *ortho*-substituted ester (Scheme 3.7).

Scheme 3.7: Synthesis of methyl 3-(β-D-galactopyranosyloxy)benzoate (**54**) and proposed synthesis of methyl 2-(β-D-galactopyranosyloxy)benzoate (**58**).

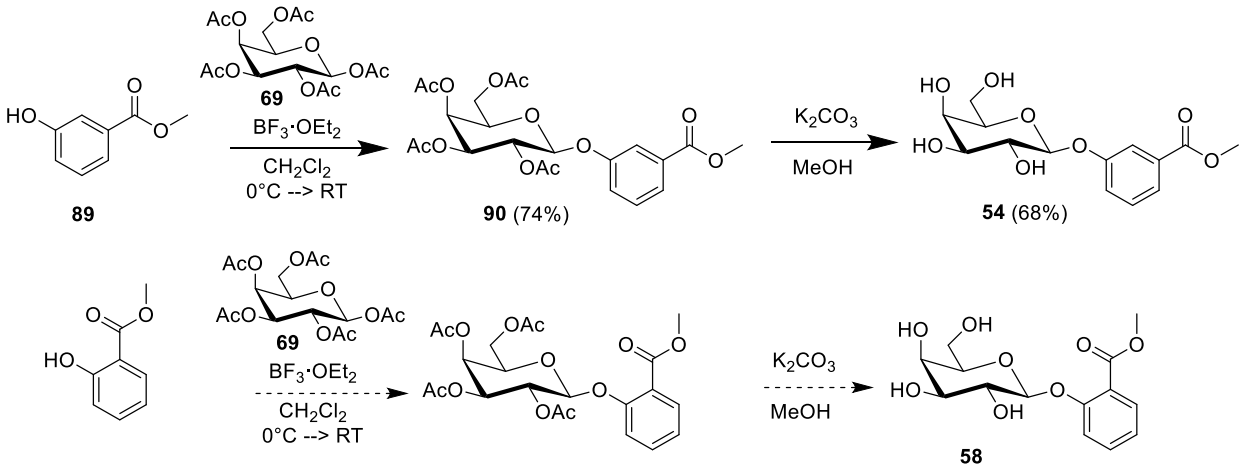

3.3.3 Preparation of 3-bromophenyl-β-D-galactopyranoside (**55**) and 2-bromophenyl-*β-D*-galactopyranoside (**59**).

The syntheses of brominated glycosides **55** and **59** were carried out under similar conditions (Scheme 3.9). Reaction of bromophenol derivatives **91** or **93** was carried out as before using galactose pentaacetate and boron trifluoride diethyletherate to give the protected meta-substituted (**92**) and ortho-substituted (**94**) glycosides. Standard deprotection of the acetate groups followed by purification via column chromatography gave 3-bromophenyl-β-D-galactopyranoside (**55**) and 2-bromophenyl-β-D-galactopyranoside (**59**) in 65% and 59% yields respectively.

Scheme 3.8: Synthesis of 3-bromophenyl-β-D-galactopyranoside (**55**) and 2-bromophenyl-β-D-galactopyranoside (**59**)

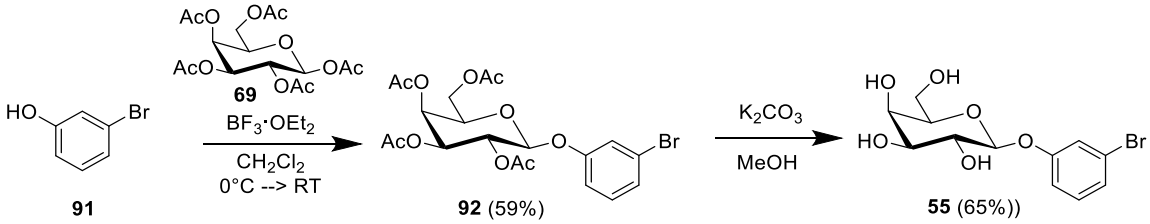

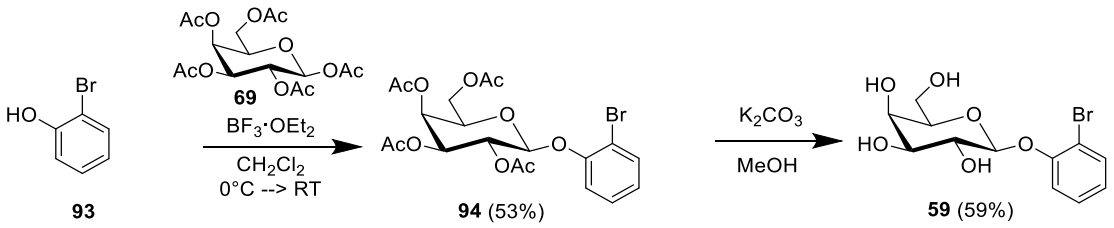

*3.3.4 Preparation of 2-methoxylphenyl-β-D-glucopyranoside (**60**)*

3-methoxylphenyl-β-D-glucopyranoside (**56**) was synthesized by Capicciotti and Mancini. The synthesis of its isomer, 2-methoxylpheny-β-D-glucopyranoside (**60**) was accomplished using the same approach (Scheme 3.9). Glycosidation was accomplished via previously-described conditions followed by standard deprotection and recrystallization to afford **60** in 29% overall yield.

Scheme 3.9: Synthesis of 2-methoxylphenyl-β-D-glucopyranoside (**60**).

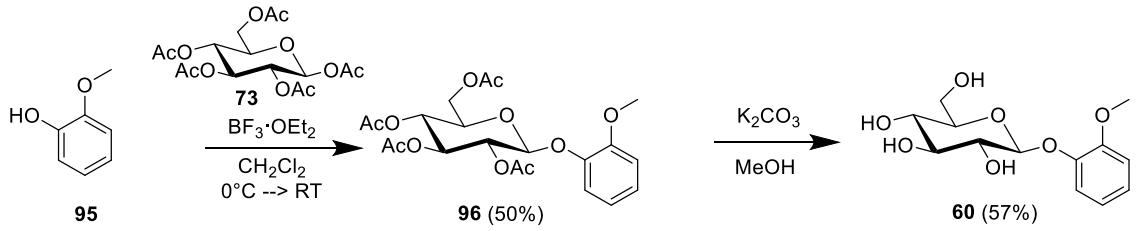

*3.3.5 Assessment of IRI activity of meta-substituted aryl glycosides (**53-56**) and ortho-substituted aryl glycosides (**57-60**).*

The *meta*- and *ortho*-substituted derivatives (**53-60**) were assessed for IRI activity at 22 mM concentration and compared with the *para*-substituted isomers (Graph 3.4). From the results, it appears that the position of the substituents on the aryl ring is important for IRI activity as there are significant variations in activity between regioisomers. In the case of the methoxyphenyl glucosides (blue bars), the observed trend in activity seems to support the hypothesis that the activity of the compounds is linked to electronic character. The electron-donating ability of the methoxy group is

expected to make the anomeric oxygen more basic in nature due to resonance. With increased electron density, this oxygen should now serve as a better hydrogen bond acceptor relative to an unsubstituted analogue. As predicted, the IRI activity of the *para*-methoxyphenyl glucoside (**33**) is almost completely eliminated when the OCH_3 group is moved to the *meta* position (**56**). This is explained by the fact that the methoxy group cannot increase the electron density of the oxygen through resonance when in the *meta* position, which renders the anomeric oxygen less basic as a result. Placement of the methoxy group at the *ortho* position (**60**) restores some of the compound's IRI activity, as would be expected since electron donation through resonance is possible at this position. However, the close proximity of the methoxy group to the pyranose ring in the *ortho* position may interfere with the ability of the sugar to interact with surrounding water molecules. This could explain the reduced IRI activity of **60**.

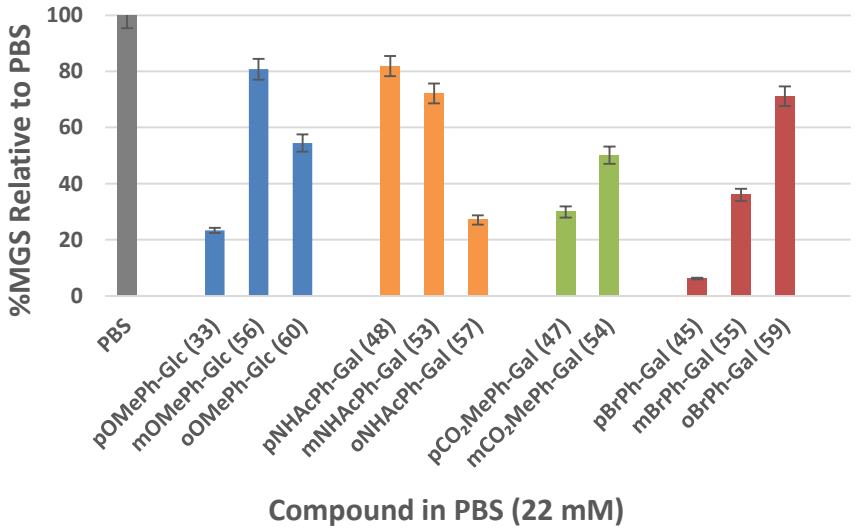

Graph 3.4: IRI activities of *meta*-substituted (**53**-**56**) and *ortho*-substituted (**57-60**) aryl glycosides in comparison with previously-tested *para*-substituted analogues (**33, 45, 47, 48**) at 22 mM in PBS.

The effect of substituent position on acetamidophenyl derivatives is less clear. A slight increase in activity is observed in *meta*-substituted compound **53** relative to *para*-substituted **48**. However, moving the amide group again to the *ortho* position (**57**) results in a substantial increase in activity. If the potency of **57** was due to electronic effects, one would expect that comparable activity would be

observed in the *para*-substituted isomer. This result is also surprising since significant steric interactions would be expected between the acetamido group and the carbohydrate hydroxyl groups. The potency of this compound suggests that a favourable interaction between the pyranose ring and the *N*-acetyl group may be responsible for the stark contrast in activity relative to the *meta* and *para* isomers.

In contrast, the bromophenyl series follows an opposite trend; movement of the bromine from the *para* to the *meta* position and then to the *ortho* position results in a loss of activity in each case. If the drop in activity of the *meta* isomer (**55**) relative to the *para* isomer (**45**) were due to electronic factors alone, it would be expected that the *ortho* isomer (**59**) would restore at least part of the IRI activity observed in **45**. This is not observed, as **59** displays the poorest IRI activity of the three. In the case of the electron-withdrawing methyl ester derivatives, movement of the substituent from the *para* position (**47**) to the *meta* position (**54**) again results in a loss of IRI activity, consistent with what is observed between *para*- and *meta*-methoxyphenyl glycosides **33** and **56**. This result is surprising given that the CO_2Me and OMe groups possess opposite electronic properties; the methyl ester is electron-withdrawing and should reduce the basicity of the anomeric oxygen, while the methoxy group is electron donating and should increase its basicity. Despite these differences, the same trend in IRI activity is observed. Unfortunately, the *ortho*-substituted derivative was not synthesized in time and therefore cannot be compared to the *meta*- and *para*-isomers.

Analysis of these results provide further evidence that electronic effects are not the only contributing factor for IRI activity in this class of compounds. The position of a given substituent on the aryl ring does appear to be an important factor since, in most cases, substantial variations in activity are observed between the different regioisomers. However, the reasons for this variation cannot be attributed to the basicity of the anomeric oxygen because the results are inconsistent between different types of functional groups. For example, in both the methoxy and the methyl ester series, movement of the R group from the *para* position to the *meta* position results in a decrease in IRI activity. This is in

spite of the fact that these functional groups confer opposite electronic effects. The methoxy group is a strong electron-donating group; by moving to the *meta* position, the phenolic oxygen experiences less electron density. In contrast, movement of the electron-withdrawing methyl ester to the *meta* position *increases* electron density on the anomeric oxygen. Hence, it was expected that movement of the substituents from the *para* to the *meta* position would have opposite effects between the two series. A notable observation is the increased activity of *o*-acetamidophenyl galactose (**57**), the only *ortho*-substituted compound which proved more potent than its *meta* or *para* isomers. While placement of a substituent at the *ortho* position may be expected to disrupt IRI activity by hindering the carbohydrate's ability to hydrogen bond, this is not the case in **57**. This suggests that *ortho*-substituted aryl glycosides should not be arbitrarily excluded from consideration in future studies.

3.4 Summary

Based on the results of these studies, we conclude that the electron density and corresponding hydrogen bonding ability of the anomeric oxygen is not a significant contributor to IRI activity in aryl glycosides. Contradictory results were observed when aryl substituents were varied from electron-donating to electron-withdrawing in nature; doing so would improve the IRI activity of the compound in some cases, while in other cases would be detrimental to its activity. Relocation of a substituent from the *para* position to the *meta* position also had a conflicting effect on the activity of the compounds examined. Additionally, the placement of a group at the *ortho* position appears to have mixed effects on IRI activity depending on the substituent. As such, the data do not support the hypothesis that a predictable and consistent effect on IRI activity would be observed by altering the electronic properties of the aryl substituent. This suggests that such an approach is not effective in the rational design of novel cryoprotectants.

Modification of the stereochemistry at C4 on the pyranose ring proved to have a significant but variable effect on IRI activity. For example, in the case of the nitro, bromo, amino and methyl ester glycosides (**31**, **45**, **47**, **49)**, the galactose-based compounds were more IRI-active than the glucose epimers. However, for all other substituents screened, glucose was optimal for IRI activity. This result is surprising since galactose (**8**) is a more potent inhibitor of ice recrystallization than glucose (**9**) without the presence of an aryl substituent at C1. In the past, this has been attributed to the increased hydration of galactose relative to glucose, which is thought to disrupt the bulk water layer through competing hydrogen bonding interactions with the carbohydrate unit.[8,14] If hydration is indeed an important modulator of IRI activity, these data would suggest that the presence of a β-phenyl ring at C1 alters the hydration of the glycosides whereby, in some cases, the aryl glucosides become more hydrated than their galactoside counterparts. Unfortunately, since the hydration numbers for these compounds have not been reported and are difficult to calculate, we are currently unable to verify this hypothesis. However, this study has conclusively demonstrated that glucose-based small molecules are an important class of compounds to be investigated as potential cryoprotectants since they are capable of proving more potent inhibitors of ice recrystallization than galactose derivatives.

One key finding from the assessment of the aryl glycoside series is that the combination of two or more structural features on a compound does not appear to have an additive effect on IRI activity. For example, since galactose (**8**) is more IRI-active than glucose (**9**), and *p*-chlorophenyl-β-D-glucopyranoside (**41**) was subsequently discovered to show potent IRI activity, it would be expected that the combination of the *p*-chlorophenyl group with a galactose unit would result in an improvement in IRI activity. However, when assessed at the same concentration, *p*-chlorophenyl-β-D-galactopyranoside (**44**) was in fact found to be less IRI-active.

In conclusion, the results from the synthesis and assessment of aryl glucosides and galactosides indicate that modulation of the electronic properties of the anomeric substituent does not impart a

predictable effect in IRI activity. The lack of a consistent electronic effect on the IRI activity of the compounds screened, along with the absence of an additive effect on IRI activity, suggests that a combination of factors are at play in governing the behaviour of these compounds. While substituting an electron-donating group for an electron-withdrawing group may have a logical effect on activity, it is difficult to separate this effect from other molecular properties which may be conferred by one substituent over another. Further studies are necessary to evaluate the changes these functional groups have on the hydrogen-bonding abilities, hydrophobicity, and solubilities of the overall compounds in question.

References

1. Eniade, A.; Hauer, L.; Ben, R. N., Synthesis of a *C*-linked Antifreeze Glycoprotein (AFGP) Mimic: Probes for Investigating the Mechanism of Action. *Org. Lett.* **1999**, 1, 1759-1762.

2. Liu, S.; Ben, R. N., *C*-Linked Galactosyl Serine AFGP Analogues as Potent Recrystallization Inhibitors. *Org. Lett.* **2005**, 7, 2385-2388.

3. Balcerzak, A. K.; Ferreira, S. S.; Trant, J. F.; Ben, R. N., Structurally diverse disaccharide analogs of antifreeze glycoproteins and their ability to inhibit ice recrystallization. *Bioorg. Med. Chem. Lett.* **2012**, 22, 1719-1721.

4. Tokarew, J., PhD Dissertation, University of Ottawa, **2010**.

5. Chaytor, J. L. *et al.*, Inhibiting ice recrystallization and optimization of cell viability after cryopreservation. *Glycobiology* **2012**, 22, 123-133.

6. Capicciotti, C. J. *et al.*, Potent inhibition of ice recrystallization by low molecular weight carbohydrate-based surfactants and hydrogelators. *Chem. Sci.* **2012**, 3, 1408-1416.

7. Balcerzak, A. K.; Febbraro, M.; Ben, R. N., The importance of hydrophobic moieties in ice recrystallization inhibitors. *RSC Adv.* **2013**, 3, 3232-3236.

8. Czechura, P.; Tam, R. Y.; Dimitrijevic, E.; Murphy, A. V.; Ben, R. N., The Importance of Hydration for Inhibiting Ice Recrystallization with *C*-Linked Antifreeze Glycoproteins. *J. Am. Chem. Soc.* **2008**, 130, 2928-2929.

9. Tam, R. Y.; Ferreira, S. S.; Czechura, P.; Chaytor, J. L.; Ben, R. N., Hydration Index – A Better Parameter for Explaining Small Molecule Hydration in Inhibition of Ice Recrystallization. *J. Am. Chem. Soc.* **2008**, 130, 17494-17501.

10. Trant, J. T.; Doshi, M.; Ben, R. N., unpublished results, **2010**.

11. Capicciotti, C. J.; Mancini, R.; Ben, R. N., unpublished results, **2011**.

12. Perron, V.; Abbott, S.; Moreau, N.; Lee, D.; Penney, C.; Zacharie, B., A Method for the Selective Protection of Aromatic Amines in the Presence of Aliphatic Amines. *Synthesis* **2009**, 2, 283-289.

13. Knight, C. A.; Hallet, J.; DeVries, A. L., Solute effects on ice recrystallization: an assessment technique. *Cryobiology* **1988**, 25, 55-60.

14. Galema, S. A.; Høiland, H., Stereochemical Aspects of Hydration of Carbohydrates in Aqueous Solutions. 3. ^{1}Density and Ultrasound Measurements, *J. Phys. Chem.* **1991**, 95, 5321-5326.

15. Høiland, H.; Hølvik, H., Partial Molar Volumes and Compressibilities of Carbohydrates in Water. *J. Solution Chem.* **1978**, 7, 587-596.

16. Dashnau, J.; Sharp, K. A.; Vanderkooi, J. M., Carbohydrate Intramolecular Hydrogen Bonding Cooperativity and its Effect on Water Structure. *J. Phys. Chem. B* **2005**, 109, 24152-24159.

17. Junquera, E.; Olmos, D.; Aicart, E., Carbohydrate-water interactions of *p*-nitrophenylglycosides in aqueous solution. Ultrasonic and densitometric studies. *Phys. Chem. Chem. Phys.* **2002**, 4, 352-357.

18. Jackman, J.; Noestheden, M.; Moffat, D.; Pezacki, J. P.; Findlay, S.; Ben, R. N., Assessing antifreeze activity of AFGP 8 using domain recognition software. *Biochem. Biophys. Res. Commun.* **2007**, 354, 340-344.

Chapter 4: The Influence of Hydrophobic Moieties on the Ice Recrystallization Inhibition activity of β-*O*-Aryl Glycosides

4.1 Introduction

The mechanism by which biological antifreezes protect organisms against freezing injury has attracted considerable interest over the past several decades. Although these compounds are known to operate by binding to the ice surface to prevent further ice growth, the driving force for this interaction is not well understood.[1] Several hypotheses have emerged suggesting that hydrophobic interactions are an important contributor to this process.[2,3] Structure-function studies carried out on native AFGP by Nishimura *et al.* determined that hydrophobic methyl groups on alanine and threonine residues are essential for antifreeze activity.[4] Unfortunately, these studies focused solely on TH activity and did not test for IRI activity. Hence, our laboratory is interested in better understanding the importance of hydrophobic interactions as they pertain specifically to IRI activity.

Studies by Chaytor and colleagues have shown that the IRI activity of *C*-allylated and fluorinated galactose derivatives is reduced relative to D-galactose.[5,6] Since these moieties are hydrophobic in nature, the results suggest that hydrophobic effects are detrimental to IRI activity. However, more recent studies have contradicted this observation. In separate reports by Capicciotti and Balcerzak, potent IRI activity was observed in amphiphilic carbohydrate- and lysine-based compounds that contain significant hydrophobic moieties.[7,8] Consequently, we sought to systematically investigate the effect of increasing hydrophobic character on the IRI activity of small-molecule carbohydrate derivatives. To this end, we have synthesized two families of aryl glycosides containing hydrophobic alkyl chains of varying size. The alkyl chains of the compounds were installed at the *para*-position of the aryl ring and sequentially lengthened by one methylene unit in order to assess the impact of increasing hydrophobic

character while minimizing steric interactions with the neighbouring carbohydrate ring. The results of this study are described herein.

4.2 Preparation and Assessment of p-alkamidophenyl-β-D-glucopyranosides

From the investigations of *para*-substituted aryl glycosides outlined in Chapter 3, it was observed that acetylation of the aniline group on *p*-aminophenyl-β-D-glucopyranoside (**52**) leads to an increase in IRI activity (Graph 3.2, page 71). This result was not believed to be a consequence of electronic effects since the *N*-acetyl substituent is a weaker activating group than the free aniline. An alternative hypothesis is that the hydrophobic nature of the methyl group on the acetamido substituent is in fact responsible for the increase in activity. To verify this hypothesis and to determine whether the IRI activity could be further optimized, analogues of **52** were synthesized containing one, two or three additional carbons on the acyl chain (**63**-**65**) and were then tested for IRI activity.

*4.2.1 Preparation of p-propionamidophenyl-β-D-glucopyranoside (**63**)*

The initial preparation of the *p*-propionamidophenol (**98**) glycosyl acceptor was envisioned through the selective acylation of *p*-aminophenol using one equivalent of propionyl chloride in pyridine. However, this approach proved unsuccessful, instead leading predominantly to acylation at both amino and hydroxyl groups. In light of this, the bis-acylated compound **97** was obtained in 70% yield using three equivalents of propionyl chloride in pyridine. Subsequent removal of the *O*-acyl group was achieved using 0.1M sodium methoxide in methanol in near-quantitative yields to provide glycosyl acceptor **98**. Reaction of **98** with glucose pentaacetate was carried out in the presence of boron trifluoride diethyletherate to provide the protected glycoside **99**, which was subsequently deprotected to give *p*-propionamidophenyl-β-D-glucopyranoside (**63**).

Scheme 4.1: Synthesis of *p*-propionamidophenyl-β-D-glucopyranoside (**63**).

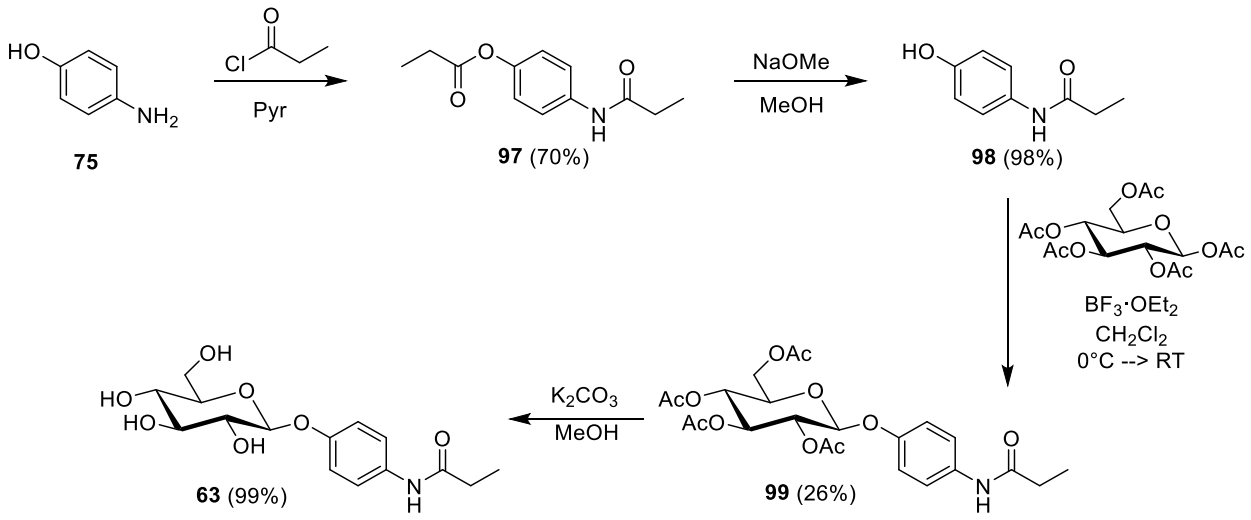

*4.2.2 Preparation of p-butyramidophenyl-*β-D-*glucopyranoside (**64**) and p-pentanamidophenyl-*β-D-*glucopyranoside (**65**).*

The syntheses of the 4- and 5-carbon amide derivatives were accomplished in a similar fashion (Scheme 4.2). In these instances, **75** was reacted with butyryl or valeryl chloride in ice-cold dichloromethane with triethylamine, which was allowed to warm to room temperature after addition. This afforded compounds **100** and **101**, which were then reacted with 0.1M NaOMe in methanol to give **102** and **103**. Subsequent reaction with glucose pentaacetate and acetate deprotection as previously-described (Scheme 4.1) afforded p-butyramidophenyl-β-D-glucopyranoside (**64**) in 16% overall yield and p-pentanamidophenyl-β-D-glucopyranoside (**65**) in 31% overall yield.

Scheme 4.2: Synthesis of *p*-butyramidophenyl-β-D-glucopyranoside (**64**) and *p*-pentanamidophenyl-β-D-glucopyranoside.

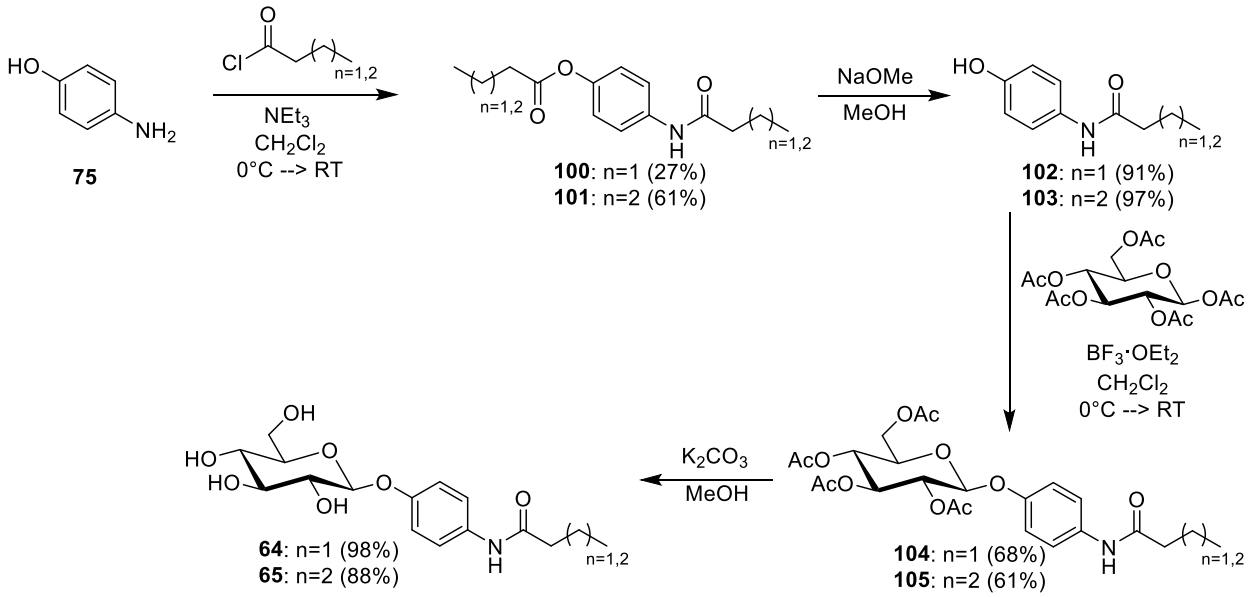

*4.2.3 Assessment of IRI activity of para-substituted alkamidophenyl glucosides (**63-65**).*

Upon completion of the syntheses of amide derivatives (**63-65**), the compounds were tested for ice recrystallization inhibition activity using the previously described IRI assay (Chapter 3, page 69). The activities of these compounds at 22 mM are presented in Graph 4.1 in comparison with *p*-acetamidophenyl-β-D-glucopyranoside (**51**) and *p*-aminophenyl-β-D-glucopyranoside (**52**). It was previously noted that acetylation of the amino group on **52** results in an increase in IRI activity. Graph 4.1 demonstrates that this trend continues as the amide chain is lengthened. The IRI activity of the compounds gradually increases as the *N*-acetyl functional group is replaced with a propionyl (**63**), butyryl (**64**) or valeryl (**65**) acyl chain. While the three-carbon chain of **63** provides only moderate IRI activity, potent activity is observed in compounds **64** and **65**.

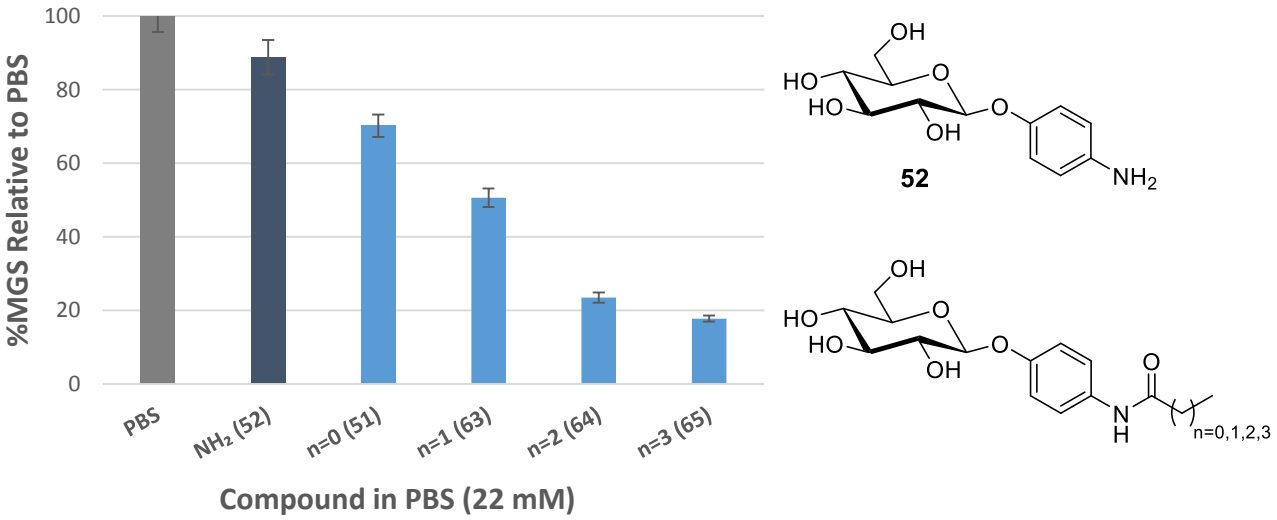

Graph 4.1: IRI activities of *p*-alkamidophenyl-β-D-glucopyranosides (**51**, **63-65**) and *p*-aminophenyl-β-D-glucopyranoside (**52**).

The consistent effect on IRI activity observed in conjunction with step-wise lengthening of the acyl chains in compounds **63-65** suggests that increasing hydrophobic character is beneficial for ice recrystallization inhibition in this series of glycosides. These results are in agreement with studies conducted by Balcerzak and coworkers demonstrating that hydrophobic moieties are important for the IRI ability of lysine derivatives.[8] In their report, the authors noted that increasing IRI activity was observed as longer alkyl and acyl chains were added to the ε-amino group of lysine. While such compounds are structurally quite different from the aryl glycosides of the present study, they are still classified as amphiphiles possessing polar head groups (either a pyranose ring or a carboxyl/α-amino group) as well as a hydrophobic component. Potent IRI activity was also observed in other previously-assessed amphiphilic compounds such as n-ocytl-β-D-galactopyranoside (**18**) and n-octylgluconamide (**21**).[7]

It has been reported that hydrophobic surfaces are capable of altering the surrounding 3D hydrogen bonding network of water.[20] In particular, the presence of these moieties causes nearby water molecules to order themselves around the solute.[20] Tam *et al.* have suggested that carbohydrate-based inhibitors of ice recrystallization act primarily by preventing the ordering of liquid water molecules necessary for the formation of ice, thus slowing the progression of water from the liquid state into a semi-ordered quasi-liquid layer (QLL, Figure 1.13, page 28).[9] Inhibiting liquid water molecules from entering the QLL before joining the ice lattice may be the mechanism by which these small molecules inhibit ice recrystallization. The *N*-acyl substituted aryl glucosides (**51**, **63**-**65**) show an increase in IRI activity with increasing hydrophobic chain length, despite the expected ordering of water molecules around the alkyl groups. This indicates that the ordering of liquid water molecules may not necessarily be detrimental to IRI activity if the induced ordering is of a different 3-dimensional arrangement than the specific arrangement required for an ice lattice. In contrast, the trend in IRI activity observed in Graph 3.1 suggests that this effect may instead be beneficial for IRI activity. It is therefore necessary to pursue further studies with compounds possessing similar hydrophobic character to corroborate this hypothesis.

4.3 Preparation and Assessment of p-alkoxyphenyl-β-D-glucopyranosides

The positive correlation identified between hydrophobic acyl chain length and IRI activity in alkamidophenyl glucosides (**51**, **63**-**65**) prompted further research into whether this phenomenon extends to other aryl glycoside analogues. A similar trend in IRI activity as hydrophobic character is increased would provide further evidence that this property is important for activity in conjunction with the hydrophilic nature of the polar carbohydrate ring. In light of the potent IRI activity of *p*-methoxylphenyl-β-D-glucopyranoside (**33**), the effect of extending the alkoxy chain of this compound

was investigated to examine whether its IRI activity could be further optimized. To this end, a series of *p*-alkoxylphenyl glucosides (**66-68**) possessing an ethoxy, propoxy and butoxy alkyl chain were synthesized and assessed for IRI activity.

*4.3.1 Preparation of p-ethoxyphenyl-β-D-glucopyranoside (**66**) and p-propoxyphenyl-β-D-glucopyranoside (**67**).*

As depicted in Scheme 4.3, the preparation of the ethoxy and propoxy derivatives was accomplished starting from commercially-available *p*-ethoxyphenol (**106**) or *p*-propoxyphenol (**107**). Reaction of the phenols with galactose pentaacetate (**73**) and boron trifluoride diethyletherate as a Lewis acid promoter afforded the acetate-protected glycosides **108** and **109** in 74% and 53% yields respectively. Deprotection of the acetate groups with potassium carbonate in methanol provided *p*-ethoxyphenyl-β-D-glucopyranoside (**66**) in 61% overall yield and *p*-propoxyphenyl-β-D-glucopyranoside (**67**) in 50% overall yield.

Scheme 4.3: Synthetic route towards *p*-ethoxyphenyl-β-D-glucopyranoside (**66**) and *p*-propoxyphenyl-β-D-glucopyranoside (**67**).

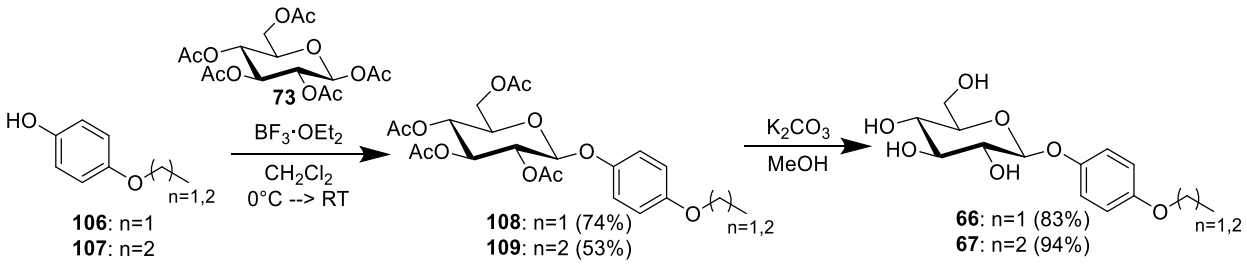

*4.3.2 Synthesis of p-butoxyphenyl-β-D-glucopyranoside (**68**).*

For the synthesis of the butoxy analogue (**68**), several attempts were made to prepare the glycosyl acceptor through alkylation of hydroquinone using butyl iodide. The initial attempt was made using one

equivalent of alkylating agent and cesium carbonate in DMF under refluxing conditions. This provided the desired product in only 12% yield, with a large proportion of bis-alkylated compound as a by-product. Another procedure was performed according to a report by Paul and Gupta involving the zinc-catalyzed alkylation of phenols under base-free conditions in DMF.[12] These conditions were also unsuccessful, as TLC analysis indicated only the presence of starting material after 18 hours at reflux.

The third attempt at alkylation, outlined in Scheme 4.4, proved successful. In this case, hydroquinone (**110**) was refluxed with one equivalent of butyl iodide and potassium carbonate in acetone. While bis-alkylated product was still formed, the yield of monoaklyated phenol was increased to 27%, providing a sufficient amount of *p*-butoxyphenol (**111**) for subsequent steps. The synthesis of the protected aryl glycoside (**112**) was accomplished using previously-described conditions (Scheme 4.3). Acetate deprotection of this compound with potassium carbonate and methanol afforded *p*-butoxyphenyl-β-D-glucopyranoside (**68**) in 19% overall yield.

Scheme 4.4: Synthesis of *p*-butoxyphenyl-β-D-glucopyranoside (**68**).

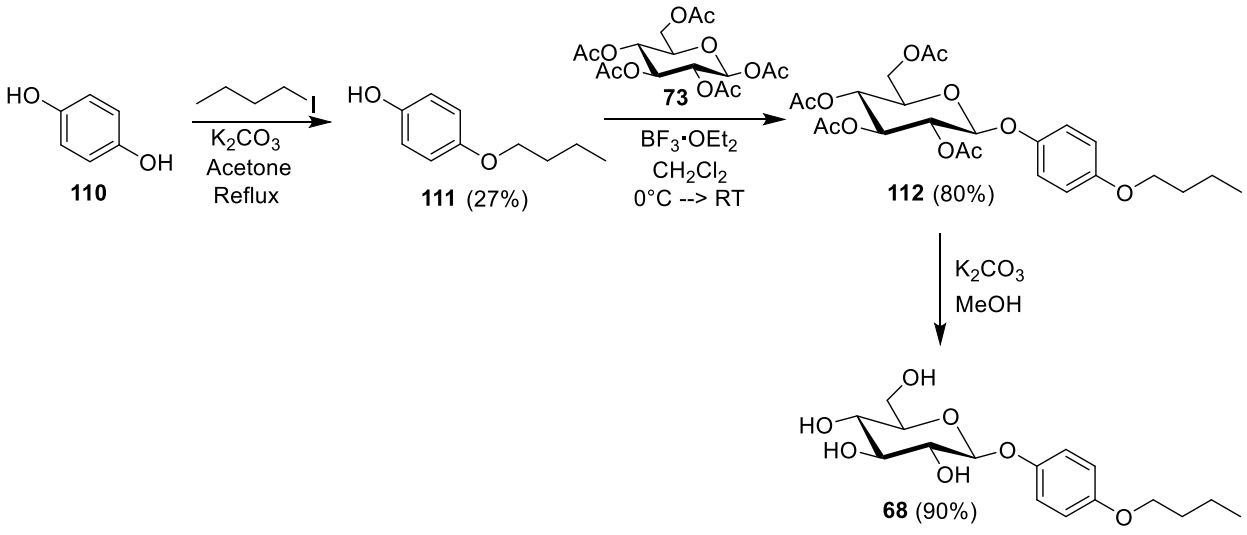

*4.3.3 Assessment of IRI activity of p-alkoxyphenyl-β-D-glucopyranosides (**66-68**).*

The IRI activities of the *p*-ethoxy, propoxy and butoxy derivatives (**66**-**68**) synthesized in this study follow an interesting trend when viewed in conjunction with the previously-assessed *p*-hydroxyphenyl and *p*-methoxyphenyl glucosides (Graph 4.2). As was the case in the acetylation of *p*-aminophenyl-β-D-glucopyranoside (**52**), the addition of a hydrophobic methyl group to the phenolic hydroxyl group of **34** produces a marked increase in IRI activity. If the alkyl substituent is extended by one carbon to an ethyl group, the IRI activity of the glycoside again increases dramatically to approximately 6% mean grain size relative to PBS, making it one of the most active aryl glycosides assessed by our laboratory to date.

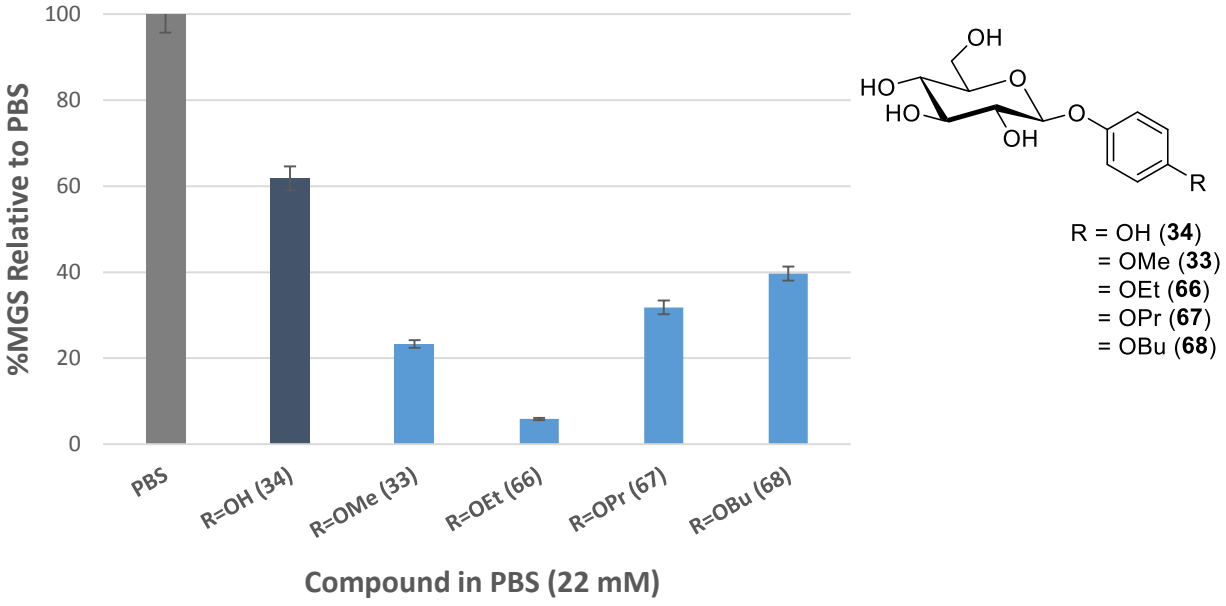

Graph 4.2: IRI activities of *p*-alkoxyphenyl-β-D-glucopyranosides (**33**, **66-68**) and *p*-hydroxyphenyl-β-D-glucopyranoside (**34**).

However, as the alkyl chain is extended further, the opposite effect is observed. Extension of the ethoxy group to a proproxy group (**67**) results in a decrease in IRI activity, while further lengthening

of the chain to a butoxy group (**68**) causes additional loss of potency. Thus, it appears from the data that there is an optimal amount of hydrophobicity that results in maximum IRI activity. The origins and cause of this phenomenon are not currently understood and require further study. However, there is precedent for the concept of an optimal alkyl chain length as it relates to IRI activity in other classes of compounds. It was observed in the lysine derivatives tested by Balcerzak *et al*. that increasing the length of the alkyl chain installed at the amino or carboxyl terminus initially proves beneficial for IRI ability, but only to a certain point as increasing the length of the hydrophobic chains eventually begins to decrease activity.[8] This was speculated to be the result of solubility issues. Similar trends have been observed during investigation of other classes of compounds by our laboratory, including *C*-linked AFGP analogues,[13] β-*S*-linked galactosyl derivatives,[14] and *N*-alkyl-acetamide galactosyl compounds.[15]

One possible reason for the loss of activity observed in compounds **67** and **68** may be that the longer hydrophobic tails they possess increase their propensity to aggregate and/or form micelles as both compounds appeared to be soluble in solution. Although the relationship between micelle formation and IRI activity has not been conclusively determined, Capicciotti *et al.* have studied the IRI abilities of non-ionic surfactants such as n-octyl-β-D-glucoside (**17**) and n-octyl-β-D-galactoside (**18**) for which critical micelle concentration (CMC) values have been reported.[7] Compound **18** was shown to be a potent inhibitor of ice recrystallization at 22 mM concentration and has a CMC value in water of approximately 30 mM. While the assay for IRI is conducted using solutions in PBS, it has been documented that CMC values of non-ionic surfactants are only slightly altered in salt solutions.[16,17] Therefore, it is not expected that **18** will form micelles at a concentration of 22 mM in PBS. In contrast, compound **17** was found to have poor IRI activity at 22 mM, but is capable of forming micelles as its CMC is 18-22 mM. It is unknown whether this difference in IRI activity is due to the presence of micelles or the change of hydroxyl group stereochemistry at C4 relative to compound **18**.

It has not been verified by our laboratory whether glucosides **67** and **68** can form micelles in aqueous solution. However, their solutions at 22 mM show detergent-like properties visible to the naked eye during mixing such as forming and emulsification. If they are capable of associating in solution at the concentrations tested, it would serve as a second example of a class of compound whose IRI activity is reduced in the presence of micelles. Future studies using dynamic light scattering (DLS) techniques will aid in determining the extent of micelle formation of these compounds in solution.[21]

*4.3.4 Assessment of p-ethoxyphenyl-β-D-glucopyranoside (**66**) for Cytotoxicity in Human Cells.*

The highly potent IRI activity of *p*-ethoxyphenyl-β-D-glucopyranoside (**66**) led to further investigation of the viability of this compound as a cryoprotectant. To identify any potential cytotoxic effects, the glycoside was tested in transformed human HepG2 cell line at five concentrations (22 mM, 10 mM, 5 mM, 2 mM, 0.5 mM) using a conventional MTT assay.[18] This assay determines the viability of a cell culture through mitochondrial function. In healthy cells, 3-(4,5-dimethylthiazol-2-yl)-2,5-diphenyltetrazolium bromide, a yellow tetrazole, is converted to a purple-coloured formazan using cellular reducing agents (i.e. NADH or NADPH) that can be quantified at 570 nm wavelength (Figure 4.1).

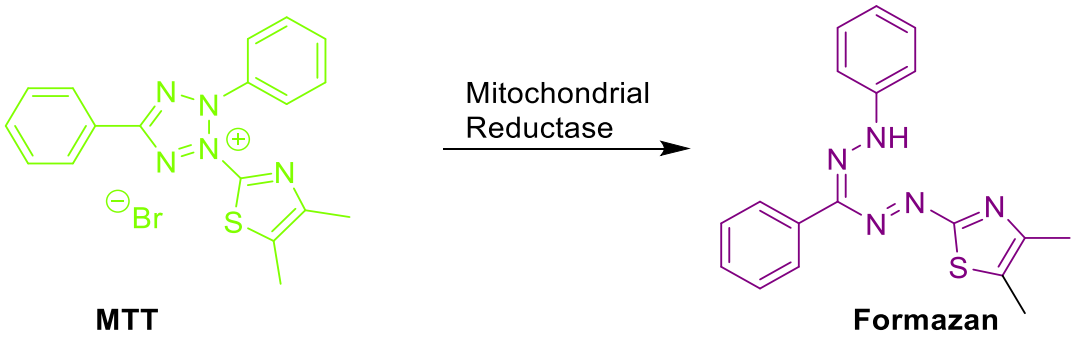

Figure 4.1: Structure of oxidized tetrazole (left) and reduced formazan (right) forms of MTT (3-(4,5-dimethylthiazol-2-yl)-2,5-diphenyltetrazolium bromide) in the colourimetric assay used to determine cell viability.

As outlined in Graph 4.3, the *p*-ethoxyphenyl glucose was not significantly toxic to HepG2 cells at the concentrations tested. At the highest concentration (22 mM), the toxicity of **66** is comparable to that of a 22 mM solution of glucose (**8**) as well as a 2.5% solution of DMSO. Further testing at higher concentrations which are used in cryopreservation protocols (0.2 M to 0.5 M) has yet to be completed. However, although this data is preliminary, initial indications suggest that **66** does not have substantially greater toxicity than the current industry standard. This warrants further investigation of the compound in cell cryopreservation studies as well as more robust cytotoxicity studies.

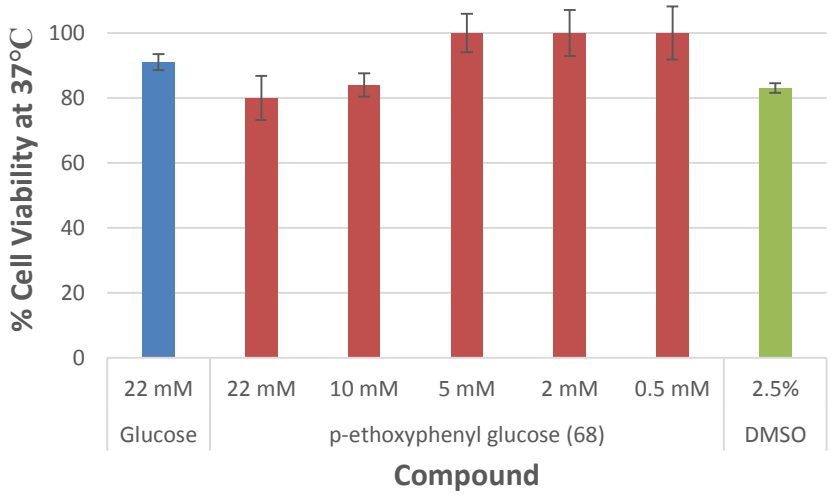

Graph 4.3: Percent viabilities of HepG2 cells incubated at physiological temperature (37°C). Cell viabilities were quantified after 24 hours of exposure using an MTT cytotoxicity assay.[18]

4.4 Summary

Over the course of this study, it has been demonstrated that the addition of hydrophobic functional groups to aryl glycosides can be used to govern the IRI activity of these compounds. In two separate sub-classes of compounds, a reproducible effect was identified whereby increasing hydrophobic character imparted increased IRI activity relative to the unmodified, more polar reference compounds. In the *p*-alkamidophenyl-β-D-glucosides (**51**, **63**-**65**), the incremental addition of carbon

atoms to the acyl chain led to increased IRI potency throughout the entire series. Similarly, the alkylation of *p*-hydroxyphenyl-β-D-glucoside (**34**) analogues results in increased IRI activity. The results show that the addition of a single methylene unit to the glycosides examined can result in significant changes in potency. As such, the installation of hydrophobic functional groups may present a novel strategy in optimizing the IRI activity of other compounds of interest.

It was noted in earlier studies that alkylation of *p*-hydroxyphenyl glucose (**34**) to *p*-methoxyphenyl glucose (**33**), or acetylation of *p*-aminophenyl glucose (**52**) to *p*-acetamidophenyl glucose (**51**) increases the IRI activity of the glycosides. In the absence of other data, this increase in potency could equally be attributed to either a loss of hydrogen bond donation by the hydroxyl or amino groups or an increase in hydrophobic character. However, further lengthening of the acetyl or methoxy groups by one methylene unit continues to improve the IRI activity of each series without changing the hydrogen bonding abilities of either functionality. This observation provides evidence that the modulation of IRI activity is indeed due to hydrophobic effects and not a change in the hydrogen bonding characteristics of the aryl substituent. Therefore, we attribute the large variations in IRI activity in the alkamidophenyl and alkoxyphenyl glucoside series to the hydrophobic nature conferred by each additional methylene unit.

In the case of the *p*-alkoxyphenyl glucoside family, the installation of propoxy and butoxy groups results in a decrease in IRI activity. This is in contrast to the addition of methoxy or ethoxy groups, which were beneficial for activity. This effect is in agreement with previous studies involving modulation of alkyl chains on *C*-linked AFGP analogues and small-molecule galactosides; assessment of these compounds also revealed that there is an optimal alkyl chain length for potent IRI activity.[13-15] We therefore conclude from this observation that a balance between hydrophobicity and hydrophilicity is required in order to maximize the IRI ability of a compound. The loss of activity caused by extension of the hydrophobic tail in the alkoxyphenyl series may be due to loss of solubility or association of the

molecules into micelles as the compound becomes more hydrophobic. It is hypothesized that further extension of the acyl chain in the *p*-alkamidophenyl glucoside series will eventually impair IRI activity in a similar fashion.

References

1. Raymond, J. A.; DeVries, A. L., Adsorption inhibition as a mechanism of freezing resistance in polar fishes. *Proc. Natl. Acad. Sci. USA.* **1977**, 74, 2589-2593.

2. Harding, M. M.; Ward, L. G.; Haymet, A. D. J., Type I "antifreeze" proteins. *FEBS J.* **1999,** 264, 653-655.

3. Davies, P. L.; Sykes, B. D., Antifreeze Proteins. *Curr. Opin. Struct. Biol.* **1997**, 7, 828-834.

4. Tachibana, Y.; Fletcher, G. L.; Fujitani, N.; Tsuda, S.; Monde, K.; Nishimura, S., Antifreeze glycoproteins: Elucidation of the structural motifs that are essential for antifreeze activity. *Angew. Chem. Int. Ed.* **2004**, 43, 856-862.

5. Chaytor, J. L.; Ben, R. N., Assessing the ability of a short fluorinated antifreeze glycopeptide and a fluorinated carbohydrate derivative to inhibit ice recrystallization. *Bioorg. Med. Chem. Lett.* **2010**, 17, 5251-5254.

6. Chaytor, J. L., Ph.D. Dissertation, University of Ottawa, **2010**.

7. Capicciotti, C. J. *et al.*, Potent inhibition of ice recrystallization by low molecular weight carbohydrate-based surfactants and hydrogelators. *Chem. Sci.* **2012**, 3, 1408-1416.

8. Balcerzak, A. K.; Febbraro, M.; Ben, R. N., The importance of hydrophobic moieties in ice recrystallization inhibitors. *RSC Adv.* **2013**, 3, 3232-3236.

9. Tam, R. Y.; Ferreira, S. S.; Czechura, P.; Chaytor, J. L.; Ben, R. N., Hydration Index – A Better Parameter for Explaining Small Molecule Hydration in Inhibition of Ice Recrystallization. *J. Am. Chem. Soc.* **2008**, 130, 17494-17501.

10. Dashnau, J.; Sharp, K. A.; Vanderkooi, J. M., Carbohydrate Intramolecular Hydrogen Bonding Cooperativity and Its Effect on Water Structure. *J. Phys. Chem. B* **2005**, 109, 24152–24159.

11. Caffarena, E. R.; Grigera, J. R., On the hydrogen bond structure of water at different densities. *Physica A*, **2004**, 342, 34-39.

12. Paul, S.; Gupta, M., Zinc-catalyzed Williamson ether synthesis in the absence of base. *Tett. Lett.* **2004**, 45, 8825-8829.

13. Tam, R. Y.; Rowley, C. N.; Petrov, I.; Zhang, T.; Afagh, N. A.; Woo, T.; Ben, R. N., Solution Conformation of C-Linked AFGP Analogues and Modulation of Ice Recrystallization Inhibition Activity. *J. Am. Chem. Soc.* **2009**, 131, 15745.

14. Tokarew, J. Ph.D. Dissertation, University of Ottawa, **2011**.

15. Trant, J. T.; Biggs, R.; Ben, R.N., unpublished results, **2009**.

16. Helenius, A.; Simons, K., Solubilization of membranes by detergents. *Biochim. Biophys. Acta, Rev. Biomembr.,* **1975**, 415, 29.

17. Ray, A.; Nemethy, G., Effects of ionic protein denaturants on micelle formation by non-ionic detergents. *J. Am. Chem. Soc.* **1971**, 93, 6787-6793.

18. Mosmann, T., Rapid colorimetric assay for cellular growth and survival: Application to proliferation and cytotoxicity assays. *J. Immunol. Methods.* **1983**, 65, 55-63.

19. Czechura, P.; Tam, R.Y.; Dimitrijevic, E; Murphy, A.V; Ben, R. N., The Importance of Hydration for Inhibiting Ice Recrystallization with C-Linked Antifreeze Glycoproteins, *J. Am. Chem. Soc.* **2008**, 130, 2928-2929.

20. Biffinger, J. C.; Kim, H. W.; DiMagno, S. G., The Polar Hydrophobicity of Fluorinated Compounds. *ChemBioChem* **2004**, 5, 622-627.

21. Gracia, C. A.; Gomez-Barreiro, S.; Gonzalez-Perez, A.; Nimo, J.; Rodriguez, J. R., Static and dynamic light-scattering studies on micellar solutions of alkyldimethylbenzylammonium chlorides. *J. Colloid Interface Sci.* **2004**, 276, 408-413.

Chapter 5: Future Directions

5.1 Continued investigation of the effect of additional hydrophobic character on the IRI activity of small molecules.

From the research presented in Chapter 4, a positive correlation was identified between the IRI activities of *p*-alkoxyphenyl and *p*-alkamidophenyl glucosides and the length of their alkyl or acyl chain. These results suggest that the hydrophobic character of the chains may be responsible for the increase in activity in the two series of glycosides. If so, the addition of hydrophobic moieties to investigational compounds would represent a novel strategy towards optimizing the IRI activity of small molecules, potentially leading to the rational discovery of new cryoprotectants. In light of these results, work should be continued on the development of other series of carbohydrate-based small molecules with varying hydrophobic character. This will provide further insight into the scope and applicability of this phenomenon and may lead to the identification of other highly-IRI active compounds. Figure 5.1 shows several potential aryl glycoside series with linear hydrophobic chains that could be prepared to this effect.

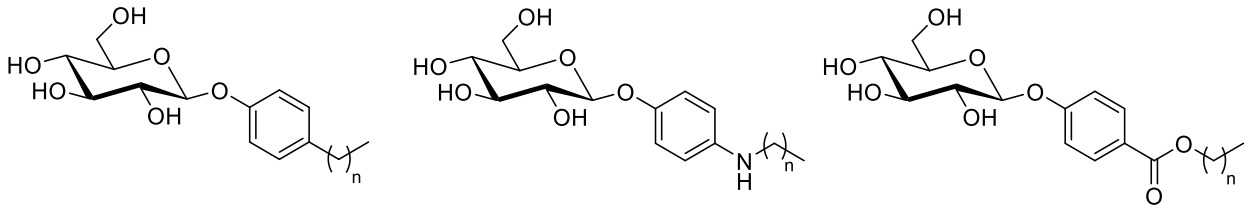

Figure 5.1: Structures of potential glucopyranoside derivatives containing alkylphenyl, *N*-alkylphenyl and alkyl benzoate aryl substituents.

Because the nature of hydrophobic effects on IRI activity are not yet understood, additional types of hydrophobic moieties should also be considered for assessment. The alkyl or acyl chains which have so far been installed have been limited to unbranched hydrocarbon chains. The addition of branched-chain derivatives (Figure 5.2A) to these compounds would represent another avenue of

investigation by adding steric bulk to the hydrophobic portion of the glycosides. Previous computational studies of nonpolar solutes in aqueous environments have indicated that branched alkanes have lower hydration values than their unbranched counterparts.[1,2] However, the effect of hydrocarbon branching on the IRI ability of a substrate has not yet been studied. Perfluorinated carbon chains are another intriguing functional group due to the enhanced hydrophobicity they possess relative to hydrocarbons (Figure 5.2B).[3] Using ultrasonic relaxation studies, Tiddy and coworkers have shown that the hydration number of perfluorinated surfactants is greater than their non-fluorinated counterparts.[4] Additionally, preliminary work by Briard *et al*. has indicated that, in some cases, fluorinated aldonamide derivatives display more potent IRI activity than non-fluorinated derivatives.[5] The mechanisms behind these differences are still being elucidated. Therefore, it is of interest to gauge the effect that these moieties may have on the IRI activity of aryl glycosides.

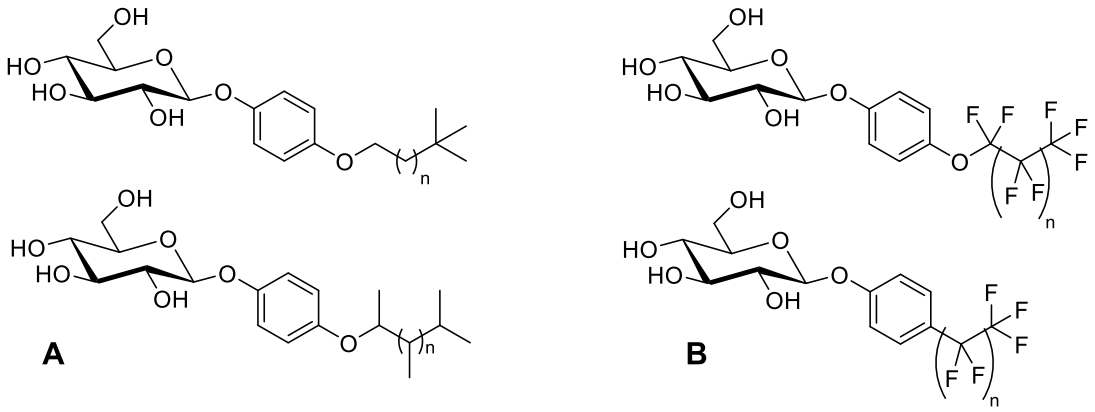

Figure 5.2: Examples of potential aryl glycoside targets possessing (**A**) branched hydrocarbon chains and (**B**) perfluorinated carbon chains.

The studies undertaken to examine the effect of hydrophobic chain length on IRI activity have so far focused exclusively on aryl glucosides. It would therefore be interesting to determine whether a similar trend in activity can be observed in the corresponding aryl galactosides. Although the aryl galactosides assessed for IRI activity in Chapter 3 were found to be generally less active overall (Graph 3.3, page 72), past studies have identified that galactose-based compounds generally display higher IRI

activity than their glucose analogues.[6] This has previously been explained by the documented correlation between carbohydrate hydration and IRI activity - galactose is more hydrated than glucose and is therefore expected to confer greater IRI activity.[7] The reasons as to why this hypothesis does not hold true in aryl glycosides is unclear and warrants further study.

5.2 Towards an understanding of the empirical basis for the link between hydrophobicity and IRI activity.

The correlation between hydrophobic character and IRI activity which was identified in Chapter 4 presents several questions which must be further addressed. Since hydrophobic surfaces have been reported to be less hydrated than hydrophilic surfaces,[8,9] it is expected that lengthening the alkyl or acyl chain of an aryl glycoside would reduce its overall hydration. However, it has been previously shown that increasing hydration generally results in an increase in IRI activity.[7] These two results at first seem contradictory. Additionally, hydrophobic moieties such as hydrocarbons and fluorocarbons have been shown to induce ordering of water molecules around the solute.[10] As a result, the increased IRI activity observed with increasing alkyl chain length in the alkamido and akoxy glycosides is suspected to be concurrent with an increase in the ordering of liquid water around the compounds. The relationship between these two processes is not yet understood.

Based on these results, further research is necessary in order to clarify the link between hydrophobicity and IRI activity. One way of doing so would be to quantitatively measure the degree of hydrophobicity of a series of compounds and then compare the IRI activities of these compounds with their hydrophobicity values. If a correlation is identified between IRI activity and hydrophobicity, it would provide further evidence that hydrophobic effects are beneficial for IRI activity in this class of compounds. One method of quantifying lipophilicity is to calculate the partition coefficient of a compound between immiscible organic and aqueous phases (usually octanol and buffer solution,

respectively).[11,12] This coefficient is termed the Log P and is commonly used in medicinal chemistry.[11,12] A number of standardized methods have been developed to measure this value, including analytical techniques such as reversed-phase HPLC, capillary electrophoresis, as well as traditional "shake flask" methods.[13] In addition, many commercial software packages are available which provide quick, reliable and inexpensive *in silico* prediction of Log P values.[13] Using these methods, the hydrophobicity of current and future aryl glycoside series can be routinely determined, which may provide insight into the specific effects of hydrophobicity on IRI activity.

The IRI activity profile of the *p*-alkoxyphenyl-β-D-glucosides (**33, 34, 66-68**) also warrants further study. In particular, it is not entirely clear as to why the activity of the series first increases with additional alkyl chain length but then begins to decrease. One possibility is that, with increasing alky chain length, the glycosides develop surfactant-like properties and begin to associate or form micelles. This may reduce their ability to interact with the surrounding network of water which would impair their IRI ability. One way of exploring this possibility is through the use of dynamic light scattering (DLS) techniques, which can assess the micelle characteristics of surfactants.[14] DLS measurements of the *p*-alkoxyphenyl and *p*-alkamidophenyl glucosides will help to determine whether these compounds are aggregating in solution. If so, the degree of micelle formation can be cross-referenced with the IRI activity of each glycoside. In addition, varying the concentration of the solutions above and below the critical micelle concentration (CMC) combined with reassessment of IRI activity at these concentrations may help to identify the relationship between micelle formation and ice recrystallization inhibition. If IRI can be modulated based on the proportion of micelles in a sample, it would provide further evidence of a link between these two processes.

References

1. Jorgensen, W. L.; Gao, J.; Ravimohan, C., Monte Carlo Simulations of Alkanes in Water: Hydration Numbers and the Hydrophobic Effect. *J. Phys. Chem.* **1985**, 89, 3470-3473.

2. Ghadar, Y.; Clark, A. E., Coupled-cluster, Möller Plesset (MP2), density fitted local MP2, and density functional theory examination of the energetic and structural features of hydrophobic solvation: Water and pentane. *J. Chem. Phys.* **2012**, 136, 05305.

3. Dalvi, V. H.; Rossky, P. J., Molecular origins of fluorocarbon hydrophobicity. *Proc. Natl. Acad. Sci.* **2010**, 107, 13603-13607.

4. Tiddy, G. J. T.; Walsh, M. F.; Wyn-Jones, E., Ultrasonic Relaxation Studies of Concentrated Surfactant Solutions and Liquid Crystals. *J. Chem. Soc., Faraday Trans. 1* **1982**, 78, 389-401.

5. Briard, J.; Capicciotti, C. J.; Ben, R.N., unpublished results, **2013**.

6. Czechura, P.; Tam, R.Y.; Dimitrijevic, E; Murphy, A.V; Ben, R. N., The Importance of Hydration for Inhibiting Ice Recrystallization with C-Linked Antifreeze Glycoproteins, *J. Am. Chem. Soc.,* **2008**, 130 (10) 2928-2929.

7. Tam, R. Y.; Ferreira, S. S.; Czechura, P.; Chaytor, J. L.; Ben, R. N., Hydration Index – A Better Parameter for Explaining Small Molecule Hydration in Inhibition of Ice Recrystallization. *J. Am. Chem. Soc.* **2008**, 130, 17494-17501.

8. Dashnau, J.; Sharp, K. A.; Vanderkooi, J. M., Carbohydrate Intramolecular Hydrogen Bonding Cooperativity and Its Effect on Water Structure. *J. Phys. Chem. B* **2005**, 109, 24152–24159.

9. Caffarena, E. R.; Grigera, J. R., On the hydrogen bond structure of water at different densities. *Physica A*, **2004**, 342, 34-39.

10. Biffinger, J. C.; Kim, H. W.; DiMagno, S. G., The Polar Hydrophobicity of Fluorinated Compounds. *ChemBioChem* **2004**, 5, 622-627.

11. Hansch, C.; Leo, A.; Hoekman, D., *Exploring QSAR. Fundamentals and applications in chemistry and biology, volume 1. Hydrophobic, electronic and steric constants, volume 2*. Oxford University Press: Oxford, **1995**.

12. Kerns, E.; Di, L., *Drug-like Properties: Concepts, Structure Design, and Methods: From ADME to Toxicity Optimization*. Academic Press: London, **2008**, p.43.

13. Kerns, E.; Di, L., *Drug-like Properties: Concepts, Structure Design, and Methods: From ADME to Toxicity Optimization*. Academic Press: London, **2008**, pp. 260-267.

14. Gracia, C. A.; Gomez-Barreiro, S.; Gonzalez-Perez, A.; Nimo, J.; Rodriguez, J. R., Static and dynamic light-scattering studies on micellar solutions of alkyldimethylbenzylammonium chlorides. *J. Colloid Interface Sci.* **2004**, 276, 408-413.

Chapter 6: Experimental

6.1 General Procedures

6.1.1 Ice Recrystallization Inhibition (IRI) Assay

IRI activities were measured using the "splat cooling" method as previously described.[1] 10 µL of the analyte dissolved in phosphate buffered saline (PBS) is dropped from a height of 2 m onto a polished, pre-cooled aluminium block at -78°C. The flash-frozen droplet forms an ice wafer of approximately 1 cm diameter and 20 µm thickness, which is then transferred to a cryostorage unit and held at -6.4°C. After 30 min of annealing, the ice wafer is photographed between crossed polarizing filters using a Nikon CoolPix 5000 digital camera fitted to a microscope. Three ice wafers are prepared for each sample and three photographs are taken of each wafer. From each photograph, the sizes of twelve ice crystals are analyzed using domain recognition software (DRS)[2] which chooses ice crystals at random and calculates their areas using the equation:

$$A = \frac{1}{2}\sum_{i=0}^{N-1}(x_i y_{i+1} - x_{i+1} y_i)$$

Where N is the number of vertices and Σ_{x0}, Σ_{y0} to Σ_{xN-1}, Σ_{yN-1} are the vertices surrounding the polygon in a clockwise direction. The mean grain (ice crystal) size (MGS) of each analyte was compared to the MGS of a PBS solution control as determined on the day of testing. All data are plotted and analyzed using Microsoft Excel with IRI activities reported as a percentage of the MGS (% MGS) relative to the PBS control. Error bars for IRI activity are calculated by dividing the standard error of the mean (SEM) by the average MGS of the PBS control for the same day of testing.

6.1.2 Cell Culture

HepG2 human liver hepatocellular carcinoma cells (ATCC, HB-8065) were cultured in Eagle's minimum essential media (MEM; Sigma-Aldrich, M4655) supplemented with 10% fetal bovine serum (FBS; Fisher, 361015856, supplier number SH30397-3C, Ottawa, ON), 1% penicillin-streptomycin (Sigma-Aldrich, P4333), 1% non-essential amino acids (Sigma, Aldrich, M7145) and sodium pyruvate (Sigma-Aldrich, P5280, final concentration of 1 mM) in 75 cm^2 flasks supplied by Corning® (Fisher, 10-126-37). Cells were incubated in a 37°C incubator supplied with 5% CO_2. All cells were removed from the plates using a trypsin-EDTA solution (Sigma-Aldrich, T4174) for use in experiments. Passages 5-18 of the cells were used in this study. No evidence of overgrowth or morphological changes consistent with apoptosis were observed.[3]

6.1.3 Cytotoxicity Assay

Assessment of cytotoxicity of test compounds was performed using the MTT assay as previously described.[3] Cells were plated in 96-well plates and were treated with 100 µL of 22, 10, 5, 2, or 0.5 mM analyte dissolved in minimum essential medium (MEM) and incubated at 37°C for 18 h. Cells incubated with MEM in the absence of analyte served as the positive control, while cells treated with 1% Triton X-100 (Aldrich, X100) served as the negative control. Following addition of 50 µL MTT (Sigma M5655) solution (5 mg/mL) in Hank's balanced salt solution (HBSS, Sigma, H8264) and 200 µL MEM, the plates were incubated at 37°C with 5% CO_2 for 4 h. The plates were then centrifuged at 1000 RPM for 5 minutes and the solution was aspirated. 100 µL of MTT solubilization solution (10% Triton X-100 with 0.1 N HCl in isopropanol) was added to each well. The plates were kept covered in the dark for 1 h at room temperature and the absorbance of each well was then read at a wavelength of 570 nm with a multi-well plate reader (AD 340C Absorbance Detector, Beckman Coulter, Inc.). Cell viabilities were reported as a percentage of the positive control. All experiments were repeated at least two times in 16 consecutive wells for each condition or analyte concentration. Error bars for cell viability was reported as the standard error of the mean (SEM) for each sample.

6.1.4 General Experimental Conditions

All anhydrous reactions were carried out in flame-dried glassware under a positive pressure of dry argon. Air- or moisture-sensitive reagents and anhydrous solvents were transferred with oven-dried syringes or cannulae. Flash chromatography was performed using E. Merck silica gel (230-400 mesh). Solution-phase reactions were monitored using analytical thin layer chromatography (TLC) with E. Merck 0.2 mm pre-coated silica gel aluminium plates 60 F254; compounds were visualized by illumination with short-wavelength (254 nm) ultraviolet light and/or staining with ceric ammonium molybdate staining solution. Anhydrous dichloromethane (DCM) used for reactions was purified using an LC Technology Solutions SPBT-1 bench top solvent purification system. Pyridine was dried extensively over activated 4Å molecular sieves under argon.

^{1}H NMR (300, 400 or 500 MHz) and ^{13}C NMR (75, 100 or 125 MHz) spectra were recorded at ambient temperature on a Bruker Avance (300, 400 or 500), Avance II 300 or Varian Inova 500 spectrometer. Deuterated chloroform ($CDCl_3$), acetone ($(CD_3)_2CO$), methanol (CD_3OD) or water (D_2O) were used as NMR solvents, unless otherwise stated. Chemical shifts are reported in ppm downfield from tetramethylsilane (TMS) and corrected using the solvent residual signal as a reference. Splitting patterns are designated as follows: s, singlet; d, doublet; t, triplet; q, quartet; quin, quintet; hex, hextet; m, multiplet and br, broad. Low-resolution mass spectrometry (LRMS) was performed on a Micromass Quattro-LC electrospray spectrometer with a pump rate of 20 µL/min using electrospray ionization (ESI).

6.2 Synthesis of O-Aryl Glycosides and Related Derivatives

6.2.1 Methyl 4-hydroxybenzoate (71) [4]

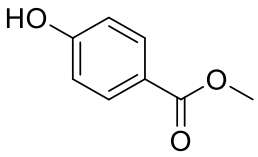

4-hydroxybenzoic acid (500 mg, 3.62 mmol) was added to a flame-dried, 100 mL round bottom flask and placed under an atmosphere of argon. The solid was dissolved in 20 mL of methanol at 0^{O}C and thionyl chloride (0.394 mL, 5.43 mmol) was added dropwise. The mixture was stirred overnight at room temperature, then the solvent was evaporated under reduced pressure. Saturated aqueous sodium bicarbonate solution was added to the residue, which was then extracted with 3x50 mL EtOAc. The combined organic layers were washed with $NaHCO_3$, brine, and dried with $MgSO_4$, and the solvent was removed under reduced pressure to yield white crystals (517 mg, 94%). ^{1}H NMR (300 MHz, $CDCl_3$) δ_H 3.89 (s, 3H), 5.48 (s, 1H), 6.86 (dd, 2H, *J*=8.9, 2.1Hz), 7.96 (dd, 2H, *J*=8.9, 2.1Hz). ^{13}C NMR (75 MHz, $CDCl_3$) δ_c 52.20, 115.39, 122.58, 132.11, 160.24, 167.42. LRMS (ESI$^-$): Calculated 152.15, Found 150.97 $[M-H]^-$.

6.2.2 Methyl 4-(2,3,4,6-tetra-*O*-acetyl-β-D-galactopyranosyloxy)benzoate (72)

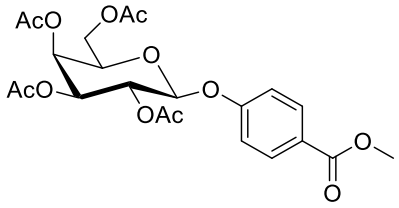

1,2,3,4,6-penta-*O*-acetyl-β-D-galactopyranoside (600 mg, 1.537 mmol) and compound **71** (257 mg, 1.691 mmol) were added to a 50 mL flame-dried round bottom flask charged with argon and 4Å molecular sieves. The compounds were dissolved in anhydrous CH_2Cl_2 (20 mL) and stirred at 0^{O}C for 30 minutes. $BF_3{\cdot}OEt_2$ (1.90 mL, 15.37 mmol) was then added dropwise and the reaction mixture was stirred overnight at room temperature. The contents were then filtered over a bed of celite and water (50 mL) was added. The organic layer was separated and the aqueous layer was extracted with CH_2Cl_2 (3 x 50 mL). The combined organic fractions were washed with $NaHCO_3$ (sat. aq.) and brine, dried with $MgSO_4$, and then filtered and concentrated under reduced pressure. The crude residue was purified by column chromatography (80:20 - 75:25 Hexanes:EtOAc) to give the product as white crystals (411 mg, 55%). ^{1}H NMR (300 MHz, $CDCl_3$) δ_H 2.02 (s, 3H), 2.06 (s, 3H), 2.07 (s, 3H), 2.18 (s, 3H), 3.89 (s, 3H), 4.06-4.26 (m, 3H), 5.12 (dd, 1H, *J*=10.5, 3.4Hz), 5.13 (d, 1H, *J*=7.9Hz), 5.47 (dd, 1H, *J*=3.5, 1.0Hz), 5.51 (dd, 1H, *J*=10.5, 7.9Hz), 7.01 (dd, 2H, *J*=8.9, 2.0Hz), 8.00 (dd, 2H, *J*=8.9, 2.0Hz). ^{13}C NMR (75 MHz, $CDCl_3$) δ_c 20.71, 20.79, 20.81, 20.86, 52.21, 61.54, 66.93, 68.60, 70.87, 71.40, 98.92, 116.27, 125.18, 131.71, 160.37, 166.60, 169.47, 170.23, 170.33, 170.49. LRMS (ESI$^+$): Calculated 482.14, Found 521.20 $[M+K]^+$.

6.2.3 Methyl 4-(β-D-galactopyranosyloxy)benzoate (47)

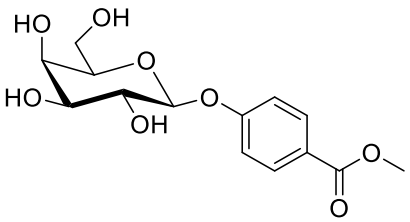

Compound **72** (409 mg, 0.848 mmol) and potassium carbonate (12 mg, 0.0848 mmol) were dissolved in methanol (15 mL) in a 100 mL round bottom flask. The contents were stirred for two hours at room temperature. Amberlite IR resin (H+ form, pH=4) was pre-rinsed with MeOH and then added to the mixture, which was stirred for an additional 10 minutes until a pH of 5 to 6. The mixture was filtered and the solvent was removed under reduced pressure. The product was recrystallized in MeOH/CH_2Cl_2 to afford white crystals (181 mg, 68%). ^{1}H NMR (300 MHz, D_2O) δ_H 3.74-3.86 (m, 4H), 3.88 (s, 3H), 3.91 (m, 1H), 4.00 (d, 1H, *J*= 3.16Hz), 5.15 (d, 1H, *J*=7.5Hz), 7.18 (dd, 2H, *J*=8.9Hz, 1.8Hz), 7.99 (dd, 2H, *J*=8.9, 1.8Hz). ^{13}C NMR (75 MHz, D_2O) δ_c 52.45, 60.64, 68.36, 70.36, 72.42, 75.48, 99.94, 116.00, 123.79, 131.61, 160.63, 168.90. LRMS (ESI$^+$): Calculated 314.29, Found 353.11 $[M+K]^+$.

6.2.4 4-(β-D-galactopyranosyloxy)-benzoic acid (46)

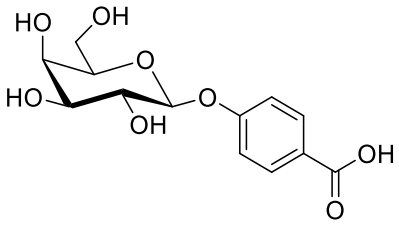

Compound **47** (160 mg, 0.509 mmol) and lithium hydroxide (37 mg, 1.527 mmol) were dissolved in a 2:1 mixture of H_2O:THF (10 mL) in a 50 mL flame-dried round bottom flask. The reaction mixture was stirred for 3 hours at room temperature. Amberlite IR-120 resin (H+ form, pH=4) was pre-rinsed with MeOH and then added to the mixture, which was stirred for an additional 10 minutes until a pH of 5 to 6. The mixture was filtered and the solvent evaporated under reduced pressure to yield the desired product as white crystals (153 mg, 99%). ^{1}H NMR (300 MHz, D_2O) δ_H 3.73-3.87 (m, 4H), 3.90 (dd, 1H, *J*=6.0Hz, 1.0Hz), 4.00 (dd, 1H, *J*=3.2Hz, 0.9Hz), 5.14, (d, 1H, *J*=7.3Hz), 7.16 (dd, 2H, 8.9Hz, 2.0Hz), 7.96 (dd, 2H, 8.9Hz, 2.0Hz). ^{13}C NMR (75 MHz, D_2O) δ_c 60.63, 68.40, 70.38, 72.44, 75.47, 100.00, 115.92, 125.29, 131.70, 160.33, 171.07. LRMS (ESI$^+$): Calculated 300.08, Found 339.10 $[M+K]^+$.

6.2.5 Methyl 4-(2,3,4,6-tetra-*O*-acetyl-β-D-glucopyranosyloxy)benzoate (74)

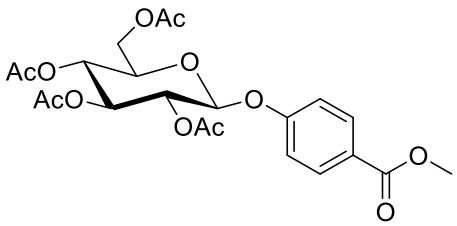

1,2,3,4,6-penta-*O*-acetyl-β-D-glucopyranoside (300 mg, 0.769 mmol) and compound **71** (129 mg, 0.845 mmol) were added to a 50 mL flame-dried round bottom flask charged with argon and 4Å molecular sieves. The compounds were dissolved in anhydrous CH_2Cl_2 (20 mL) and stirred at 0^{O}C for 30 minutes. $BF_3{\cdot}OEt_2$ (1.90 mL, 15.37 mmol) was then added dropwise and the reaction mixture was stirred overnight at room temperature. The contents were then filtered over a bed of celite and then quenched with sodium bicarbonate (sat. aq., 50 mL). The organic layer was separated and the aqueous layer was extracted with CH_2Cl_2 (3 x 50 mL). The combined organic fractions were washed with $NaHCO_3$ (sat. aq.) and brine, dried with $MgSO_4$, and then filtered and concentrated under reduced pressure. The crude residue was purified by column chromatography (80:20 - 75:25 Hexanes:EtOAc) to give the product as white crystals (190 mg, 39%). ^{1}H NMR (300 MHz, $CDCl_3$) δ_H 2.02 (s, 3H), 2.03 (s, 3H), 2.04 (s, 3H), 2.05 (s, 3H), 3.87 (s, 3H), 3.89-3.94 (m, 1H), 4.15 (dd, *J*= 12.2 Hz, 2.5 Hz, 1H), 4.27 (dd, *J*=12.2 Hz, 5.4 Hz, 1H), 5.12-5.19 (m, 2H), 5.24-5.31 (m, 2H), 6.99 (d, *J*=8.9 Hz, 2H), 7.97 (d, *J*=8.9 Hz, 2H). ^{13}C NMR (75 MHz, $CDCl_3$) δ_c 51.94, 61.82, 68.11, 70.94, 72.06, 72.49, 98.04, 116.07, 124.91, 131.46, 160.11, 166.27, 169.12, 169.29, 170.03, 170.36. LRMS (ESI$^+$): Calculated 482.14, Found 521.02 $[M+K]^+$.

6.2.6 Methyl 4-(β-D-glucopyranosyloxy)benzoate (37)

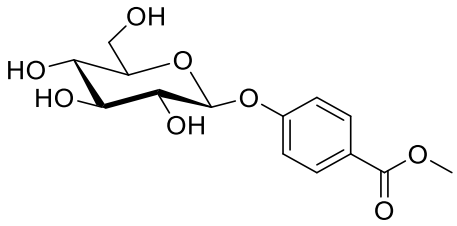

Compound **74** (248 mg, 0.514 mmol) and potassium carbonate (7 mg, 0.0514 mmol) were dissolved in methanol (10 mL) in a 50 mL round bottom flask. The contents were stirred overnight at room temperature. Amberlite IRC-76 resin (H+ form, pH=4) was pre-rinsed with MeOH and then added to the mixture, which was stirred for an additional 10 minutes until a pH of 5 to 6. The mixture was filtered and the solvent was removed under reduced pressure to yield white crystals (160 mg, 99%). ^{1}H NMR (300 MHz, D_2O) δ_H 3.46-3.53 (m, 1H), 3.54-3.78 (m, 3H), 3.89 (s, 3H), 3.93 (dd, *J*=12.1, 2.1 Hz, 1H), 5.22 (d, *J*=7.6 Hz, 1H), 7.18 (d, *J*=8.9 Hz, 2H), 8.01 (d, *J*=8.9 Hz, 2H). ^{13}C NMR (75 MHz, D_2O) δ_c 53.16, 61.10, 69.99, 73.46, 76.11, 76.84, 100.06, 116.73, 132.33, 161.18, 169.60. LRMS (ESI$^-$): Calculated 314.10, Found 312.99 $[M-H]^-$.

6.2.7 4-(β-D-glucopyranosyloxy)-benzoic acid (50)

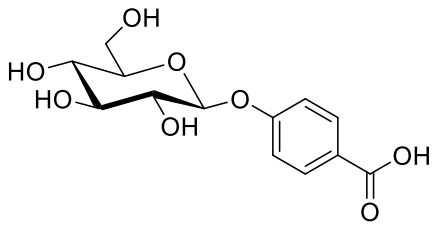

Compound **37** (150 mg, 0.477 mmol) and lithium hydroxide (34 mg, 1.413 mmol) was dissolved in a 3:1 mixture of H_2O:THF (10 mL) in a 50 mL flame-dried round bottom flask. The reaction mixture was stirred for 3 hours at room temperature. Amberlite IR-120 resin (H+ form, pH=4) was pre-rinsed with MeOH and then added to the mixture, which was stirred for an additional 10 minutes until a pH of 5 to 6. The mixture was filtered and the solvent evaporated under reduced pressure. The crude product was dissolved in a minimum of methanol and precipitated with diethyl ether to afford white crystals (136 mg, 95%). ^{1}H NMR (500 MHz, D_2O) δ_H 3.53 (dd, *J*=9.2, 9.2 Hz, 1H), 3.59-3.71 (m, 3H), 3.78 (dd, *J*=12.5, 5.6 Hz, 1H), 3.96, (dd, *J*=12.2, 1.8 Hz, 1H), 5.23 (d, *J*= 7.4 Hz, 1H), 7.17 (d, *J*= 8.7 Hz, 2H), 7.91 (d, *J*=8.7 Hz, 2H). ^{13}C NMR (125 MHz, D_2O) δ_c 61.12, 70.02, 73.51, 76.13, 76.76, 100.27, 116.43, 130.21, 131.75, 159.72, 174.71. LRMS (ESI^-): Calculated 300.08, Found 298.94 $[M-H]^-$.

6.2.8 4-(benzyloxycarbonyl)aminophenol (76)

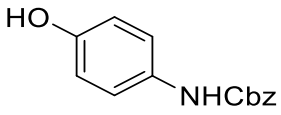

4-aminophenol (500 mg, 4.58 mmol) was dissolved in 10mL of 10% aqueous AcOH in a 50 mL round bottom flask and stirred for 5 minutes. A solution of benzyl chloroformate (1.17 g, 6.87 mmol) in 1,4-dioxane (10 mL) was added dropwise, and the mixture was left to react at room temperature for 36 hours. The mixture was then quenched with water (50 mL) and extracted with CH_2Cl_2 (3x50 mL). The combined organic extracts were washed with sodium bicarbonate (sat. aq., 50 mL), brine (50 mL), dried with $MgSO_4$, filtered and evaporated under reduced pressure. The crude product was purified by column chromatography (5:95 MeOH:CH_2Cl_2) to give light brown crystals (0.98 g, 88%). ^{1}H NMR (300 MHz, MeOD) δ_H 5.14 (s, 2H), 6.71 (d, *J*=8.9 Hz, 2H), 7.21 (d, *J*=8.8 Hz, 2H), 7.26-7.41 (m, 5H). ^{13}C NMR (75 MHz, MeOD) δ_c 67.40, 116.27, 122.15, 128.89, 129.02, 129.48, 131.92, 138.24, 154.63, 156.34. LRMS (ESI^+): Calculated 243.09, Found 243.08 $[M+H]^+$.

6.2.9 4-(benzyloxycarbonyl)aminophenyl-2,3,4,6-tetra-*O*-acetyl-β-D-galactopyranoside (77)

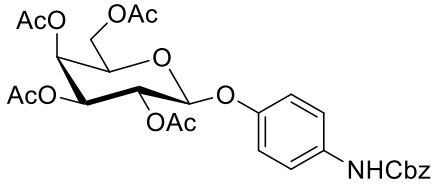

1,2,3,4,6-penta-*O*-acetyl-β-D-galactopyranoside (300 mg, 0.769 mmol) and compound **76** (206 mg, 0.845 mmol) were added to a 50 mL flame-dried round bottom flask charged with argon and 4Å molecular sieves. The compounds were dissolved in anhydrous CH_2Cl_2 (20 mL) and stirred at 0^{O}C for 30 minutes. $BF_3{\cdot}OEt_2$ (1.09 mL, 15.37 mmol) was then added dropwise and the reaction mixture was stirred overnight at room temperature. The contents were filtered over a bed of celite and then quenched with sodium bicarbonate (sat. aq., 50 mL). The organic layer was separated and the aqueous layer was extracted with CH_2Cl_2 (3 x 50 mL). The combined organic fractions were washed with $NaHCO_3$ (sat. aq.) and brine, dried with $MgSO_4$, and then filtered and concentrated under reduced pressure. The crude residue was purified by column chromatography (75:25 - 70:30 (Hexanes:EtOAc) to give a yellow oil (327 mg, 74%). ^{1}H NMR (300 MHz, $CDCl_3$) δ_H 1.94 (s, 3H), 1.97 (s, 3H), 2.01 (s, 3H), 2.09 (s, 3H), 3.97 (dd, *J*=6.7, 6.6 Hz, 1H), 4.08-4.18 (m, 2H), 4.93 (d, *J*=8.0 Hz, 1H), 5.08 (dd, *J*= 10.4, 3.3 Hz, 1H), 5.12 (s, 2H), 5.39-5.40 (m, 1H), 5.41 (dd, *J*=10.4, 8.0 Hz, 1H), 6.90 (d, *J*=9.0 Hz, 2H), 7.24-7.33 (m, 7H). ^{13}C NMR (75 MHz, $CDCl_3$) δ_c 20.38, 20.40, 20.43, 20.53, 61.25, 66.68, 66.86, 68.57, 70.64, 70.76, 99.91, 117.51, 120.07, 128.05, 128.12, 128.41, 133.54, 136.00, 152.81, 153.60, 169.34, 169.96, 170.21, 170.27. LRMS (ESI$^-$): Calculated 573.18, Found 571.99 [M-H]$^-$.

6.2.10 4-(benzyloxycarbonyl)aminophenyl-2,3,4,6-tetra-*O*-acetyl-β-D-glucopyranoside (78)

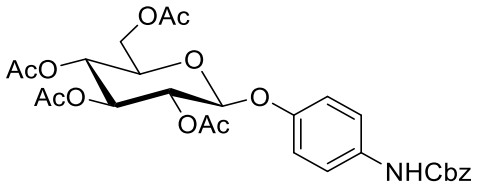

1,2,3,4,6-penta-*O*-acetyl-β-D-glucopyranoside (300 mg, 0.769 mmol) and compound **76** (206 mg, 0.845 mmol) were added to a 50 mL flame-dried round bottom flask charged with argon and 4Å molecular sieves. The compounds were dissolved in anhydrous CH_2Cl_2 (20 mL) and stirred at 0^{O}C for 30 minutes. $BF_3{\cdot}OEt_2$ (1.09 mL, 15.37 mmol) was then added dropwise and the reaction mixture was stirred overnight at room temperature. The contents were then filtered over a bed of celite and then quenched with sodium bicarbonate (sat. aq., 50 mL). The organic layer was separated and the aqueous layer was extracted with CH_2Cl_2 (3 x 50 mL). The combined organic fractions were washed with $NaHCO_3$ (sat. aq.) and brine, dried with $MgSO_4$, and then filtered and concentrated under reduced pressure. The crude residue was purified by column chromatography (75:25 - 70:30 Hexanes:EtOAc) to afford the title compound as a yellow oil (372 mg, 84%). ^{1}H NMR (300 MHz, $CDCl_3$) δ_H 2.03 (s, 3H), 2.04 (s, 3H), 2.06 (s, 3H), 2.07 (s, 3H), 3.79-3.86 (m, 1H), 4.15 (dd, *J*=12.3, 2.4 Hz, 1H), 4.28 (dd, *J*=12.2, 5.4 Hz, 1H), 5.00 (d, *J*=7.6 Hz, 1H), 5.12-5.17 (m, 1H), 5.19 (s, 2H), 5.23-5.29 (m, 2H), 6.69 (br s, 1H), 6.95 (d, *J*=9.0 Hz, 2H), 7.30 (d, *J*=8.9 Hz, 2H), 7.35-7.42 (m, 5H). ^{13}C NMR (75 MHz, $CDCl_3$) δ_c 20.47, 20.50, 20.53, 20.59, 61.88, 68.21, 71.15, 71.83, 172.68, 99.52, 117.70, 120.19, 128.17, 128.25, 128.52, 133.60, 136.02, 152.85, 166.19, 169.52, 170.30, 170.74, 175.63. LRMS (ESI$^-$): Calculated 573.18 Found 571.98 [M-H]$^-$.

6.2.11 4-(benzyloxycarbonyl)aminophenyl-β-D-galactopyranoside (79)

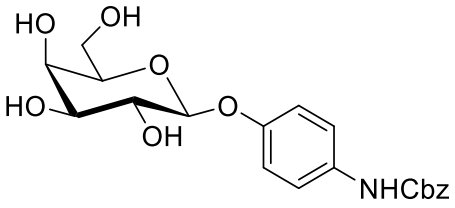

Compound **77** (325 mg, 0.567 mmol) and potassium carbonate (8 mg, 0.0567 mmol) were dissolved in methanol (10 mL) in a 50 mL round bottom flask and stirred overnight at room temperature. Amberlite IRC-76 resin (H+ form, pH=4) was pre-rinsed with MeOH and then added to the mixture, which was stirred for an additional 10 minutes until a pH of 5 to 6. The mixture was filtered and the solvent was removed under reduced pressure. The crude product was purified by recrystallization in EtOAc to yield white crystals (122 mg, 53%). ^{1}H NMR (300 MHz, $(CD_3)_2CO$) δ_H 3.61 (dd, *J*=9.4, 3.4 Hz, 1H), 3.69-3.82 (m, 4H), 3.94-3.97 (m, 1H), 4.83 (d, *J*=7.7 Hz, 1H), 5.15 (s, 2H), 7.03 (d, *J*=9.0 Hz, 2H), 7.29-7.48 (m, 7H), 8.62 (br s, 1H). ^{13}C NMR (75 MHz, $(CD_3)_2CO$) δ_C 62.35, 66.76, 69.82, 72.14, 74.67, 76.44, 103.01, 117.91, 120.39, 128.80, 128.90, 129.27, 134.51, 138.00, 154.48, 154.62. LRMS (ESI^-): Calculated 405.14, Found 404.00 $[M-H]^-$.

6.2.12 4-(benzyloxycarbonylamino)phenyl-β-D-glucopyranoside (80)

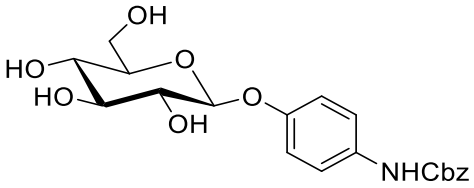

Compound **78** (370 mg, 0.645 mmol) and potassium carbonate (9 mg, 0.0645 mmol) were dissolved in methanol (10 mL) in a 50 mL round bottom flask and stirred overnight at room temperature. Amberlite IRC-76 resin (H+ form, pH=4) was pre-rinsed with MeOH and then added to the mixture, which was stirred for an additional 10 minutes until a pH of 5 to 6. The mixture was filtered and the solvent was removed under reduced pressure. The crude product was purified by column chromatography (90:10 CH_2Cl_2:MeOH) to afford white crystals (142 mg, 54%). ^{1}H NMR (300 MHz, MeOD) δ_H 3.36-3.46 (m, 4H), 3.96 (dd, *J*= 11.9, 4.9 Hz, 1H), 3.89 (d, *J*=11.9 Hz, 1H), 4.83 (d, *J*=7.6 Hz, 1H), 7.04 (d, *J*=9.0 Hz, 2H), 7.28-7.43 (m, 7H). ^{13}C NMR (75 MHz, MeOD) δ_c 62.69, 67.01, 71.37, 74.79, 77.92, 77.97, 102.67, 118.11, 120.61, 129.01, 129.05, 129.48, 134.73, 138.18, 154.71, 154.86. LRMS (ESI^-): Calculated 405.14, Found 403.93 $[M-H]^-$.

6.2.13 4-aminophenyl-β-D-galactopyranoside (49)

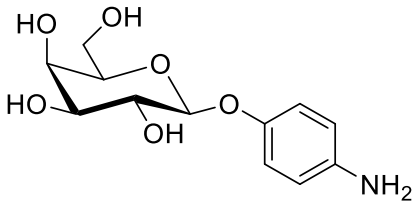

Compound **79** (110 mg, 0.271 mmol) was dissolved in methanol (10 mL) in a 50 mL flame-dried round bottom flask. 20% palladium (II) hydroxide on carbon (19 mg, 0.0271 mmol) was added, the atmosphere was removed from the flask using a water aspirator, and a positive pressure of hydrogen gas was added. The contents were stirred overnight at room temperature, after which the mixture was filtered over a bed of celite and the solvent evaporated under reduced pressure to yield the title compound as light brown crystals (56 mg, 100%). ^{1}H NMR (300 MHz, D_2O) δ_H 3.71-3.79 (m, 5H), 3.96 (m, 1H), 4.88 (d, *J*=7.8 Hz, 1H), 6.80 (d, *J*=9.0 Hz, 2H), 6.98 (d, *J*=9.0 Hz, 2H). ^{13}C NMR (75 MHz, D_2O) δ_C 61.38, 69.11, 71.24, 73.23, 75.93, 102.58, 118.17, 118.71, 142.22, 150.90. LRMS (ESI^-): Calculated 271.11, Found 270.02 $[M-H]^-$.

6.2.14 4-aminophenyl-β-D-glucopyranoside (52)

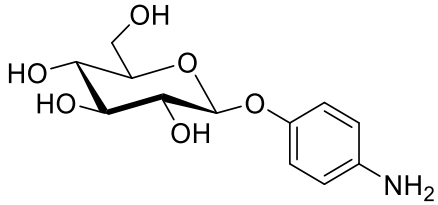

Compound **80** (142 mg, 0.35 mmol) was dissolved in methanol (10 mL) in a 50 mL flame-dried round bottom flask. 20% palladium (II) hydroxide on carbon (25 mg, 0.0350 mmol) was added, the atmosphere was removed from the flask using a water aspirator, and a positive pressure of hydrogen gas was added. The contents were stirred overnight at room temperature, after which the mixture was filtered over a bed of celite and the solvent evaporated under reduced pressure to give light brown crystals (96 mg, 100%). ^{1}H NMR (300 MHz, D_2O) δ_H 3.42-3.61 (m, 4H), 3.72 (dd, *J*=12.3, 5.3 Hz, 1H), 3.90 (dd, *J*=12.4, 2.2 Hz, 1H), 4.95 (d, *J*=7.6 Hz, 1H), 6.80 (d, *J*=9.0 Hz, 2H), 6.98 (d, *J*=8.9 Hz, 1H). ^{13}C NMR (75 MHz, D_2O) δ_C 61.17, 70.07, 73.60, 76.21, 76.64, 101.99, 118.16, 118.79, 142.32, 150.72. LRMS (ESI^-): Calculated 271.11, Found 269.97 $[M-H]^-$.

6.2.15 4-acetamidophenol (81)

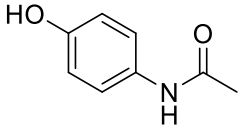

4-aminophenol (500 mg, 4.58 mmol) was suspended in H_2O (1.5 mL) and stirred vigourously in a 25 mL round bottom flask. Acetic anhydride (0.463 mL, 4.90 mmol) was added dropwise and the mixture was stirred for approximately 10 minutes. It was then filtered and washed with cold H_2O and dried under vacuum to yield the desired product as white crystals (380 mg, 55%). ^{1}H NMR (300 MHz, DMSO-*d*6) δ_H 1.97 (s, 3H), 6.66 (d, *J*=8.9 Hz, 2H), 7.33 (d, *J*=8.9 Hz, 2H), 9.13 (br s, 1H), 9.64 (br s, 1H). ^{13}C NMR (75 MHz, DMSO-*d*6) δ_c 23.75, 114.98, 120.77, 131.04, 153.10, 167.48. LRMS (ESI$^+$): Calculated 151.06, Found 174.07 $[M+Na]^+$.

6.2.16 4-acetamidophenyl-2,3,4,6-tetra-*O*-acetyl-β-D-galactopyranoside (82)

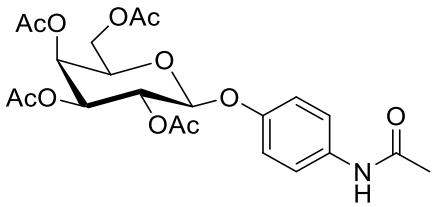

1,2,3,4,6-penta-*O*-acetyl-β-D-glucopyranoside (300 mg, 0.769 mmol) and compound **81** (128 mg, 0.845 mmol) were added to a 50 mL flame-dried round bottom flask charged with argon and 4Å molecular sieves. The compounds were dissolved in anhydrous CH_2Cl_2 (20 mL) and stirred at 0^{O}C for 30 minutes. $BF_3{\cdot}OEt_2$ (1.09 mL, 15.37 mmol) was then added dropwise and the reaction mixture was stirred overnight at room temperature. The contents were then filtered over a bed of celite and then quenched with sodium bicarbonate (sat. aq., 50 mL). The organic layer was separated and the aqueous layer was extracted with CH_2Cl_2 (3 x 50 mL). The combined organic fractions were washed with $NaHCO_3$ (sat. aq.) and brine, dried with $MgSO_4$, and then filtered and concentrated under reduced pressure. The crude residue was purified by column chromatography (60:40 Hexanes:EtOAc) to afford the title compound as a colourless oil (148 mg, 40%). ^{1}H NMR (300 MHz, $CDCl_3$) δ_H 1.99 (s, 3H), 2.04 (s, 3H), 2.05 (s, 3H), 2.11 (s, 3H), 2.14 (s, 3H), 4.03 (dd, *J*=6.6 Hz, 1H), 4.10-4.18 (m, 2H), 5.05 (d, *J*=7.9 Hz, 1H), 5.09 (dd, *J*=10.3, 3.4 Hz, 1H), 5.45 (dd, *J*=10.2, 7.8 Hz, 1H), 5.42 (m, 1H), 6.91 (d, *J*=9.0 Hz, 2H), 7.39 (d, *J*=9.0 Hz, 2H), 7.63 (br s, 1H). ^{13}C NMR (75 MHz, $CDCl_3$) δ_C 20.73, 20.81, 20.82, 20.89, 24.55, 61.49, 67.08, 68.79, 70.95, 71.17, 100.26, 117.77, 121.71, 133.52, 153.73, 168.41, 169.57, 170.27, 170.40, 170.53. LRMS (ESI): Calculated 481.16, Found 504.25 $[M+Na]^+$.

6.2.17 4-acetamidophenyl-β-D-galactopyranoside (48)

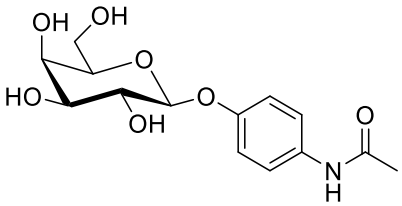

Compound **82** (25 mg, 0.051 mmol) and potassium carbonate (7 mg, 0.0051 mmol) were dissolved in methanol (10 mL) in a 50 mL round bottom flask and stirred overnight at room temperature. Amberlite IRC-76 resin (H+ form, pH=4) was pre-rinsed with MeOH and then added to the mixture, which was

stirred for an additional 10 minutes until a pH of 5 to 6. The mixture was filtered and the solvent was removed under reduced pressure. The crude product was purified by column chromatography (85:15 CH_2Cl_2:MeOH) to yield white crystals (8 mg, 53%). ^{1}H NMR (300 MHz, D_2O) δ_H 2.15 (s, 3H), 3.76-3.81 (m, 4H), 3.86 (dd, *J*=12.1, 6.1 Hz, 1H), 4.00 (d, *J*=3.1 Hz, 1H), 5.04 (d, *J*=7.2 Hz, 1H), 7.14 (d, *J*=9.0 Hz, 2H), 7.35 (d, *J*=9.0 Hz, 2H). ^{13}C NMR (75 MHz, D_2O) δ_C 30.87, 61.38, 69.11, 71.18, 73.19, 76.07, 101.57, 117.66, 124.83, 132.41, 154.93, 173.86. LRMS (ESI): Calculated 313.12, Found 336.20 $[M+Na]^+$.

6.2.18 4-acetamidophenyl- β-D-glucopyranoside (51)

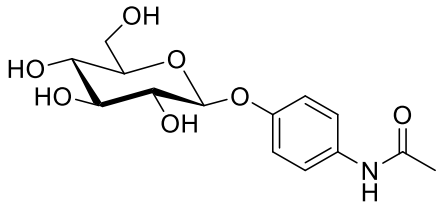

Compound **52** (86 mg, 0.320 mmol) was dissolved in water (3 mL) in a 50 mL round bottom flask. Acetic anhydride (32 uL, 0.337 mmol) was added, and the solution was stirred overnight at room temperature. The reaction mixture was concentrated under reduced pressure, and the crude product was dissolved in a minimum of methanol and precipitated with ether to afford light brown crystals (73 mg, 74%). ^{1}H NMR (300 MHz, D_2O) δ_H 2.14 (s, 3H), 3.45-3.65 (m, 4H), 3.74 (dd, *J*=12.4, 5.7 Hz, 1H), 3.92 (dd, *J*=12.4, 2.2 Hz, 1H), 5.10 (d, *J*=7.5 Hz, 1H), 7.12 (d, *J*=9.0 Hz, 2H), 7.35 (d, *J*=9.0 Hz, 2H). ^{13}C NMR (75 MHz, D_2O) δ_C 22.46, 60.43, 69.33, 72.83, 75.44, 76.03, 100.28, 116.98, 124.06, 131.79, 154.03, 172.97. LRMS (ESI): Calculated 313.12, Found 312.03 $[M-H]^-$.

6.2.19 3-acetamidophenol (84)

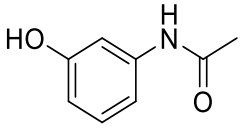

3-aminophenol (500 mg, 4.58 mmol) was suspended in water (10 mL) and stirred vigorously in a 50 mL round bottom flask. Acetic anhydride (0.476 mL, 5.04 mmol) was added dropwise, and the mixture was stirred overnight at room temperature. The contents were then filtered and the residue was washed with cold water (5 mL) and then dried under high vacuum to yield white crystals (363 mg, 52%). ^{1}H NMR (300 MHz, $CDCl_3$) δ_H 7.16 (dd, *J*=2.2 Hz, 1H), 7.08 (dd, *J*=8.0 Hz, 1H), 6.91 (ddd, *J*=8.1, 2.0, 1.0 Hz, 1H), 6.52 (ddd, *J*=8.1, 2.4, 0.9 Hz, 1H), 2.09 (s, 3H). ^{13}C NMR (75 MHz, MeOD) δ_C 171.58, 158.89, 140.95, 130.45, 112.26, 112.11, 108.36, 23.82. LRMS (ESI): Calculated 151.06, Found 190.09 $[M+K]^+$.

6.2.20 3-acetamidophenyl-2,3,4,6-tetra-*O*-acetyl-β-D-galactopyranoside (85)

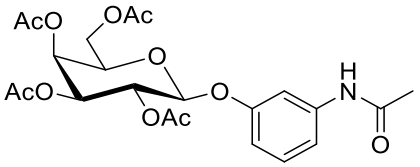

1,2,3,4,6-penta-*O*-acetyl-β-D-galactopyranoside (500 mg,1.281 mmol) and compound **84** (213mg, 1.41 mmol) were added to a 50 mL flame-dried round bottom flask charged with argon and 4Å molecular sieves. The compounds were dissolved in anhydrous CH_2Cl_2 (20 mL) and stirred at 0^{O}C for 30 minutes. $BF_3{\cdot}OEt_2$ (1.58 mL, 12.81 mmol) was then added dropwise and the reaction mixture was stirred overnight at room temperature. The contents were then filtered over a bed of celite and water (50 mL) was added. The organic layer was separated and the aqueous layer was extracted with CH_2Cl_2 (3 x 50 mL). The combined organic fractions were washed with $NaHCO_3$ (sat. aq.) and brine, dried with $MgSO_4$, and then filtered and concentrated under reduced pressure. The crude residue was purified by column chromatography (80:20 - 60:40 Hexanes:EtOAc) to furnish a yellow oil (136 mg, 22%). ^{1}H NMR (300 MHz, $CDCl_3$) δ_H 7.40 (dd, *J*=1.7, 1.6 Hz, 1H), 7.19 (dd, *J*=8.2, 8.2 Hz, 1H), 7.10 (dd, *J*=8.1, 1.6 Hz, 1H), 6.73 (dd, *J*=8.2, 1.7 Hz, 1H), 5.45 (dd, *J*=10.4, 7.9 Hz, 1H), 5.43 (dd, *J*=3.5, 1.0 Hz, 1H), 5.08 (dd, *J*=10.4, 3.5 Hz, 1H), 5.05 (d, *J*=8.0 Hz, 1H), 4.22-4.06 (m, 3H), 2.15 (s, 3H), 2.14 (s, 3H), 2.06 (s, 3H), 2.03 (s, 3H), 1.99 (s, 3H). ^{13}C NMR (75 MHz, $CDCl_3$) δ_C 170.56, 170.36, 170.21, 169.62, 168.63, 157.40, 139.46, 129.87, 114.52, 112.76, 108.70, 99.60, 71.10, 70.91, 68.42, 66.99, 61.36, 24.63, 20.83, 20.71, 20.67. LRMS (ESI): Calculated 481.45, Found 504.25 $[M+Na]^+$.

6.2.21 3-acetamidophenyl β-D-galactopyranoside (53)

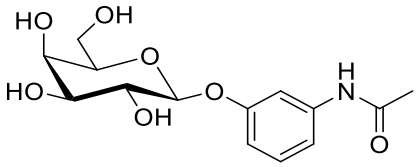

Compound **85** (136 mg, 0.282 mmol) and potassium carbonate (4 mg, 0.0282 mmol) were dissolved in methanol (5 mL) in a 50 mL round bottom flask and were stirred overnight at room temperature. Amberlite IRC-76 resin (H+ form, pH=4) was pre-rinsed with MeOH and then added to the mixture, which was stirred for an additional 10 minutes until a pH of 5 to 6. The mixture was filtered and the solvent was removed under reduced pressure to yield white crystals (70 mg, 79%). ^{1}H NMR (300 MHz, D_2O) δ_H 7.34 (dd, *J*=8.2, 8.2 Hz, 1H), 7.31 (dd, *J*=2.4, 2.3 Hz, 1H), 7.13 (ddd, *J*=8.1, 1.9, 0.8 Hz, 1H), 6.94 (ddd, *J*=8.2, 2.4, 0.7 Hz, 1H), 5.02 (d, *J*=7.2 Hz, 1H), 4.02 (dd, *J*=3.1, 0.7 Hz, 1H), 3.89-3.77 (m, 3H), 2.16 (s, 3H). ^{13}C NMR (75 MHz, $CDCl_3$) δ_C 170.56, 170.36, 170.21, 169.62, 168.63, 157.40, 139.46, 129.87, 114.52, 112.76, 108.70, 99.60, 71.10, 70.91, 68.72, 66.99, 61.36, 24.63, 20.83, 20.71, 20.67. LRMS (ESI^+): Calculated 313.12, Found 372.26 $[M+CH3CN-NH3]^+$.

6.2.22 2-acetamidophenol (87)

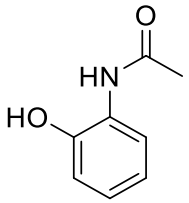

2-aminophenol (500 mg, 4.58 mmol) was dissolved in H_2O (5 mL) in a 25 mL round bottom flask and stirred vigourously. Acetic anhydride (0.476 mL, 5.04 mmol) was added dropwise and the mixture was stirred for 36 hours at room temperature. It was then filtered, washed with cold H_2O and dried under vacuum to afford light brown crystals (611 mg, 88%). ^{1}H NMR (300 MHz, $CDCl_3$) δ_H 2.28 (s, 3H), 6.87 (ddd, 1H, J= 8.4Hz, 7.8Hz, 1.4Hz), 6.99 (dd, 1H, J=8.1Hz, 1.4Hz), 7.09 (dd, 1H, J=8.0Hz, 1.6Hz), 7.12 (ddd, 1H, J=8.5, 7.4, 1.6Hz). ^{13}C NMR (125 MHz, ($CDCl_3$) δ_C 23.88, 53.58, 119.72, 120.92, 122.33, 127.51, 148.40, 171.11. LRMS (ESI^-): Calculated 151.06, Found 149.99 $[M-H]^-$.

6.2.23 2-acetamidophenyl-2,3,4,6-tetra-*O*-acetyl-β-D-galactopyranoside (88)

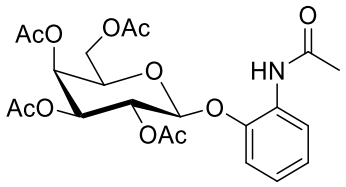

1,2,3,4,6-penta-*O*-acetyl-β-D-galactopyranoside (300 mg,0.769 mmol) and compound **87** (128 mg, 0.846 mmol) were added to a 50 mL flame-dried round bottom flask charged with argon and 4Å molecular sieves. The compounds were dissolved in anhydrous CH_2Cl_2 (10 mL) and stirred at 0^{O}C for 30 minutes. $BF_3{\cdot}OEt_2$ (570 uL, 4.61 mmol) was then added dropwise and the reaction mixture was stirred overnight at room temperature. The contents were then filtered over a bed of celite and water (50 mL) was added. The organic layer was separated and the aqueous layer was extracted with CH_2Cl_2 (3 x 50 mL). The combined organic fractions were washed with $NaHCO_3$ (sat. aq.) and brine, dried with $MgSO_4$, and then filtered and concentrated under reduced pressure. The crude residue was purified by column chromatography (85:15 - 60:40 Hexanes:EtOAc) to give the desired product as a colourless solid (28 mg, 8%). ^{1}H NMR (300 MHz, $CDCl_3$) δ_H 2.03 (s, 3H), 2.07 (s, 3H), 2.09 (s, 3H), 2.19 (s, 3H), 2.22 (s, 3H), 4.08-4.26 (m, 3H), 5.03 (d, 1H, *J*=8.1Hz), 5.17 (dd, 1H, J=10.6Hz, 3.5Hz), 5.46-5.52 (m, 2H), 6.93-7.09 (m, 3H), 7.89 (s, 1H), 8.40 (dd, 1H, *J*=8.0Hz, 1.7Hz). ^{13}C NMR (75 MHz, $CDCl_3$) δ_c 20.53, 20.60, 20.61, 21.01, 24.52, 61.26, 66.67, 69.11, 70.08, 71.16, 99.94, 113.23, 120.24, 123.40, 123.63, 128.67, 144.95, 168.83, 169.92, 170.10, 170.33, 170.83. LRMS (ESI^+): Calculated 481.45, Found 596. $[M+CH_3CN\text{-}NH_4]^+$.

6.2.24 2-acetamidophenyl β-D-galactopyranoside (57)

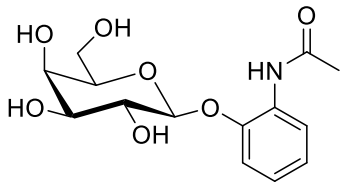

Compound **88** (25 mg, 0.0519 mmol) and potassium carbonate (0.7 mg, 0.00519 mmol) were dissolved in methanol (5 mL) in a 50 mL flame dried, round bottom flask and were stirred overnight at room temperature. Amberlite IRC-76 resin (H+ form, pH=4) was pre-rinsed with MeOH and then added to the mixture, which was stirred for an additional 10 minutes until a pH of 5 to 6. The mixture was filtered and the solvent was removed under reduced pressure. The product was purified by column chromatography (85:15 CH_2Cl_2:MeOH) to yield white crystals (9.9 mg, 61%). ^{1}H NMR (300 MHz, D_2O) δ_H 2.20 (s, 3H), 3.73-3.87 (m, 5H), 4.00 (d, 1H, *J*=3.4Hz), 5.01 (d, 1H, *J*=7.5 Hz), 7.12-7.18 (m, 1H), 7.27 (d, 2H, J=3.8Hz), 7.64 (dt, 1H, J=7.8Hz, 1.0Hz). ^{13}C NMR (75 MHz, D_2O) δ_c 22.59, 60.71, 68.42, 70.42, 72.54, 75.42, 101.56, 116.53, 123.42, 125.19, 127.12, 148.89, 173.40. LRMS (ESI$^+$): Calculated 313.12, Found 352.11. $[M+K]^+$.

6.2.25 Methyl 3-(2,3,4,6-tetra-*O*-acetyl-β-D-galactopyranosyloxy)benzoate (90)

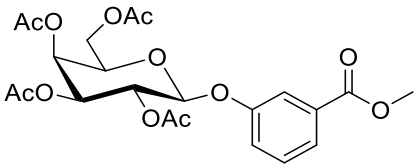

1,2,3,4,6-penta-*O*-acetyl-β-D-galactopyranoside (300 mg, 0.769 mmol) was added to a 50 mL flame-dried round bottom flask charged with argon and 4Å molecular sieves. The solid was dissolved in dry CH_2Cl_2 (20 mL) and $BF_3{\cdot}OEt_2$ (570 uL, 4.614 mmol) was added at 0^{O}C for 20 minutes. Methyl 3-hydroxybenzoate (129 mg, 0.845 mmol) was then added and the reaction mixture was stirred overnight at room temperature. The contents were then filtered over a bed of celite and water (50 mL) was added. The organic layer was separated and the aqueous layer was extracted with CH_2Cl_2 (3 x 50 mL). The combined organic fractions were washed with $NaHCO_3$ (sat. aq.) and brine, dried with $MgSO_4$, and then filtered and concentrated under reduced pressure. The crude residue was purified by column chromatography (85:15 - 25:75 Hexanes:EtOAc) to afford a light yellow oil (274 mg, 74%). ^{1}H NMR (300 MHz, $CDCl_3$) δ_H 2.02 (s, 3H), 2.07 (s, 3H), 2.08 (s, 3H), 2.19 (s, 3H), 3.92 (s, 3H), 4.07-4.13 (m, 3H), 5.09-5.15 (m, 2H), 5.46-5.54 (m, 2H), 7.20 (ddd, 1H, J=8.2Hz, 2.7Hz, 1.1Hz), 7.37 (t, 1H, J=8.1Hz), 7.66 (dd, 1H, J= 2.7Hz, 1.6Hz), 7.76 (dt, 1H, J= 7.7Hz, 1.1Hz). ^{13}C NMR (75 MHz, $CDCl_3$) δ_c 20.69, 20.76, 20.85, 52.42, 61.63, 67.05, 68.69, 70.91, 71.34, 99.47, 117.47, 122.00, 124.57, 129.73, 131.82, 156.86, 166.58, 169.57, 170.25, 170.40, 170.67. LRMS (ESI$^+$): Calculated 482.43, Found 505.20 $[M+Na]^+$.

6.2.26 Methyl 3-(β-D-galactopyranosyloxy)benzoate (54)

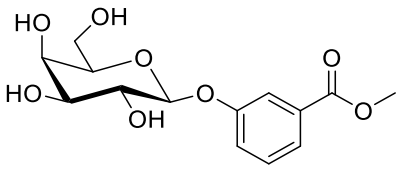

Compound **90** (216 mg, 0.448 mmol) and potassium carbonate (6.2 mg, 0.0448 mmol) were dissolved in methanol (10 mL) in a 50 mL flame dried, round bottom flask and stirred overnight at room temperature. Amberlite IRC-76 resin (H+ form, pH=4) was pre-rinsed with MeOH and then added to the mixture, which was stirred for an additional 10 minutes until a pH of 5 to 6. The mixture was filtered and the solvent was removed under reduced pressure. The crude product was recrystallized in MeOH:Et_2O to yield white crystals (96 mg, 68%). ^{1}H NMR (300 MHz, MeOD) δ_H 3.59 (dd, 1H, J= 9.7Hz, 3.4Hz), 3.69-3.83 (m, 4H), 3.90 (s, 3H), 3.92 (d, 1H, J=3.4Hz), 4.91 (d, 1H, J= 7.7Hz), 7.33-7.43 (m, 2H), 7.67 (dt, 1H, J=7.1Hz, 1.4Hz), 7.74 (m, 1H). ^{13}C NMR (75 MHz, MeOD) δ_c 52.70, 62.33, 70.15, 72.721, 74.81, 77.04, 102.97, 122.65, 124.34, 130.63, 132.64, 159.24. LRMS (ESI^+): Calculated 314.10, Found 337.17 $[M+Na]^+$.

6.2.27 3-bromophenyl-2,3,4,6-tetra-*O*-acetyl-β-D-galactopyranoside (92)

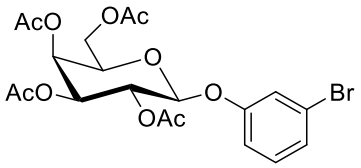

1,2,3,4,6-penta-*O*-acetyl-β-D-galactopyranoside (200 mg, 0.512 mmol) and 3-bromophenol (98 mg, 0.563 mmol) were added to a 50 mL flame-dried round bottom flask charged with argon and 4Å molecular sieves. The compounds were dissolved in anhydrous CH_2Cl_2 (20 mL) and stirred at 0^{O}C for 30 minutes. $BF_3{\cdot}OEt_2$ (1.58 mL, 12.81 mmol) was then added dropwise and the reaction mixture was stirred overnight at room temperature. The contents were then filtered over a bed of celite and water (50 mL) was added. The organic layer was separated and the aqueous layer was extracted with CH_2Cl_2 (3 x 50 mL). The combined organic fractions were washed with $NaHCO_3$ (sat. aq.) and brine, dried with $MgSO_4$, and then filtered and concentrated under reduced pressure. The crude residue was purified by column chromatography (85:15 – 60:40 Hexanes:EtOAc) to give a yellow oil (53 mg, 59%). ^{1}H NMR (300 MHz, $CDCl_3$) δ_H 2.01 (s, 3H), 2.07 (s, 3H), 2.09 (s, 3H), 2.18 (s, 3H), 4.04-4.24 (m, 3H), 5.02 (d, *J*=7.9 Hz, 1H), 5.10 (dd, *J*=10.4, 3.4 Hz, 1H), 5.46 (dd, *J*=3.5, 1.0 Hz, 1H), 5.48 (dd, *J*=10.4, 7.9 Hz, 1H), 6.93 (ddd, *J*=7.9, 2.4, 1.3 Hz, 1H), 7.16 (dd, *J*=7.9, 7.9 Hz, 1H), 7.19-7.24 (m, 2H). ^{13}C NMR (75 MHz, CDCl) δ_C 20.59, 20.66, 20.73, 20.74, 61.68, 66.98, 68.52, 70.77, 71.32, 99.35, 115.98, 120.05, 122.69, 126.38, 130.73, 157.48, 169.36, 170.08, 170.23, 170.46. LRMS (ESI): Calculated 502.05, Found 561.16 $[M+CH_3CN\text{-}NH_3]^+$.

6.2.28 3-bromophenyl-β-D-galactopyranoside (55)

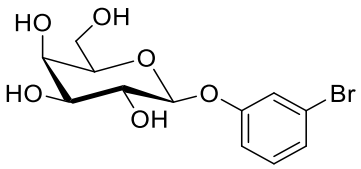

Compound **92** (138 mg, 0.275 mmol) and potassium carbonate (4 mg, 0.0275 mmol) were dissolved in methanol (5 mL) in a 50 mL round bottom flask and stirred for two hours at room temperature. Amberlite IRC-76 resin (H+ form, pH=4) was pre-rinsed with MeOH and then added to the mixture, which was stirred for an additional 10 minutes until a pH of 5 to 6. The mixture was filtered and the solvent was removed under reduced pressure. The product purified by column chromatography (85:15 CH_2Cl_2:MeOH) to yield white crystals (60 mg, 65%). ^{1}H NMR (300 MHz, D_2O) δ_H 3.70-3.85 (m, 5H), 3.98 (d, *J*=3.1 Hz, 1H), 5.00 (d, *J*=7.3 Hz, 1H), 7.08 (m, 1H), 7.25 (dd, *J*= 8.9, 8.9 Hz, 1H), 7.27-7.32 (m, 2H). ^{13}C NMR (75 MHz, D_2O) δ_C 60.62, 68.34, 70.40, 72.46, 75.40, 100.62, 115.40, 119.62, 122.14, 126.00, 131.10, 157.32. LRMS (ESI): Calculated 334.01, Found 373.04 $[M+K]^+$.

6.2.29 2-bromophenyl-2,3,4,6-tetra-*O*-acetyl-β-D-galactopyranoside (94)

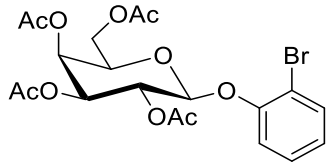

1,2,3,4,6-penta-*O*-acetyl-β-D-galactopyranoside (500 mg, 1.281 mmol) and 2-bromophenol (443 mg, 2.56 mmol) were added to a 50 mL flame-dried round bottom flask charged with argon and 4Å molecular sieves. The compounds were dissolved in anhydrous CH_2Cl_2 (20 mL) and stirred at 0^{O}C for 30 minutes. $BF_3{\cdot}OEt_2$ (1.58 mL, 12.81 mmol) was then added dropwise and the reaction mixture was stirred overnight at room temperature. The contents were then filtered over a bed of celite and water (50 mL) was added. The organic layer was separated and the aqueous layer was extracted with CH_2Cl_2 (3 x 50 mL). The combined organic fractions were washed with $NaHCO_3$ (sat. aq.) and brine, dried with $MgSO_4$, and then filtered and concentrated under reduced pressure. The crude residue was purified by column chromatography (85:15 - 60:40 Hexanes:EtOAc) to yield a yellow oil (341 mg, 53%). ^{1}H NMR (300 MHz, $CDCl_3$) δ_H 7.53 (dd, *J*=8.0, 1.6 Hz, 1H), 7.25 (ddd, *J*=8.8, 7.3, 1.6 Hz, 1H), 7.16 (dd, *J*=8.3, 1.6Hz, 1H), 6.96 (ddd, *J*=7.9, 7.3, 1.6 Hz, 1H), 5.59 (dd, *J*=10.6, 8.0 Hz, 1H), 5.46 (dd, *J*=3.4, 1.0 Hz, 1H), 5.10 (dd, *J*=10.5, 3.4 Hz, 1H), 4.48 (d, *J*=8.0 Hz, 1H), 4.29-4.02 (m, 3H), 2.18 (s, 3H), 2.10 (s, 3H), 2.06 (s, 3H), 2.01 (s, 3H). ^{13}C NMR (75 MHz, $CDCl_3$) δ_C 170.35, 170.28, 170.17, 169.38, 153.70, 133.55, 128.55, 124.71, 117.83, 133.21, 100.56, 71.22, 70.75, 68.18, 66.90, 61.43, 21.04, 20.69, 20.63. LRMS (ESI^+): Calculated 502.05, Found 561.16 $[M+CH3CN-NH3]^+$.

6.2.30 2-bromophenyl-β-D-galactopyranoside (59)

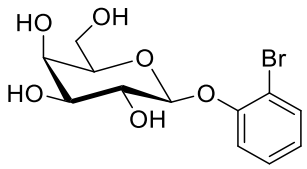

Compound **94** (320 mg, 0.636 mmol) and potassium carbonate (9 mg, 0.0636 mmol) were dissolved in methanol (5 mL) in a 50 mL round bottom flask and stirred for two hours at room temperature. Amberlite IRC-76 resin (H+ form, pH=4) was pre-rinsed with MeOH and then added to the mixture, which was stirred for an additional 10 minutes until a pH of 5 to 6. The mixture was filtered and the solvent was removed under reduced pressure. The product purified by dissolving in methanol and precipitating with diethyl ether to yield white crystals (126 mg, 59%). ^{1}H NMR (500 MHz, MeOD) δ_H 7.53 (dd, *J*=7.8, 1.2 Hz, 1H), 7.31-7.25 (m, 2H), 6.91 (ddd, 1H, *J*=8.2, 6.2, 1.8 Hz), 4.95 (d, *J*=7.8 Hz, 1H), 3.91 (d, *J*=3.3 Hz, 1H), 3.88 (dd, *J*=9.7, 7.7 Hz, 1H), 3.79-3.74 (m, 2H), 3.71-3.68 (m, 1H), 3.59 (dd, *J*=9.7, 3.5Hz, 1H). ^{13}C NMR (125 MHz, MeOD) δ_C 155.50, 134.30, 129.66, 124.37, 117.72, 113.42, 102.86, 77.15, 75.01, 72.17, 70.21, 62.38. LRMS (ESI$^+$): Calculated 334.01, Found 356.99 $[M+Na]^+$.

6.2.31 2-methoxyphenyl-2,3,4,6-tetra-*O*-acetyl-β-D-glucopyranoside (96)

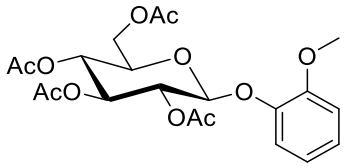

1,2,3,4,6-penta-*O*-acetyl-β-D-glucopyranoside (300 mg, 0.769 mmol) was added to a 50 mL flame-dried round bottom flask charged with argon and 4Å molecular sieves. The solid was dissolved in dry CH_2Cl_2 (10 mL) and $BF_3{\cdot}OEt_2$ (0.950mL, 7.69 mmol) was added at 0^{O}C for 20 minutes. 2-methoxyphenol (105 mg, 0.845 mmol) was then added and the reaction mixture was stirred overnight at room temperature. The contents were then filtered over a bed of celite and water (50 mL) was added. The organic layer was separated and the aqueous layer was extracted with CH_2Cl_2 (3 x 50 mL). The combined organic fractions were washed with $NaHCO_3$ (sat. aq.) and brine, dried with $MgSO_4$, and then filtered and concentrated under reduced pressure. The crude residue was purified by column chromatography (75:25 Hexanes:EtOAc) to afford white crystals (175 mg, 50%). ^{1}H NMR (300 MHz, $CDCl_3$) δ_H 2.00 (s, 3H), 1.97 (s, 3H), 2.01 (s, 3H), 2.12 (s, 3H), 3.70-3.73 (m, 1H), 3.75 (s, 3H), 4.09 (dd, *J*=12.2, 2.4 Hz, 1H), 4.22 (dd, *J*=12.2, 5.4 Hz, 1H), 4.91 (d, *J*=7.7 Hz, 1H), 5.05-5.12 (m, 1H), 5.20-5.24 (m, 2H), 6.80 (ddd, *J*= 7.8, 7.8, 1.4 Hz, 1H), 6.84 (dd, *J*= 8.2, 1.4 Hz, 1H), 7.00 (ddd, *J*= 8.0, 8.0, 1.5 Hz, 1H), 7.05 (dd, *J*=8.0, 1.5 Hz, 1H). ^{13}C NMR (75 MHz, $CDCl_3$) δ_c 20.70, 20.74, 20.79, 20.85, 56.14, 62.10, 68.58, 71.37, 72.07, 72.78, 100.99, 112.88, 120.42, 120.97, 124.88, 146.25, 150.85, 169.56, 169.59, 170.48, 170.81. LRMS (ESI$^+$): Calculated 454.15, Found 513.23 $[M+CH3CN-NH_4]^+$.

6.2.32 2-methoxyphenyl-β-D-glucopyranoside (60)

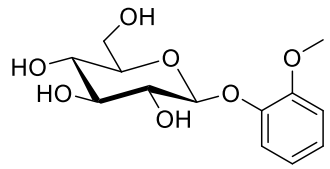

Compound **96** (175 mg, 0.385 mmol) and potassium carbonate (5 mg, 0.0139 mmol) were dissolved in methanol (10 mL) in a 50 mL round bottom flask and stirred overnight at room temperature. Amberlite IRC-76 resin (H+ form, pH=4) was pre-rinsed with MeOH and then added to the mixture, which was stirred for an additional 10 minutes until a pH of 5 to 6. The mixture was filtered and the solvent was removed under reduced pressure to yield white crystals (63 mg, 57%). ^{1}H NMR (300 MHz, D_2O) δ_H 3.48-3.52 (m, 1H), 3.55-3.62 (m, 3H), 3.73 (dd, *J*= 12.2, 5.3 Hz, 1H), 3.87 (s, 3H), 3.89 (dd, *J*=12.2, 2.1 Hz, 1H), 5.10-5.13 (m, 1H), 6.96-7.03 (m, 1H), 7.10-7.14 (m,2H), 7.18 (dd, *J*=8.8, 1.2, 1H). ^{13}C NMR (75 MHz, $CDCl_3$) δ_c 55.76, 60.34, 69.25, 72.81, 75.48, 76.04, 112.94, 116.18, 121.50, 123.82, 145.37, 148.67. LRMS (ESI^+): Calculated 286.11, Found 325.11 $[M+K]^+$.

6.2.33 4-propionamidophenyl propionate (97)

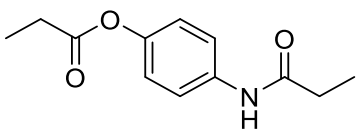

4-aminophenol (200mg, 1.833 mmol) was dissolved in anhydrous pyridine (10 mL) in a flame-dried round bottom flask under an atmosphere of argon and stirred at 0°C for 10 minutes. Propionyl chloride (0.48 mL, 5.50 mmol) was added dropwise, then the mixture was stirred overnight at room temperature. Upon completion, the mixture was concentrated under reduced pressure, taken up in saturated aqueous sodium bicarbonate (50 mL) and then extracted with CH_2Cl_2 (3x50 mL). The combined organic fractions were washed with sodium bicarbonate (sat. aq., 50 mL), brine (50 mL), dried with $MgSO_4$, filtered and concentrated. The crude product was then purified by column chromatography (80:20 Hex:EtOAc) to yield white crystals (284 mg, 70%). ^{1}H NMR (500 MHz, $CDCl_3$) δ_H 1.22 (t, *J*=7.6 Hz, 3H), 1.25 (t, *J*=7.6 Hz, 3H), 2.35 (q, *J*=7.6 Hz, 2H), 2.58 (q, *J*=7.6 Hz, 2H), 7.00 (d, *J*=8.9 Hz, 2H), 7.45 (br s, 1H), 7.48 (d, *J*=8.9 Hz, 2H). ^{13}C NMR (125 MHz, $CDCl_3$) δ_c 9.17, 9.78, 27.82, 30.70, 120.87, 120.01, 135.78, 146.84, 172.23, 173.44. LRMS (ESI^-): Calculated 221.11, Found 220.03 $[M-H]^-$.

6.2.34 *N*-(4-hydroxyphenyl)propionamide (98)

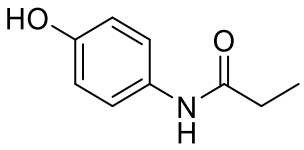

Compound **97** (284 mg, 1.28 mmol) was dissolved in a 0.1 M solution of sodium methoxide in methanol (10 mL) in a 50 mL round bottom flask and stirred overnight at room temperature. Amberlite IR-120 resin (H+ form, pH=4) was pre-rinsed with MeOH and then added to the mixture, which was stirred for an additional 10 minutes until a pH of 5 to 6. The mixture was filtered and concentrated under reduced pressure to yield the pure product as off-white crystals (208 mg, 98%). ^{1}H NMR (300 MHz, $(CD_3)_2CO$) δ_H 1.13 (t, *J*=7.6 Hz, 3H), 2.34 (q, *J*=7.6 Hz, 2H), 6.76 (d, *J*=8.9 Hz, 2H), 7.46 (d, *J*=8.8 Hz, 2H), 8.28 (br s, 1H), 8.98 (br s, 1H). ^{13}C NMR (75 MHz, $(CD_3)_2CO$) δ_c 10.11, 30.54, 115.86, 121.96, 132.38, 154.31, 172.54. LRMS (ESI^-): Calculated 165.08, Found 164.00 $[M-H]^-$.

6.2.35 4-propionamidophenyl-2,3,4,6-tetra-*O*-acetyl-β-D-glucopyranoside (99)

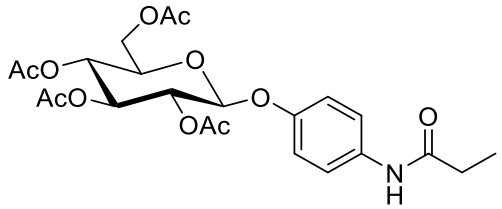

1,2,3,4,6-penta-*O*-acetyl-β-D-glucopyranoside (250 mg, 0.639 mmol) and compound **98** (116 mg, 0.704 mmol) were added to a 50 mL flame-dried round bottom flask charged with argon and 4Å molecular sieves. The compounds were dissolved in anhydrous CH_2Cl_2 (20 mL) and stirred at 0^{O}C for 30 minutes. $BF_3{\cdot}OEt_2$ (1.18 mL, 9.59 mmol) was then added dropwise and the reaction mixture was stirred overnight at room temperature. The contents were then filtered over a bed of celite and then quenched with sodium bicarbonate (sat. aq., 50 mL). The organic layer was separated and the aqueous layer was extracted with CH_2Cl_2 (3 x 50 mL). The combined organic fractions were washed with $NaHCO_3$ (sat. aq.) and brine, dried with $MgSO_4$, and then filtered and concentrated under reduced pressure. The crude residue was purified by column chromatography (1:1 Hexanes:EtOAc) to give the title compound as white crystals (83 mg, 26%). ^{1}H NMR (300 MHz, $CDCl_3$) δ_H 1.23 (t, *J*=7.6 Hz, 3H), 2.03 (s, 3H), 2.04 (s, 3H), 2.06 (s, 3H), 2.07 (s, 3H), 2.36 (t, *J*=7.6 Hz, 2H), 3.80-3.87 (m, 1H), 4.15 (dd, *J*=12.3, 2.5 Hz, 1H), 4.28 (dd, *J*=12.3, 5.3 Hz, 1H), 5.01 (d, *J*=7.6 Hz, 1H), 5.15 (dd, *J*=9.8, 9.8 Hz, 1H), 5.23-5.31 (m, 2H), 6.94 (d, *J*=9.0 Hz, 2H), 7.21 (br s, 1H), 7.43 (d, *J*=9.0 Hz, 2H). ^{13}C NMR (75 MHz, $CDCl_3$) δ_c 9.62, 20.56, 20.68, 20.62, 20.69, 30.54, 61.90, 68.23, 71.13, 72.00, 76.67, 99.59, 117.67, 121.31, 133.56, 153.32, 169.30, 169.39, 170.20, 170.58, 171.88. LRMS (ESI^-): Calculated 495.17, Found 494.06 $[M-H]^-$.

6.2.36 4-propionamidophenyl-β-D-glucopyranoside (63)

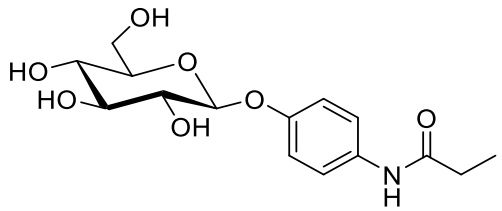

Compound **99** (83 mg, 0.168 mmol) and potassium carbonate (2.3 mg, 0.0168 mmol) were dissolved in methanol (10 mL) in a 50 mL round bottom flask. The contents were stirred overnight at room

temperature. Amberlite IRC-76 resin (H+ form, pH=4) was pre-rinsed with MeOH and then added to the mixture, which was stirred for an additional 10 minutes until a pH of 5 to 6. The mixture was filtered and the solvent was removed under reduced pressure to afford white crystals (55 mg, 99%). ^{1}H NMR (300 MHz, D_2O) δ_H 1.20 (t, *J*=7.5 Hz, 3H), 2.42 (q, *J*=7.5 Hz, 2H), 3.51 (dd, *J*=9.3 Hz, 9.3 Hz, 1H), 3.55-3.65 (m, 3H), 3.76 (dd, *J*=12.3, 5.5 Hz, 1H), 3.94 (dd, *J*=12.3, 1.5 Hz, 1H), 5.11 (d, *J*=7.6 Hz, 1H), 7.15 (d, *J*=8.9 Hz, 2H), 7.38 (d, *J*=8.9 Hz, 2H). ^{13}C NMR (75 MHz, D_2O) δ_c 9.33, 29.56, 60.44, 69.33, 72.83, 75.44, 76.03, 100.29, 116.99, 124.08, 131.83, 154.00, 176.89. LRMS (ESI^-): Calculated 327.13, Found 326.02 $[M-H]^-$.

6.2.37 4-butyramidophenyl butyrate (100)

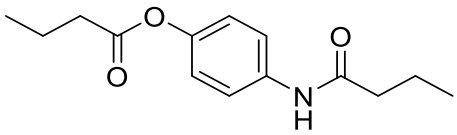

4-aminophenol (200mg, 1.833 mmol) and butyryl chloride (0.57 mL, 5.50 mmol) were dissolved in anhydrous CH_2Cl_2 (15 mL) in a flame-dried round bottom flask under an atmosphere of argon and stirred at 0°C for 10 minutes. Triethylamine (1.28 mL, 9.17 mmol) was added dropwise and the mixture was stirred overnight at room temperature. Upon completion, hydrochloric acid solution (1% aq., 50 mL) was added and the mixture extracted with CH_2Cl_2 (3x50 mL). The combined organic fractions were washed with sodium bicarbonate (sat. aq., 3 x 50 mL), brine (50 mL), dried with $MgSO_4$, filtered and concentrated. The crude product was then recrystallized in hexanes/Et_2O to afford white crystals (123 mg, 27%). ^{1}H NMR (500 MHz, $CDCl_3$) δ_H 0.99 (t, *J*=7.4 Hz, 3H), 1.04 (t, *J*=7.4 Hz, 3H), 1.71-1.81 (m, 4H), 2.31 (t, *J*=7.4 Hz, 2H), 2.53 (t, *J*=7.4 Hz, 2H), 7.00 (d, *J*=8.9 Hz, 2H), 7.37 (br s, 1H), 7.49 (d, *J*=8.9 Hz, 2H). ^{13}C NMR (125 MHz, $CDCl_3$) δ_c 13.62, 13.72, 18.41, 19.01, 36.15, 39.50, 120.72, 121.92, 135.57, 146.71, 171.27, 172.40. LRMS (ESI^-): Calculated 249.14, Found 248.05 $[M-H]^-$.

6.2.38 4-pentanamidophenyl pentanoate (101)

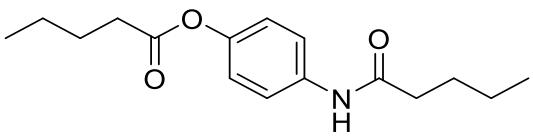

4-aminophenol (500mg, 4.58 mmol) and valeryl chloride (1.14 mL, 9.26 mmol) were dissolved in anhydrous CH_2Cl_2 (20 mL) in a flame-dried round bottom flask under an atmosphere of argon and stirred at 0°C for 10 minutes. Triethylamine (3.19 mL, 22.9 mmol) was added dropwise and the mixture was stirred overnight at room temperature. Upon completion, hydrochloric acid solution (1% aq., 50 mL) was added and the mixture extracted with CH_2Cl_2 (3x50 mL). The combined organic fractions were washed with sodium bicarbonate (sat. aq., 3 x 50 mL), brine (50 mL), dried with $MgSO_4$, filtered and concentrated. The crude product was then recrystallized in hexanes/Et_2O to yield the desired product as white crystals (780 mg, 61%). ^{1}H NMR (500 MHz, $CDCl_3$) δ_H 0.94 (t, *J*=7.4 Hz, 3H), 0.97 (t, *J*=7.4 Hz, 3H), 1.35-1.48 (m, 4H), 1.67-1.77 (m, 4H), 2.32 (t, *J*=7.6 Hz, 2H), 2.55 (t, *J*=7.6 Hz, 2H), 6.99 (d, *J*=8.9 Hz, 2H), 7.44 (br s, 1H), 7.48 (d, *J*=8.8 Hz, 2H). ^{13}C NMR (75 MHz, $CDCl_3$) δ_c 13.74, 13.82, 22.47, 22.38, 26.98,

27.67, 34.08, 37.64, 120. 78, 121.89, 135.67, 146.71, 171.52, 172.67. LRMS (ESI^-): Calculated 277.17, Found 276.06 $[M-H]^-$.

6.2.39 *N*-(4-hydroxyphenyl)butyramide (102)

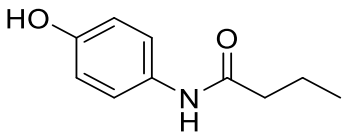

Compound **100** (123 mg, 0.493 mmol) was dissolved in a 0.1 M solution of sodium methoxide in methanol (10 mL) in a 50 mL round bottom flask and stirred overnight at room temperature. Amberlite IR-120 resin (H+ form, pH=4) was pre-rinsed with MeOH and then added to the mixture, which was stirred for an additional 10 minutes until a pH of 5 to 6. The mixture was filtered and concentrated under reduced pressure. The crude product was purified by column chromatography (70:30 EtOAc:Hexanes) to yield white crystals (80 mg, 91%). ^1H NMR (500 MHz, $(CD_3)_2CO$) δ_H 0.94 (t, *J*=7.5 Hz, 3H), 1.64-1.71 (m, 2H), 2.28 (t, *J*=7.7 Hz, 2H), 6.75 (d, *J*=8.8 Hz, 2H), 7.46 (d, *J*=8.8 Hz, 2H), 8.13 (br s, 1H), 8.98 (br s, 1H). ^{13}C NMR (100 MHz, $(CD_3)_2CO$) δ_c 14.02, 19.71, 39.47, 115.85, 121.82, 132.59, 154.24, 171.40. LRMS (ESI^-): Calculated 179.09, Found 178.03 $[M-H]^-$.

6.2.40 *N*-(4-hydroxyphenyl)pentanamide (103)

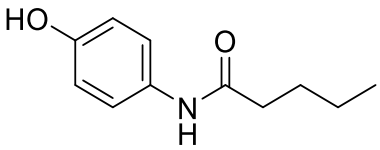

Compound **101** (658 mg, 2.37 mmol) was dissolved in a 0.1 M solution of sodium methoxide in methanol (20 mL) in a 50 mL round bottom flask and stirred overnight at room temperature. Amberlite IR-120 resin (H+ form, pH=4) was pre-rinsed with MeOH and then added to the mixture, which was stirred for an additional 10 minutes until a pH of 5 to 6. The mixture was filtered and concentrated under reduced pressure to yield the pure product as white crystals (447 mg, 97%). ^1H NMR (500 MHz, $(CDCl_3)$ δ_H 0.95 (t, *J*=7.4 Hz, 3H), 1.37-1.46 (m, 2H), 1.68-1.74 (m, 2H), 2.34 (t, *J*=7.6 Hz, 2H), 6.76 (d, *J*=8.8 Hz, 2H), 7.08 (br s, 1H), 7.29 (d, *J*=8.8 Hz, 2H). ^{13}C NMR (75 MHz, $CDCl_3$) δ_c 13.66, 22.33, 27.86, 36.86, 115.32, 122.21, 130.15, 153.59, 172.61. LRMS (ESI^-): Calculated 193.11, Found 192.06 $[M-H]^-$.

6.2.41 4-butyramidophenyl-2,3,4,6-tetra-*O*-acetyl-β-D-glucopyranoside (104)

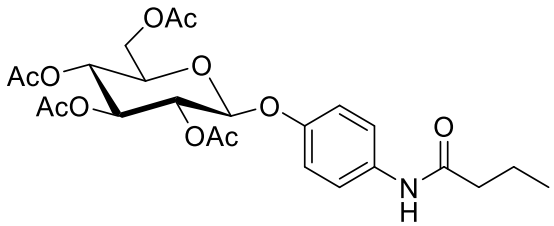

1,2,3,4,6-penta-*O*-acetyl-β-D-glucopyranoside (125 mg, 0.320 mmol) and compound **102** (65 mg, 0.363 mmol) were added to a 50 mL flame-dried round bottom flask charged with argon and 4Å molecular sieves. The compounds were dissolved in anhydrous CH_2Cl_2 (20 mL) and stirred at 0^{O}C for 30 minutes. $BF_3{\cdot}OEt_2$ (0.593 mL, 4.80 mmol) was then added dropwise and the reaction mixture was stirred overnight at room temperature. The contents were then filtered over a bed of celite and then quenched with sodium bicarbonate (sat. aq., 50 mL). The organic layer was separated and the aqueous layer was extracted with CH_2Cl_2 (3 x 50 mL). The combined organic fractions were washed with $NaHCO_3$ (sat. aq.) and brine, dried with $MgSO_4$, and then filtered and concentrated under reduced pressure. The crude residue was purified by column chromatography (60:40 Hexanes:EtOAc) to give white crystals (111 mg, 68%). ^{1}H NMR (300 MHz, $CDCl_3$) δ_H 1.00 (t, *J*=7.4 Hz, 3H), 1.76 (hex, 2H), 2.03 (s, 3H), 2.04 (s, 3H), 2.06 (s, 3H), 2.08 (s, 3H), 2.32 (t, *J*=7.4 Hz, 2H), 3.80-3.87 (m, 1H), 4.16 (dd, *J*=12.3, 2.4 Hz, 1H), 4.28 (dd, *J*=12.3, 5.4 Hz, 1H), 5.01 (d, *J*=7.6 Hz, 1H), 5.15 (dd, *J*=9.8, 9.8 Hz, 1H), 5.21-5.32 (m, 2H), 6.95 (d, *J*=9.0, 2H), 7.09 (br s, 1H), 7.43 (d, *J*=9.0 Hz, 2H). ^{13}C NMR (75 MHz, $CDCl_3$) δ_c 13.70, 19.01, 20.54, 20.56, 20.60, 20.66, 39.39, 61.89, 68.23, 71.13, 71.96, 72.65, 99.59, 117.62, 121.39, 133.66, 153.29, 169.32, 169.40, 170.17, 170.58, 171.33. LRMS (ESI$^-$): Calculated 509.19, Found 508.04 $[M-H]^-$.

6.2.42 4-pentanamidophenyl-2,3,4,6-tetra-*O*-acetyl-β-D-glucopyranoside (105)

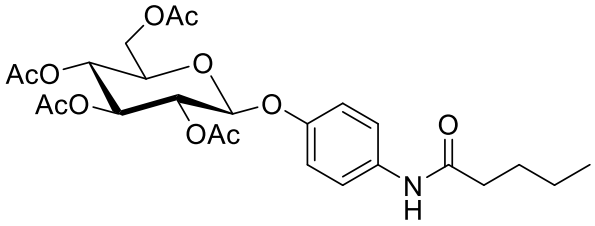

1,2,3,4,6-penta-*O*-acetyl-β-D-glucopyranoside (300 mg, 0.769 mmol) and compound **103** (163 mg, 0.846 mmol) were added to a 50 mL flame-dried round bottom flask charged with argon and 4Å molecular sieves. The compounds were dissolved in anhydrous CH_2Cl_2 (20 mL) and stirred at 0^{O}C for 30 minutes. $BF_3{\cdot}OEt_2$ (1.42 mL, 11.5 mmol) was then added dropwise and the reaction mixture was stirred overnight at room temperature. The contents were then filtered over a bed of celite and then quenched with sodium bicarbonate (sat. aq., 50 mL). The organic layer was separated and the aqueous layer was extracted with CH_2Cl_2 (3 x 50 mL). The combined organic fractions were washed with $NaHCO_3$ (sat. aq.) and brine, dried with $MgSO_4$, and then filtered and concentrated under reduced pressure. The crude residue was purified by column chromatography (60:40 Hexanes:EtOAc) to afford a white solid (245 mg, 61%). ^{1}H NMR (500 MHz, $CDCl_3$) δ_H 0.93 (t, *J*=7.4 Hz, 3H), 1.39 (hex, *J*=7.5 Hz, 2H), 1.69 (quin, *J*=7.4 Hz, 2H), 2.02 (s, 3H), 2.04 (s, 3H), 2.06 (s, 3H), 2.07 (s, 3H), 2.33, *J*=7.6 Hz, 2H), 3.81-3.85 (m, 1H), 4.15 (dd,

J=12.3, 2.4 Hz, 1H), 4.27 (dd, *J*=12.3, 5.4 Hz, 1H), 5.00 (d, *J*=7.6 Hz, 1H), 5.15 (dd, *J*=9.2, 9.2 Hz, 1H), 5.21-5.30 (m, 2H), 6.94 (d, *J*=8.8 Hz, 2H), 7.23 (br s, 1H), 7.42 (d, *J*=8.8 Hz, 2H). ^{13}C NMR (75 MHz, $CDCl_3$) δ_c 13.86, 20.63, 20.65, 20.69, 20.76, 22.43, 27.75, 37.31, 61.99, 68.33, 71.24, 72.04, 72.75, 99.67, 117.69, 121.51, 133.83, 153.36, 169.45, 169.52, 170.27 170.70, 171.75. LRMS (ESI^-): Calculated 523.21, Found 522.12 $[M-H]^-$.

6.2.43 4-butyramidophenyl-β-D-glucopyranoside (64)

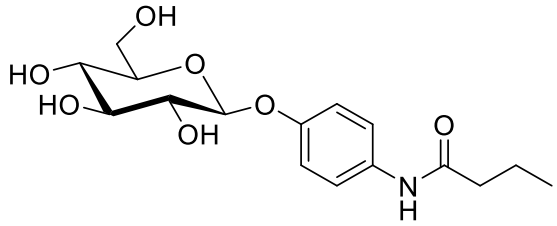

Compound **104** (78 mg, 0.153 mmol) and potassium carbonate (2.1 mg, 0.0153 mmol) were dissolved in methanol (10 mL) in a 50 mL round bottom flask and stirred overnight at room temperature. Amberlite IRC-76 resin (H+ form, pH=4) was pre-rinsed with MeOH and then added to the mixture, which was stirred for an additional 10 minutes until a pH of 5 to 6. The mixture was filtered and the solvent was removed under reduced pressure to yield white crystals (51 mg, 98%). ^{1}H NMR (300 MHz, D_2O/MeOD) δ_H 0.93 (t, *J*=7.4 Hz, 3H), 1.65 (hex, *J*=7.4 Hz, 2H), 2.32 (t, *J*=7.3 Hz, 2H), 3.38-3.55 (m, 4H), 3.69 (dd, *J*=12.4, 5.5 Hz, 1H), 3.86 (dd, *J*=12.3, 2.1 Hz, 1H), 4.98 (d, *J*=7.4, Hz, 1H), 7.07 (d, *J*= 9.0 Hz, 2H), 7.34 (d, *J*=9.1 Hz, 2H). ^{13}C NMR (75 MHz, D_2O/MeOD) δ_c 14.26, 20.57, 39.78, 62.16, 71.07, 74.58, 77.28, 77.75, 102.16, 118.52, 142.76, 133.75, 155.61, 176.78. LRMS (ESI^-): Calculated 341.15, Found 340.08 $[M-H]^-$.

6.2.44 4-pentanamidophenyl-β-D-glucopyranoside (65)

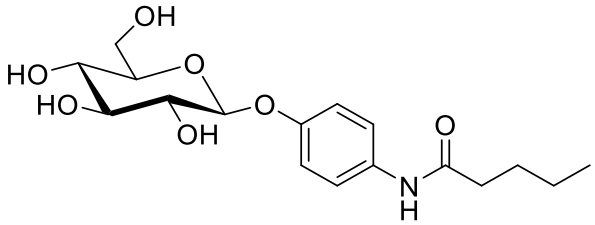

Compound **105** (245 mg, 0.468 mmol) and potassium carbonate (6.5mg, 0.0153 mmol) were dissolved in methanol (10 mL) in a 50 mL round bottom flask and stirred overnight at room temperature. Amberlite IRC-76 resin (H+ form, pH=4) was pre-rinsed with MeOH and then added to the mixture, which was stirred for an additional 10 minutes until a pH of 5 to 6. The mixture was filtered and the solvent was removed under reduced pressure to yield white crystals (147 mg, 88%). ^{1}H NMR (300 MHz, D_2O/MeOD) δ_H 0.97 (t, *J*=7.4 Hz, 3H), 1.41 (hex, *J*=7.6 Hz, 2H), 1.67 (quin, *J*=7.6 Hz, 2H), 2.34 (t, *J*=7.6 Hz, 2H), 3.35-3.46 (m, 4H), 3.70 (dd, *J*=12.1, 5.4 Hz, 1H), 3.89 (dd, *J*=12.1, 1.9 Hz, 1H), 4.82 (m, 1H), 7.06 (d, *J*=9.0 Hz, 2H), 7.45 (d, *J*=9.0 Hz, 2H). ^{13}C NMR (75 MHz, D_2O/MeOD) δ_C 12.75, 22.01, 27.72, 36.21, 61.11, 69.97, 73.50, 76.56, 76.72, 101.30, 116.65, 121.24, 133.12, 154.26, 173.10. LRMS (ESI^-): Calculated 355.16, Found 354.15 $[M-H]^-$.

6.2.45 4-ethoxyphenyl-2,3,4,6-tetra-*O*-acetyl-β-D-glucopyranoside (108)

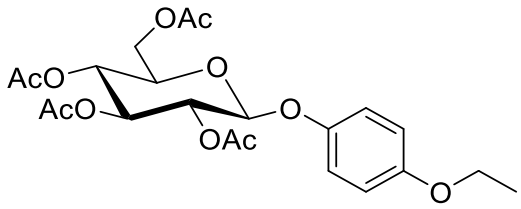

1,2,3,4,6-penta-*O*-acetyl-β-D-glucopyranoside (300 mg, 0.769 mmol) and 4-ethoxyphenol (117 mg, 0.845 mmol) were added to a 50 mL flame-dried round bottom flask charged with argon and 4Å molecular sieves. The compounds were dissolved in anhydrous CH_2Cl_2 (20 mL) and stirred at 0^{O}C for 30 minutes. $BF_3{\cdot}OEt_2$ (1.42 mL, 11.54 mmol) was then added dropwise and the reaction mixture was stirred overnight at room temperature. The contents were then filtered over a bed of celite and then quenched with sodium bicarbonate (sat. aq., 50 mL). The organic layer was separated and the aqueous layer was extracted with CH_2Cl_2 (3 x 50 mL). The combined organic fractions were washed with $NaHCO_3$ (sat. aq.) and brine, dried with $MgSO_4$, and then filtered and concentrated under reduced pressure. The crude residue was purified by column chromatography (75:25 - 70:30 Hexanes:EtOAc) to give a colourless solid (327 mg, 74%). ^{1}H NMR (300 MHz, $CDCl_3$) δ_H 1.34 (t, *J*=7.0 Hz, 3H), 1.99 (s, 3H), 2.00 (s, 3H), 2.03 (s, 3H), 2.04 (s, 3H), 3.74-3.81 (m, 1H), 3.94 (q, *J*=7.0 Hz, 2H), 4.12 (dd, *J*=12.3, 2.3 Hz, 1H), 4.25 (dd, *J*=12.3, 5.3 Hz, 1H), 4.92 (d, *J*=7.6 Hz, 1H), 5.11 (dd, *J*=9.7, 9.7 Hz, 1H), 5.18-5.27 (m, 2H), 6.76 (d, *J*=9.0 Hz, 2H), 6.89 (d, *J*=9.0 Hz, 2H). ^{13}C NMR (75 MHz, $CDCl_3$) δ_c 14.85, 20.59, 20.61, 20.65, 20.70, 61.94, 63.87, 63.32, 71.23, 71.91, 72.75, 100.27, 115.19, 118.66, 150.82, 155.13, 169.31, 169.41, 170.23, 170.57. LRMS (ESI$^+$): Calculated 468.16, Found 507.12 $[M+K]^+$.

6.2.46 4-propoxyphenyl-2,3,4,6-tetra-*O*-acetyl-β-D-glucopyranoside (109)

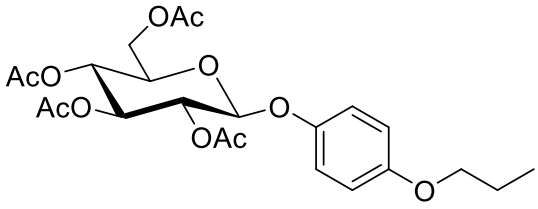

1,2,3,4,6-penta-*O*-acetyl-β-D-glucopyranoside (300 mg, 0.769 mmol) and 4-propoxyphenol (129 mg, 0.845 mmol) were added to a 50 mL flame-dried round bottom flask charged with argon and 4Å molecular sieves. The compounds were dissolved in anhydrous CH_2Cl_2 (20 mL) and stirred at 0^{O}C for 30 minutes. $BF_3{\cdot}OEt_2$ (1.42 mL, 11.54 mmol) was then added dropwise and the reaction mixture was stirred overnight at room temperature. The contents were then filtered over a bed of celite and then quenched with sodium bicarbonate (sat. aq., 50 mL). The organic layer was separated and the aqueous

layer was extracted with CH_2Cl_2 (3 x 50 mL). The combined organic fractions were washed with $NaHCO_3$ (sat. aq.) and brine, dried with $MgSO_4$, and then filtered and concentrated under reduced pressure. The crude residue was purified by column chromatography (80:20 - 70:30 Hexanes:EtOAc) to afford white crystals (195 mg, 53%). ^{1}H NMR (500 MHz, $CDCl_3$) δ_H 0.98 (t, *J*=7.5 Hz, 3H), 1.70-1.77 (m, 2H), 1.99 (s, 3H), 2.00 (s, 3H), 2.03 (s, 3H), 2.04 (s, 3H), 3.76-3.80 (m, 1H), 3.83 (t, *J*=6.6 Hz, 2H), 4.13 (dd, *J*=12.3, 2.4 Hz, 1H), 4.25 (dd, *J*=12.3, 5.3 Hz, 1H), 4.92 (d, *J*=7.7 Hz, 1H), 5.11 (dd, *J*=9.4, 9.4 Hz, 1H), 5.17-5.26 (m, 2H), 6.77 (d, *J*=9.1 Hz, 2H), 6.89 (d, *J*=9.1 Hz, 2H). ^{13}C NMR (125 MHz, $CDCl_3$) δ_c 10.48, 20.59, 20.62, 20.66, 20.71, 22.56, 61.91, 68.28, 69.97, 71.19, 71.90, 72.73, 100.32, 115.18, 118.65, 150.75, 155.33, 169.31, 169.39, 170.27, 170.60. LRMS (ESI$^+$): Calculated 482.18, Found 521.13 $[M+K]^+$.

6.2.47 4-ethoxyphenyl-β-D-glucopyranoside (66)

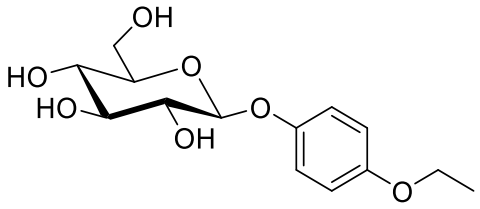

Compound **108** (234 mg, 0.500 mmol) and potassium carbonate (7 mg, 0.050 mmol) were dissolved in methanol (10 mL) in a 50 mL round bottom flask and stirred overnight at room temperature. Amberlite IRC-76 resin (H+ form, pH=4) was pre-rinsed with MeOH and then added to the mixture, which was stirred for an additional 10 minutes until a pH of 5 to 6. The mixture was filtered and the solvent was removed under reduced pressure to yield white crystals (124 mg, 83%). ^{1}H NMR (300 MHz, D_2O) δ_H 1.35 (t, *J*=7.0 Hz, 3H), 3.44-3.62 (m, 4H), 3.74 (dd, *J*=12.4, 5.6 Hz, 1H), 3.91 (dd, *J*=12.4, 2.1 Hz, 1H), 4.09 (q, *J*=7.1 Hz, 2H), 5.01 (d, *J*=7.5 Hz, 1H), 6.97 (d, *J*=9.2 Hz, 2H), 7.10 (d, *J*=9.2 Hz, 2H). ^{13}C NMR (125 MHz, D_2O) δ_c 13.83, 60.40, 64.83, 69.30, 72.83, 75.43, 75.95, 101.49, 115.81, 118.05, 150.86, 153.70. LRMS (ESI): Calculated 300.12, Found 299.06 $[M-H]^-$.

6.2.48 4-propoxyphenyl-β-D-glucopyranoside (67)

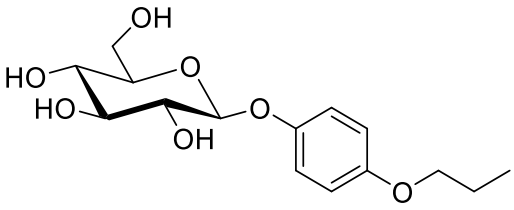

Compound **109** (185 mg, 0.384 mmol) and potassium carbonate (5 mg, 0.038 mmol) were dissolved in methanol (10 mL) in a 50 mL round bottom flask and stirred overnight at room temperature. Amberlite IRC-76 resin (H+ form, pH=4) was pre-rinsed with MeOH and then added to the mixture, which was stirred for an additional 10 minutes until a pH of 5 to 6. The mixture was filtered and the solvent was removed under reduced pressure to yield white crystals (114 mg, 94%). ^{1}H NMR (500 MHz, D_2O) δ_H 0.95

(t, *J*=7.5 Hz, 3H), 1.68-1.75 (m, 2H), 3.43-3.57 (m, 4H), 3.71 (dd, *J*=12.5, 5.7 Hz, 1H), 3.89 (dd, *J*=12.4, 2.2 Hz, 1H), 3.96 (t, *J*=6.6 Hz, 2H), 4.96 (d, *J*=7.7 Hz, 1H), 6.95 (d, *J*=9.2 Hz, 2H), 7.07 (d, *J*=9.1 Hz, 2H). ^{13}C NMR (125 MHz, D_2O) δ_c 9.54, 21.79, 60.43, 69.33, 70.89, 72.86, 75.46, 75.97, 101.07, 115.93, 118.08, 150.88, 153.93. LRMS (ESI$^-$): Calculated 314.14, Found 313.03 $[M-H]^-$.

6.2.49 4-butoxyphenol (111)

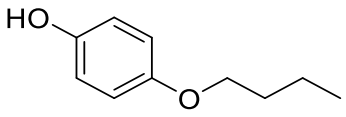

Hydroquinone (200 mg, 1.816 mmol) and potassium carbonate (376 mg, 2.724 mmol) were dissolved in acetone in a 50 mL round bottom flask. Butyl iodide (207 uL, 1.816 mmol) was added dropwise, and the reaction mixture was heated to reflux and stirred overnight. Once complete, the acetone was evaporated under reduced pressure, and the residue was taken up in 1% aq. HCl (50 mL) and extracted with dichloromethane (3 x 50 mL). The combined organic fractions were washed with $NaHCO_3$ (sat. aq., 50 mL), brine (50 mL), dried with $MgSO_4$, filtered and concentrated. The crude product was purified by column chromatography (90:10 Hex:EtOAc) to afford a brown solid (81 mg, 27%). ^{1}H NMR (300 MHz, $CDCl_3$) δ_H 0.97 (t, *J*=7.5 Hz, 3H), 1.48 (hex, *J*=7.6 Hz, 2H), 1.74 (quin, *J*=7.6 Hz, 2H), 3.91 (t, *J*=6.6 Hz, 2H), 5.04 (br s, 1H), 6.73-6.81 (m, 4H).

All spectral data were consistent with previous reports.[5]

6.2.50 4-butoxyphenyl-2,3,4,6-tetra-*O*-acetyl-β-D-glucopyranoside (112)

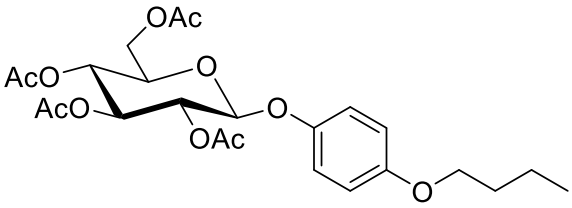

1,2,3,4,6-penta-*O*-acetyl-β-D-glucopyranoside (250 mg, 0.639 mol) and compound **111** (117 mg, 0.704 mmol) were added to a 50 mL flame-dried round bottom flask charged with argon and 4Å molecular sieves. The compounds were dissolved in anhydrous CH_2Cl_2 (20 mL) and stirred at 0^{O}C for 30 minutes. $BF_3{\cdot}OEt_2$ (1.18 mL, 11.54 mmol) was then added dropwise and the reaction mixture was stirred overnight at room temperature. The contents were then filtered over a bed of celite and then quenched with sodium bicarbonate (sat. aq., 50 mL). The organic layer was separated and the aqueous layer was extracted with CH_2Cl_2 (3 x 50 mL). The combined organic fractions were washed with $NaHCO_3$ (sat. aq.) and brine, dried with $MgSO_4$, and then filtered and concentrated under reduced pressure. The crude residue was purified by column chromatography (70:30 Hexanes:EtOAc) to give the title compound as white crystals (255 mg, 80%). ^{1}H NMR (300 MHz, $CDCl_3$) δ_H 0.95 (d, *J*=7.4 Hz, 3H), 1.40-1.53 (m, 2H), 1.68-1.78 (m, 2H), 2.02 (s, 3H), 2.03 (s, 3H), 2.06 (s, 3H), 2.08 (s, 3H), 3.76-3.83 (m, 1H), 3.90 (t, *J*=6.6 Hz, 2H), 4.15 (dd, *J*=12.4, 2.5 Hz, 1H), 4.28 (dd, *J*=12.3, 5.2 Hz, 1H), 4.94 (d, *J*=7.6Hz, 1H), 5.15 (dd, *J*=9.6, 9.6 Hz, 1H), 5.22-5.31 (m, 2H), 6.79 (d, *J*=9.1 Hz, 2H), 6.92 (d, *J*=9.1 Hz, 2H). ^{13}C NMR (75

MHz, $CDCl_3$) δ_c 13.96, 19.32, 20.71, 20.78, 20.83, 31.43, 62.04, 68.26, 68.41, 71.33, 72.02, 72.86, 100.43, 115.29, 118.77, 150.87, 155.47, 169.43, 169.51, 170.38, 170.72. LRMS (ESI^+): Calculated 496.19, Found 535.18 $[M+K]^+$.

6.2.51 4-butoxyphenyl-β-D-glucopyranoside (68)

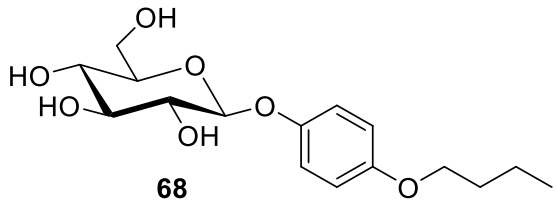

68

Compound **112** (245 mg, 0.493 mmol) and potassium carbonate (7 mg, 0.049 mmol) were dissolved in methanol (10 mL) in a 50 mL round bottom flask and stirred overnight at room temperature. Amberlite IRC-76 resin (H+ form, pH=4) was pre-rinsed with MeOH and then added to the mixture, which was stirred for an additional 10 minutes until a pH of 5 to 6. The mixture was filtered and the solvent was removed under reduced pressure to afford white crystals (145 mg, 90%). ^1H NMR (300 MHz, MeOD) δ_H 0.98 (t, *J*=7.4 Hz, 3H), 1.43-1.55 (m, 2H), 1.68-1.78 (m, 2H), 3.36-3.46 (m, 4H), 3.66-3.74 (m, 1H), 3.86-3.90 (m, 1H), 3.92 (t, *J*=6.6 Hz, 2H), 4.77 (d, =7.6 Hz, 1H), 6.82 (d, *J*=9.1 Hz, 2H), 7.04 (d, *J*=9.1 Hz, 2H). ^{13}C NMR (75 MHz, MeOD) δ_c 14.19, 20.29, 32.58, 62.52, 69.14, 71.39, 74.95, 77.97, 78.06, 103.41, 116.12, 119.15, 153.14, 156.04. LRMS (ESI^-): Calculated 328.15, Found 327.06 $[M-H]^-$.

References

1. Tam, R. Y.; Ferreira, S. S.; Czechura, P.; Chaytor, J. L.; Ben, R. N., Hydration Index: A Better Parameter for Explaining Small Molecule Hydration in Inhibition of Ice Recrystallization. *J. Am. Chem. Soc.* **2008**, 130, 17494-17501.

2. Jackman, J.; Noestheden, M.; Moffat, D.; Pezacki, J. P.; Findlay, S.; Ben, R. N., Assessing antifreeze activity of AFGP 8 using domain recognition software. *Biochem. Biophys. Res. Commun.* **2007**, 354, 340-344.

3. Inada, T.; Modak, P. R., Growth control of ice crystals by poly(vinyl alcohol) and antifreeze protein in ice slurries. *Chem. Eng. Sci*. **2006**, 61, 3149-3158.

4. Soulère, L.; Aldrich, C.; Daumke, O.; Gail, R.; Kissau, L.; Wittinghofer, Al; Waldmann, H., Synthesis of GTP-Derived Ras Ligands. *Chem. Bio. Chem.* **2004**, 5, 1448-1453.

5. Paduraru, P. M.; Popoff, R. T. W.; Nair, R.; Gries, R.; Gries, G.; Plettner, E., Synthesis of Substituted Alkoxy Benzene Minilibraries for the Discovery of New Insect Olfaction or Gustation Inhibitors. *J. Comb. Chem.* **2008**, 10, 123-134.

Appendix: Selected 1H and 13C NMR Spectra

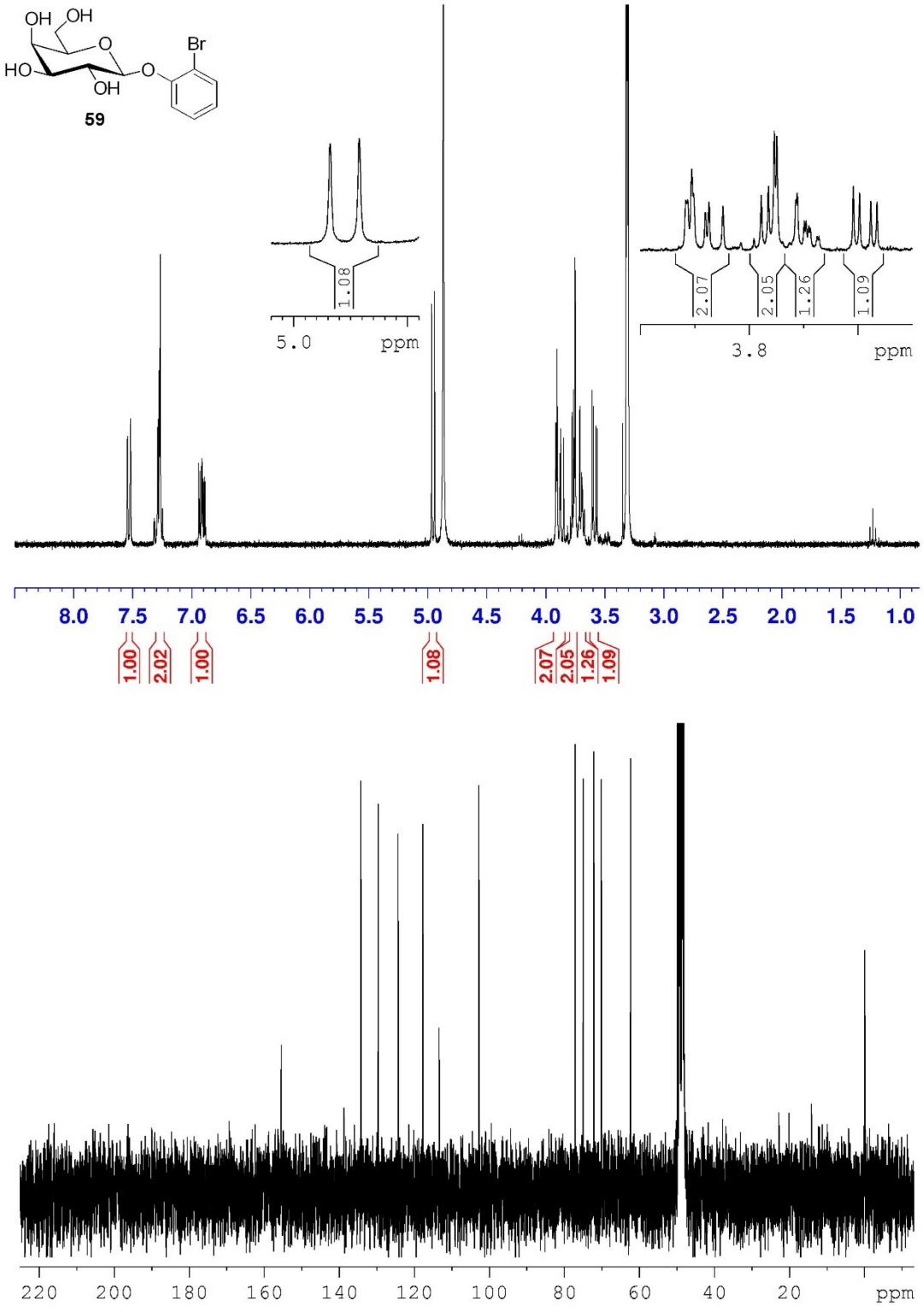
OH
OH
O
Br
HO
O
OH
59
1.08
5.0
ppm
2.07
2.05
1.26
1.09
3.8
ppm
8.0
7.5
7.0
6.5
6.0
5.5
5.0
4.5
4.0
3.5
3.0
2.5
2.0
1.5
1.0
1.00
2.02
1.00
1.08
2.07
2.05
1.26
1.09
220
200
180
160
140
120
100
80
60
40
20
ppm

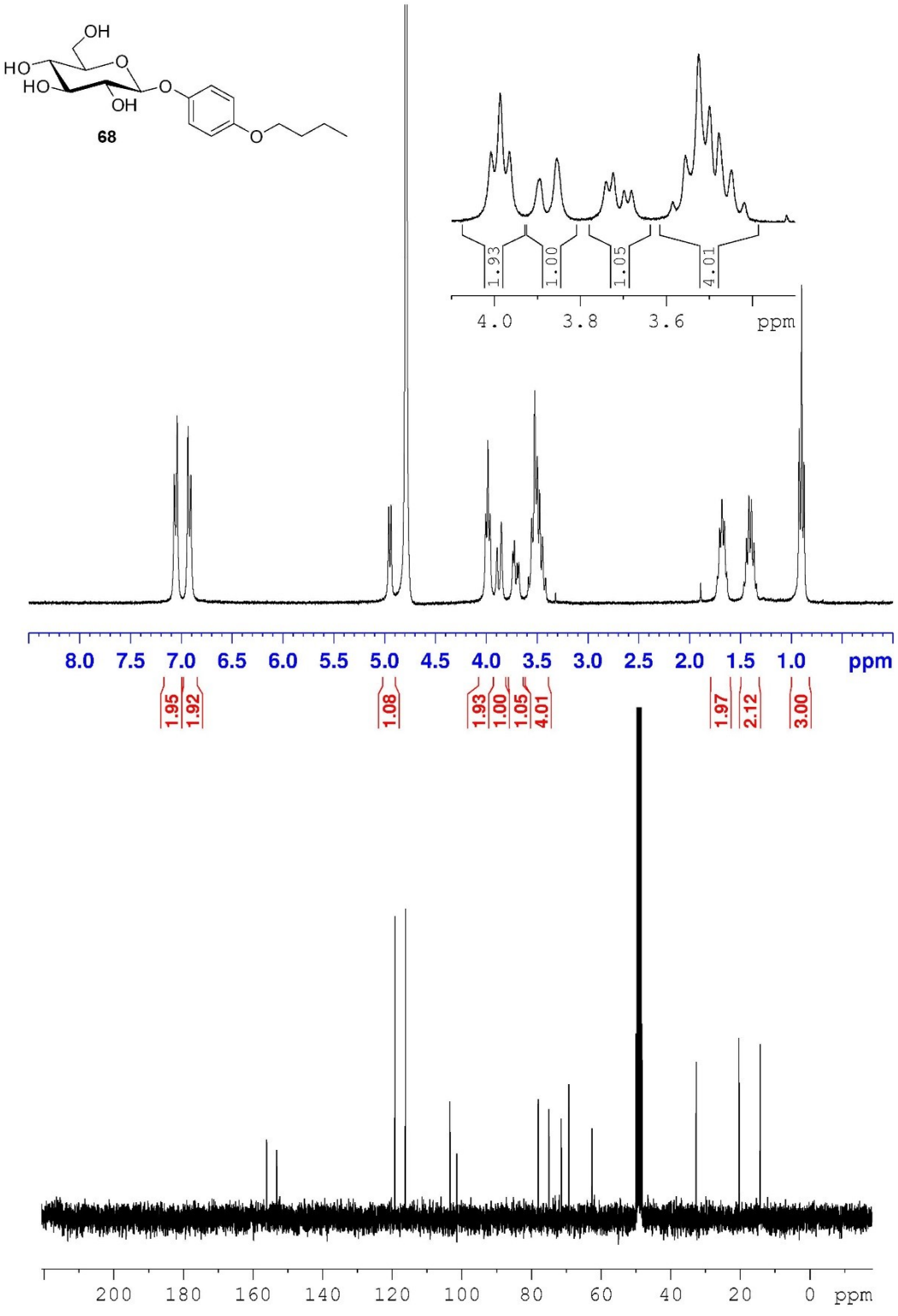
OH
HO
HO
OH
O
O
O
68
1.93
1.00
1.05
4.01
4.0
3.8
3.6
ppm
8.0
7.5
7.0
6.5
6.0
5.5
5.0
4.5
4.0
3.5
3.0
2.5
2.0
1.5
1.0
ppm
1.95
1.92
1.08
1.93
1.00
1.05
4.01
1.97
2.12
3.00
200
180
160
140
120
100
80
60
40
20
0
ppm

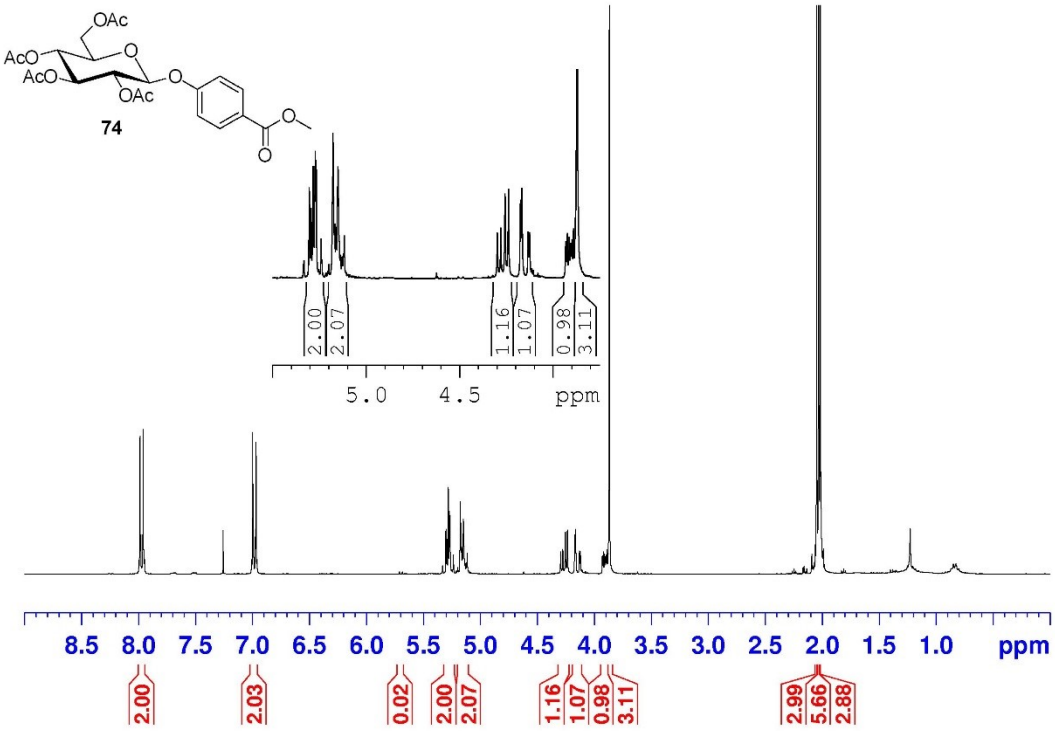
OAc
AcO
AcO
OAc
O
O
O
74
2.00
2.07
1.16
1.07
0.98
3.11
5.0
4.5
ppm
8.5 8.0 7.5 7.0 6.5 6.0 5.5 5.0 4.5 4.0 3.5 3.0 2.5 2.0 1.5 1.0 ppm
2.00
2.03
0.02
2.00
2.07
1.16
1.07
0.98
3.11
2.99
5.66
2.88

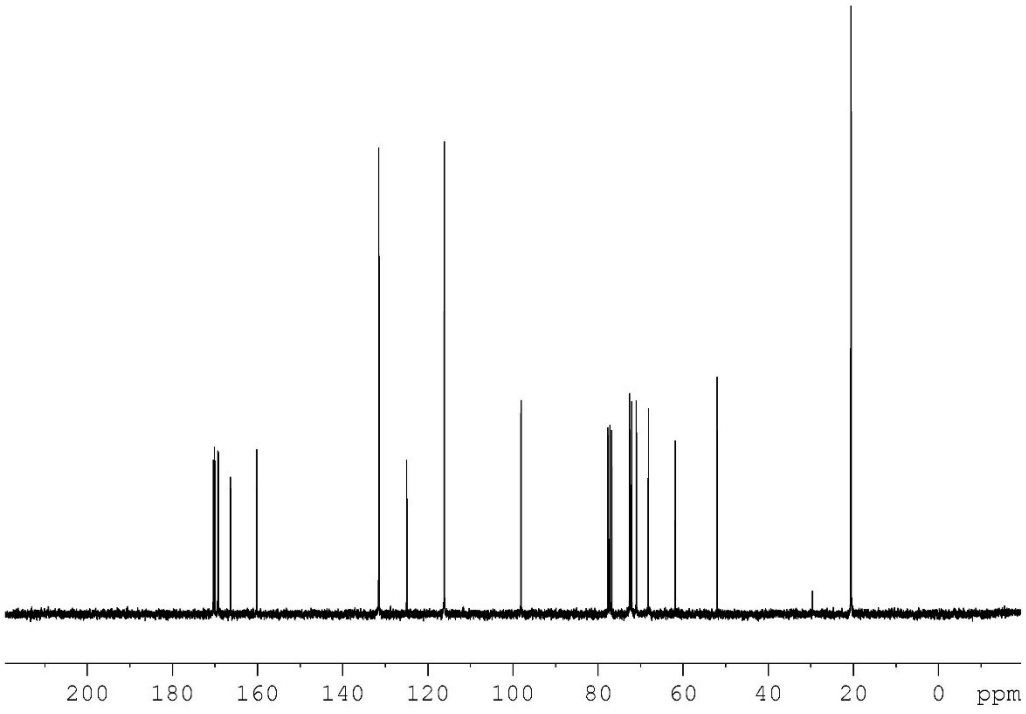
200 180 160 140 120 100 80 60 40 20 0 ppm

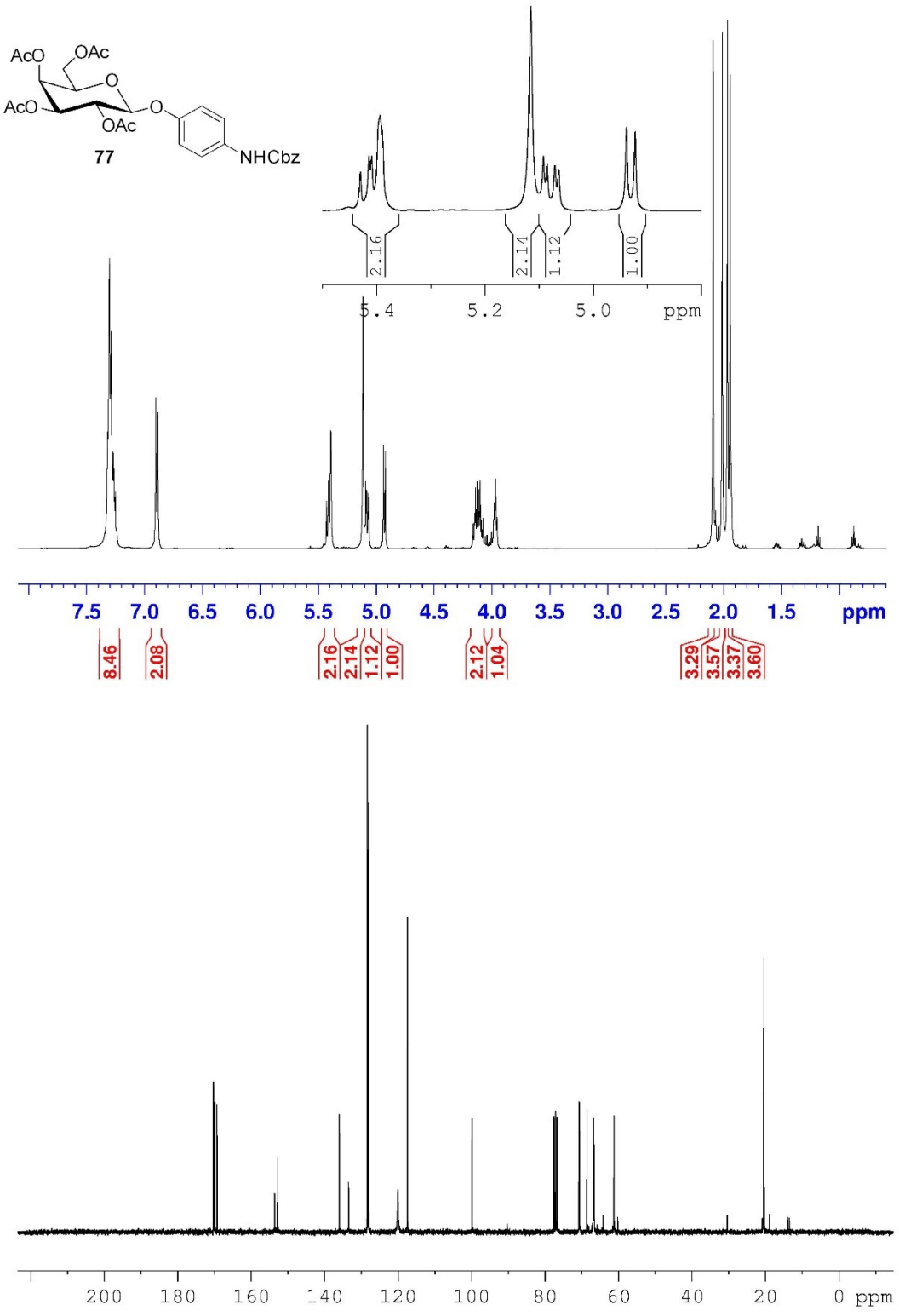
AcO
OAc
AcO
OAc
O
O
NHCbz
77
2.16
2.14
1.12
1.00
5.4
5.2
5.0
ppm
7.5
7.0
6.5
6.0
5.5
5.0
4.5
4.0
3.5
3.0
2.5
2.0
1.5
ppm
8.46
2.08
2.16
2.14
1.12
1.00
2.12
1.04
3.29
3.57
3.37
3.60
200
180
160
140
120
100
80
60
40
20
0 ppm

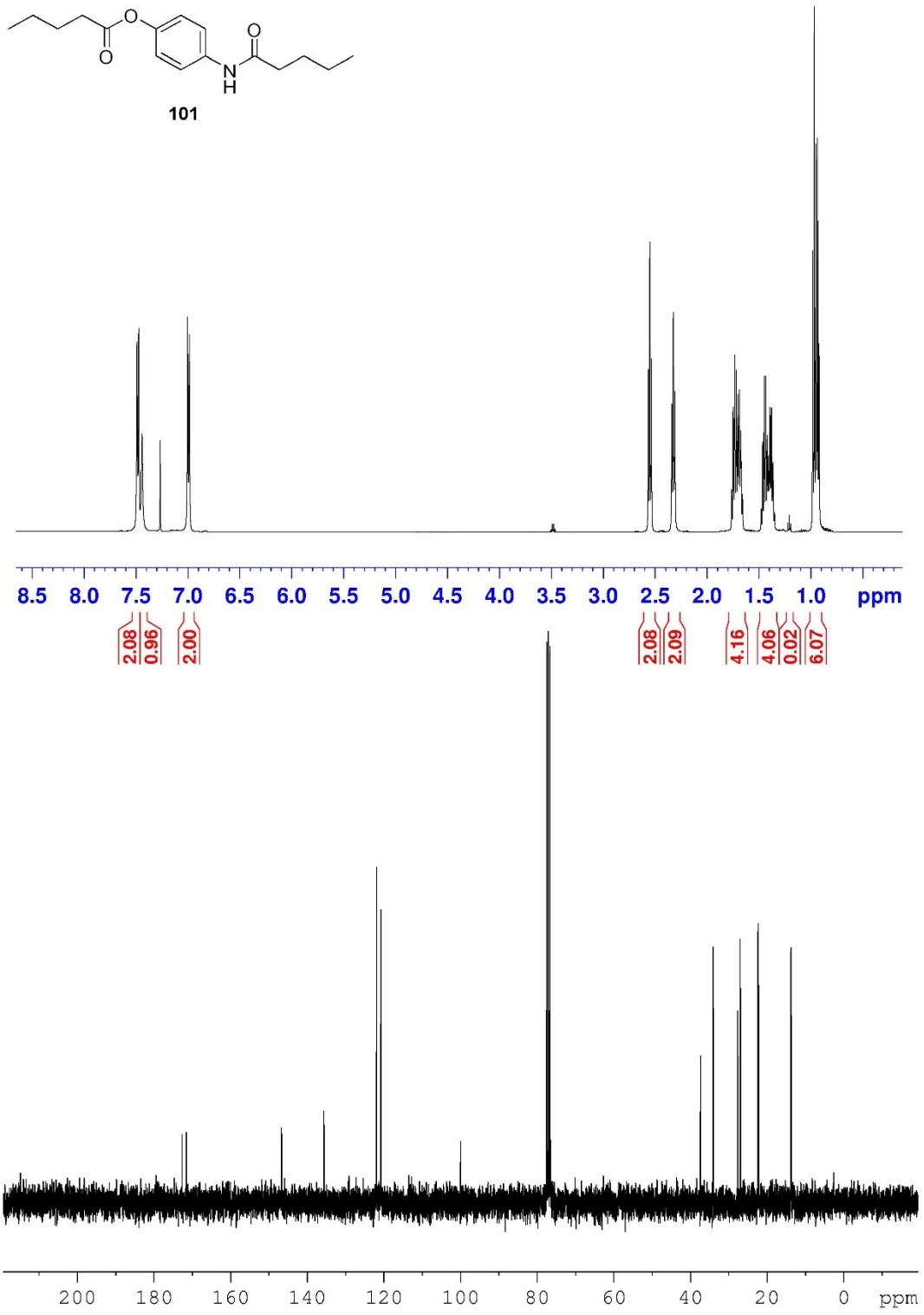
101
8.5 8.0 7.5 7.0 6.5 6.0 5.5 5.0 4.5 4.0 3.5 3.0 2.5 2.0 1.5 1.0 ppm
2.08 0.96 2.00 2.08 2.09 4.16 4.06 0.02 6.07
200 180 160 140 120 100 80 60 40 20 0 ppm

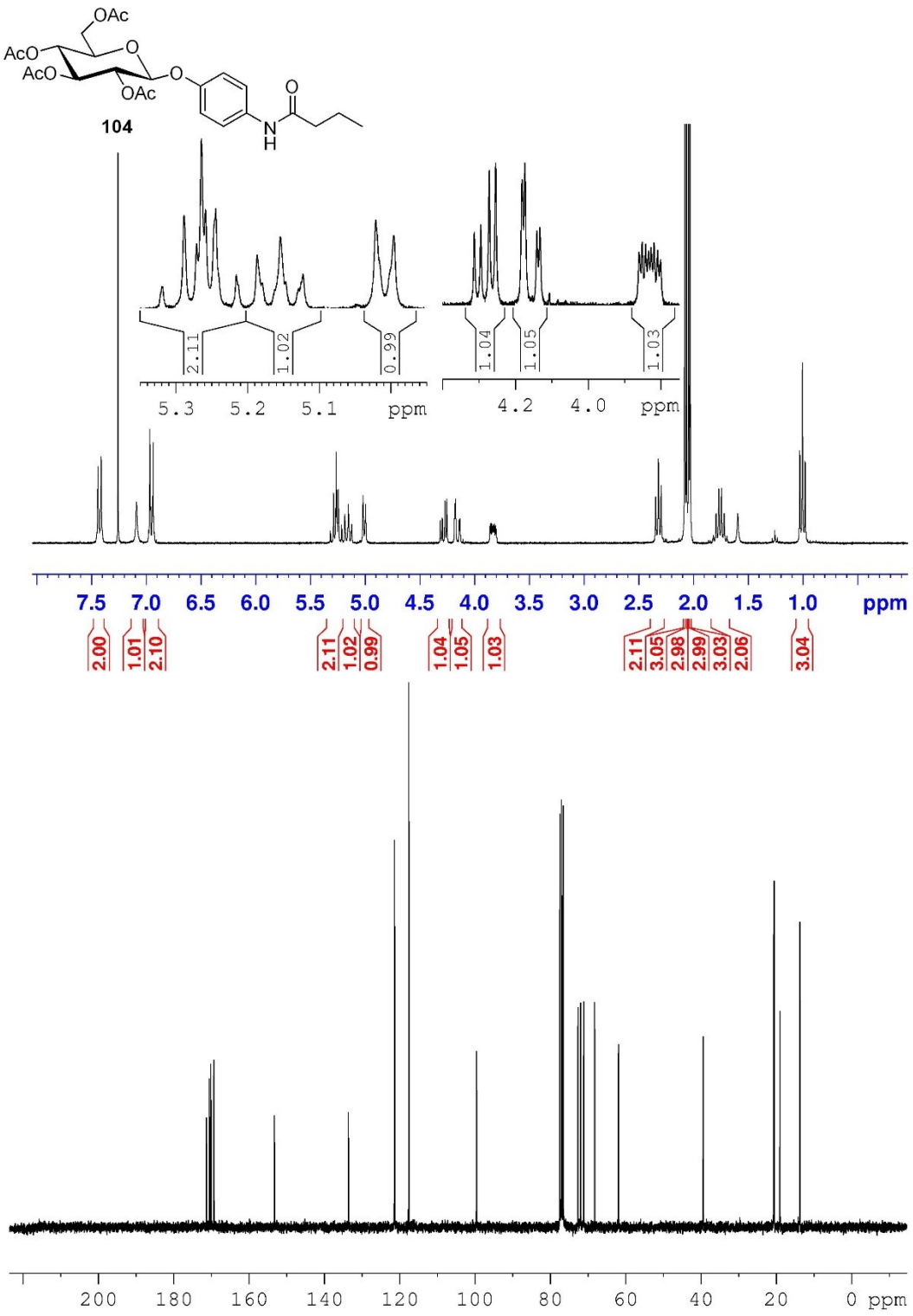
OAc
AcO
AcO
OAc
O
O
N
H
O
104
2.11
1.02
0.99
5.3
5.2
5.1
ppm
1.04
1.05
1.03
4.2
4.0
ppm
7.5
7.0
6.5
6.0
5.5
5.0
4.5
4.0
3.5
3.0
2.5
2.0
1.5
1.0
ppm
2.00
1.01
2.10
2.11
1.02
0.99
1.04
1.05
1.03
2.11
3.05
2.98
2.99
3.03
2.06
3.04
200
180
160
140
120
100
80
60
40
20
0 ppm

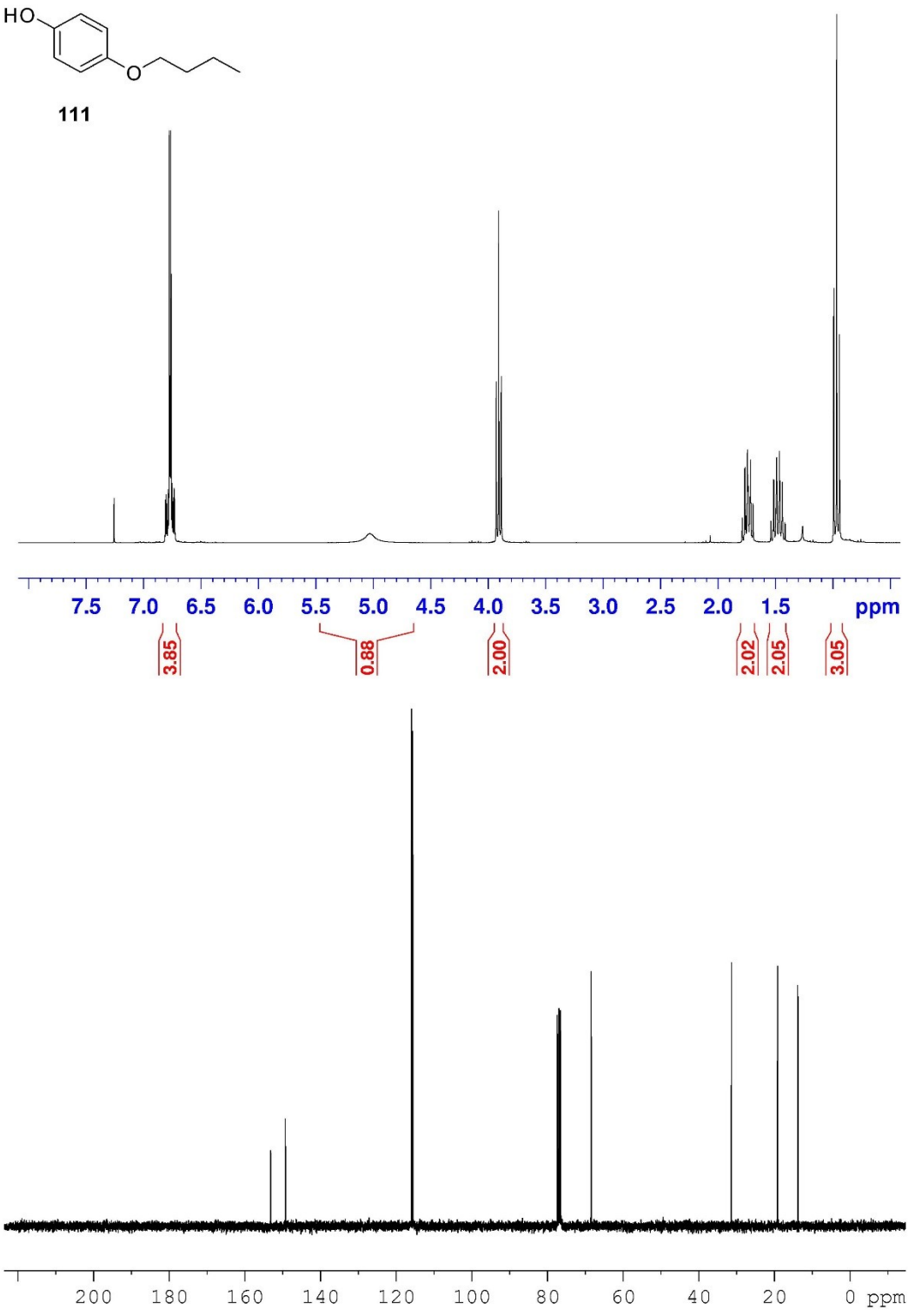
HO
O
111
7.5
7.0
6.5
6.0
5.5
5.0
4.5
4.0
3.5
3.0
2.5
2.0
1.5
ppm
3.85
0.88
2.00
2.02
2.05
3.05
200
180
160
140
120
100
80
60
40
20
0 ppm